Quantitative Ultrasonography in Regional Anesthesia

LI, Xiang

A Thesis Submitted in Partial Fulfilment

of the Requirements for the Degree of

Doctor of Philosophy

in

Anaesthesia and Intensive Care

The Chinese University of Hong Kong

June 2009

ProQuest LLC.
789 East Eisenhower Parkway
P.O. Box 1346
Ann Arbor, MI 48106 - 1346

STATEMENT OF WORK

The work in this thesis was performed at the Department of Anaesthesia and Intensive Care of The Chinese University of Hong Kong, Prince of Wales Hospital, Shatin, Hong Kong SAR between 2006 and 2009. All work presented in this thesis is my own original work under the supervision of Prof. Manoj Kumar Karmakar. None of the work in this thesis has previously been submitted either in whole or in part, for a degree or diploma to The Chinese University of Hong Kong or any other academic institution.

ACKNOWLEDGMENTS

I would like to express my sincere gratitude to my supervisor, Professor Manoj Kumar Karmakar for his guidance, patience and friendship throughout the past three years. He generously shared his experience, knowledge and opinion with me throughout this project. I would also like to thank his wife, Mrs. Mala Karmakar and her family for all the happy moments that we shared together as a family.

I would also like to thank Professor Lester Critchley, Professor Anna Lee, Dr. P. T. Chui, Dr. W. H. Kwok, Dr. Y. E. Chee, Professor Anthony Ho, and Professor Tony Gin for their advice, help and guidance rendered during my various studies. I would also like to thank all my colleagues from the Department of Anaesthesia & Intensive Care for their supports.

To

My Family during the Past Seven Years

My wife, Yun Fen, for her devotion to our family & her sacrifice...

My son, Hao hao, who gives me great joy...

My parents, who inspire me to sing a brave song...

My sisters, Jing Li & Qiong Li, for their help and support...

ABSTRACT

Regional anesthetic procedures (peripheral and central neuraxial blocks) are frequently performed for anesthesia or analgesia during the perioperative period. Success of these techniques depends on one's ability to accurately place the needle and thereby the local anesthetic drug closes to the target nerve. Currently one has to rely on anatomical landmarks, fascial clicks, loss of resistance, eliciting paresthesia or nerve stimulation to position the block needle in the vicinity of the nerve.

Recently there has been an increase in interest in the use of ultrasound to guide peripheral and central neuraxial blocks in both adults and children. Ultrasound allows the target peripheral nerve and the surrounding structures to be directly visualized in real-time during block placement. It also helps one to decide on the best possible site and maximum safe depth for needle insertion, allows real-time guidance of the needle to the target site, and visualizes the spread of the injected local anesthetic in real-time. This leads to fewer needle insertions, improved patient comfort during block placement, speeds the execution of peripheral nerve blocks, reduces the amount of local anesthetic required, speeds the onset of sensory blockade and prolongs the duration of sensory blockade. Currently the majority of published data on ultrasound guided regional anesthesia have largely focused on the application and efficacy of ultrasound guidance for peripheral nerve blockade. The peripheral nerves are visualized using ultrasound, and qualitative sonographic characteristics of peripheral nerves are described in the literature. However, to the best of our knowledge, there are no quantitative data on musculoskeletal structures during ultrasound guided regional anesthesia. Quantitative ultrasonographic methods have been used in radiology to evaluate the echogenicity and echotexture of

musculoskeletal structures. Therefore, it seemed plausible to extend these methods to quantify ultrasound images during regional anesthesia.

The aims of this research project were to develop quantitative ultrasonography methods to evaluate ultrasound images that were obtained during ultrasound guided regional anesthesia, test the reproducibility of these methods, evaluate how ultrasound system settings affect the echo intensity of an ultrasound image, assess the agreement between "off-cart" and "in-cart" measurements made on ultrasound images, evaluate gender and age-related differences in the musculoskeletal sonoanatomy at the infraclavicular fossa, characterize the echogenicity and echotexture of a peripheral nerve and compare the differences in the echo intensity and echotexture of a peripheral nerve in the young and the elderly, and quantify the changes in echo intensity of a peripheral nerve during ultrasound-guided nerve blockade.

This work was conducted in the Department of Anesthesia and Intensive Care of The Chinese University of Hong Kong at the Prince of Wales Hospital, Shatin, Hong Kong. The measurements of dimension, echo intensity and texture were performed on the ultrasound images using computer assisted image analysis techniques.

My work has shown that the quantitative ultrasonographic methods that were used in this project are reproducible. Varying the setting in an ultrasound system can affect the echo intensity, indicating that it is essential to standardize the scan settings of an ultrasound system during quantitative ultrasonography. A good correlation was seen between the measurements that were made by "off-cart" and "in-cart" methods, indicating that "off-cart" measurements can substitute "in-cart" measurements for research purposes. We also found age and gender-related differences in

measurements of musculoskeletal structure made at the infraclavicular fossa. The echo intensity of the median nerve and the flexor muscles of the forearm are significantly increased, and there is a reduction in contrast between the median nerve and the adjoining flexor muscles in the elderly. Furthermore, there is also an increase in the white area index, a reduction in the black area index and the cross sectional area of the median nerve in the elderly. Finally, we have also demonstrated a dynamic change in the cross sectional area and echo intensity of the sciatic nerve after local anesthetic injection during ultrasound-guided sciatic nerve blockade.

In conclusion, in this project several computer-assisted image analysis methods were developed and used to quantitatively evaluate ultrasound images during regional anesthesia. Parameters that were evaluated included "off-cart" measurement of distance, area, echo intensity and echotexture. The methods used for computer assisted image analysis were found to be accurate and reproducible. The echo intensity measurement is affected by the settings in the ultrasound system. There is a good correlation between "off-cart" and "in-cart" measurements, and "off-cart" measurements that were made at the infraclavicular fossa demonstrated significant age and gender-related differences in the dimension of musculoskeletal structure. There are significant differences in the cross sectional area, echo intensity and echotexture of the median nerve in the young and the elderly. There are also significant differences in the echo intensity of the flexor muscles, and contrast between the median nerve and the adjoining flexor muscles in the young and the elderly. Moreover, the changes in echo intensity and cross sectional area of the sciatic nerve after local anesthetic injection during ultrasound-guided nerve blockade were quantified. Future research correlating echotexture and histology of a peripheral nerve is warranted.

中文摘要

區域麻醉技術（周圍和中樞神經阻滯）是一項在圍手術期對病人進行術中麻醉和術后鎮痛的常用技術。成功進行阻滯的關鍵依賴於操作者對目標神經的準確定位和隨之進行麻醉藥物在神經周圍的良好擴散。目前，神經定位技術仍然依賴於解剖標志、筋膜突破感、阻力損失、感覺异常和神經刺激定位。

目前，超聲波引導下周圍神經、中樞神經區域痲醉技術由于其高效性及安全性而日漸普及于成人和兒童臨床工作之中。在超聲波掃描下，周圍神經和神經周圍結構得以實時、直接顯示，穿刺針的最佳安全穿刺深度得以確立，而且注射藥物的過程也可以在實時超聲波掃描下進行觀察。超聲波的應用減少了穿刺次數、增加病人舒適度、增加阻滯的準確性、減少麻醉藥物的使用劑量、加快區域麻醉起傚時間、并且延長區域麻醉藥物對感覺神經阻滯作用時間。目前超聲波在區域麻醉學領域的研究主要集中僅僅側重於其實用技術方面。雖然，量化超聲技術在骨骼肌超聲領域已經得到應用，但是對于周圍神經結構量化聲學特性研究却未見到報道。

該實驗課題的目的是應用量化超聲對于在超聲波引導下區域麻醉過程中獲得的超聲波影像進行量化客觀檢測。基于該項量化超聲波分析研究方法，在該項科研課題中的一系列實驗得以進行。其中包括對于實驗方法的重復興的評價、體外檢測不同的超聲波系統參數設定對回聲密度的影響、在綫和離綫測量技術間的相關性進行評價。此外，使用離綫測量技術對于鎖骨下區域的聲學解剖結構進行量化測量，并且比較該處結構在性別和年齡中的差异。而且，還使用計算機輔導下的圖像分析技術對于正中神經的回聲密度和紋理特徵進行了系

統之分析測量，對于它們在年輕人和老年人組別的差异也進行了系統比較。最後，觀測了坐骨神經的橫截麵積和聲學密度在超聲引導下區域麻醉的過程中的動態變化過程。

該課題的全部實驗均在中文大學威爾士親王醫院麻醉与深切治療系進行。實驗結果發現證實項圖像分析技術具有良好可重復性，確定了超聲波系統參數設定對于聲學密度影響的正性和負性相關性，離綫和在綫測量技術的相關性得以證實，這也表明離綫測量可以在科研中替代在綫測量。實驗中發現不同年齡和性別的鎖骨下區域解剖結構也存在顯著差別。老年人前臂的正中神經和屈肌聲學密度增高、二者對比度卻減少，并且還發現在對老年人紋理檢測中，老年人的正中神經白色面積指數也顯著增加但是神經橫截麵積卻減少。最後，坐骨神經在區域麻醉中聲學密度動態變化和橫截面積特點也進行觀察闡述。

總之，在這一課題中量化超聲波分析方法被應用於定量分析獲得於超聲波引導區域麻醉中的影像資料，這些方法包括聲學密度、紋理、離綫測量。這些分析方法被證實具有準確性和可重復性，超聲波系統參數的設定可以影響聲學密度，超聲波的離綫測量和在綫測量具有很好的相關性，鎖骨下區域的骨骼肌結構上存在性別和年齡差异。此外，在青年和老年人間正中神經的橫截面積、聲學密度、聲學紋理存在顯著差异，正中神經周圍屈肌的聲學密度以及正中神經和周圍屈肌之間的聲學密度對比度也存在顯著差异性。坐骨神經在超聲引導下區域麻醉中的橫截麵積和聲學密度變化也得以定量闡明。未來的實驗將對周圍神經的組織學和聲學紋理間關聯性進行研究。

PUBLICATIONS

The following publications have arisen from this research work to date:

1). **Li X,** Karmakar MK, Padmanabhan U, Gin T. Echotexture of the Median Nerve in the Young and the Elderly -- A Quantitative Analysis. 3rd Pan-Asian Symposium of the New York School of Regional Anesthesia (NYSORA 2009) on Regional Anesthesia and Pain Medicine, Kuala Lumpur, Malaysia. 6th-8th February 2009.(***Awarded the Best Poster Presentation***)

2). **Li X,** Karmakar MK, Lee A, Ho A.M.-H, Critchley L.A.H. Quantitative Evaluation of the Echogenicity of a Peripheral Nerve in the Young and the Elderly. The 82nd Annual Meeting of International Anesthesia Research Society (IARS 2008). San Francisco, California, USA. 27th March-2nd April 2008.

3). **Li X,** Karmakar MK, Kwok W.H, Critchley L.A.H, Gin T. Echogenicity of Peripheral Nerve in the Young and the Elderly. 2nd Pan-Asian Symposium of the New York School of Regional Anesthesia (NYSORA 2008) on Regional Anesthesia and Pain Medicine, Hong Kong, China. 12th-13th January 2008. (***Awarded the Best Poster Presentation***)

4). Karmakar MK, **Li X,** Ho AM, Kwok WH, Chui PT. Real-time ultrasound-guided paramedian epidural access: evaluation of a novel in-plane technique. Br J Anaesth. 2009 Jun;102(6):845-54

CONTENTS

Chapter1

Introduction 1

1.1 Introduction 1

1.2 Aims of the Project 6

1.3 Outline of the Thesis 7

Chapter 2

Literature Review 10

2.1 History 10

2.2 Basis of Ultrasound 13

2.3 Muscle and Nerve Dimension Measurements 18

2.3.1 Muscle Dimension Measurements 18

2.3.2 Nerve Dimension Measurements 20

2.4 Anatomy of a Peripheral Nerve 21

2.5 Sonoanatomy of a Normal Peripheral Nerve 24

2.6 Correlation between Anatomy and Qualitative Echotexture of a Peripheral Nerve 25

2.7 Limitations of Qualitative Ultrasonography in Assessing the Echotexture of a Peripheral Nerve 27

2.8 Quantitative Ultrasonographic Methods of Assessing the Echogenicity of Musculoskeletal Structures 28

2.8.1 Heckmatt's Visual Scale 28

2.8.2 Computer Assisted Grey-Scale Analysis 29

2.8.3 Computer Assisted Texture Analysis 31

2.9 Limitations of the Quantitative Ultrasonography Assessing the Echogenicity of Musculoskeletal Structures 32

2.10 Summary 33

Chapter 3

Methods Used for Quantitative Ultrasonography 34

3.1 Introduction and Objective 34

3.2 Equipment and Software Used 34

3.2.1 Ultrasound Equipment 34

3.2.2 Data Storage Device 35

3.2.3 Image Process Software 35

3.3 Scanning Routine 36

3.4 Image Acquisition and Data Transfer 37

3.4.1 Image Recording 37

3.4.2 Video Data Transfer 37

3.4.3 Still Image Capture 38

3.5 Method for "off-cart" Measurements of Distance and Area 38

3.5.1 Spatial Calibration 40

3.5.2 Distance Measurement 42

3.5.3 Area Measurement 42

3.6 Method for Measuring Echo Intensity 43

3.6.1 Standardization of the Ultrasound System Setting 43

3.6.2 Image Normalization 44

3.6.3 ROI Selection and Echo Intensity Measurement 45

3.7 Method for Measuring Texture 46

3.7.1 Standardization of the Ultrasound System Setting 47

3.7.2 Image Normalization 47

3.7.3 Noise Reduction and ROI Selection 47

3.7.4 Thresholding 48

3.7.5 Black and White Area Index Measurement 49

3.8 Summary 51

Chapter 4

Reproducibility of Quantitative Ultrasonography 52

4.1 Introduction and Objective 52

4.2 Materials and Methods 52

4.2.1 Study Design 52

4.2.2 Inclusion and Exclusion Criteria 52
4.2.3 Equipment and Software Used 53
4.2.4 System Settings 53
4.2.5 Preparation for Subjects 54
4.2.6 Scan Methods 54
4.2.7 Image Acquisition and Transfer 56
4.2.8 "Off-cart" Measurement of Distance and Area 56
4.2.9 Echo Intensity and Texture Measurements 57
4.2.10 Repeated Measurements 58
4.2.11 Statistical Analysis 59
4.3 Results 60
4.4 Discussion 60
4.5 Conclusion 61
Chapter 5
Effect of Ultrasound System Settings on the Echo Intensity of an Ultrasound Image: An In-Vitro Phantom Study 64
5.1 Introduction and Objective 64
5.2 Materials and Methods 64
5.2.1 Ultrasound Phantom 64
5.2.2 Equipment and Software Used 65
5.2.3 Preparation before the US Scan 66
5.2.4 Standardization of the Ultrasound System Settings 67
5.2.5 Image Acquisition and Transfer 70
5.2.6 Image Normalization 71
5.2.7 ROI Selection and Echo Intensity Measurement 71
5.2.8 Statistical Analysis 72
5.3 Results 72
5.3.1 Gain 72
5.3.2 Frequency 73
5.3.3 Dynamic Range 73
5.3.4 Depth 73
5.3.5 Power Output 73
5.4 Discussion 74
5.4.1 Effect of Gain on the Echo Intensity 74
5.4.2 Effect of Frequency on the Echo Intensity 74

5.4.3 Effect of Dynamic Range on the Echo Intensity 75
5.4.4 Effect of Depth on the Echo Intensity 76
5.4.5 Effect of Power Output on the Echo Intensity 77
5.5 Limitations 77
5.6 Conclusion 78

Chapter 6

"Off-cart" Measurements of Musculoskeletal Structures at the Infraclavicular Fossa 82

6.1 Introduction and Objective 82
6.2 Material and Methods 83
6.2.1 Study Design 83
6.2.2 Inclusion and Exclusion Criteria 83
6.2.3 Equipment and Software Used 84
6.2.4 System Setting 84
6.2.5 Preparation for the Patient 84
6.2.6 Scan Method 85
6.2.7 Infraclavicular Fossa Sonoanatomy 86
6.2.8 "In-cart" Measurements 88
6.2.9 Image Acquisition and Data Transfer 90
6.2.10 Spatial Calibration 90
6.2.11 "Off-cart" Measurements 91
6.2.12 Reproducibility Testing 91
6.2.13 Statistical Analysis 91
6.3 Results 93
6.3.1 Demographic Data 93
6.3.2 Correlation between "In-cart" and "Off-cart" Measurements 93
6.3.3 Parameter Measured at the Infraclavicular Fossa 94
6.4 Discussion 95
6.4.1 Reproducibility of "Off-cart" Measurement 95
6.4.2 Correlation between "In-cart" and "Off-cart" Measurements 95
6.4.3 Distance from the Skin to the Axillary Vessels 96
6.4.4 Dimensions of the Axillary Vessels 97
6.4.5 Width of the Pectoral Muscles 98
6.5 Limitations 100

6.6 Conclusion 101

Chapter 7

Echogenicity of the Median Nerve and the Flexor Muscles of the Forearm in the Young and the Elderly 107

7.1 Introduction and Objective 107

7.2 Material and Methods 107

7.2.1 Study Design 107

7.2.2 Sample Size Estimation 108

7.2.3 Inclusion and Exclusion Criteria 108

7.2.4 Equipment and Software Used 109

7.2.5 Standardization of the Ultrasound System Setting 109

7.2.6 Preparation for Subjects 110

7.2.7 Scan Method 110

7.2.8 Image Acquisition and Transfer 111

7.2.9 Image Normalization 112

7.2.10 ROI Selection 112

7.2.11 Echo Intensity Measurement 112

7.2.12 Reproducibility Testing 115

7.2.13 Statistical Analysis 115

7.3 Results 116

7.3.1 Demographic Data 116

7.3.2 Echo Intensity of the Flexor Muscles 116

7.3.3 Echo Intensity of the Median Nerve 116

7.3.4 Contrast between the Median Nerve and the Flexor Muscles 116

7.4 Discussion 117

7.4.1 Reproducibility of Echo Intensity Measurement 117

7.4.2 Effect of Age on the Echo Intensity of the Flexor Muscles 118

7.4.3 Effect of Age on the Echo Intensity of the Median Nerve 119

7.4.4 Effect of Age on the Contrast between the Median Nerve and the Flexor Muscles 119

7.5 Limitations 120

7.6 Conclusion 121

Chapter 8

Echotexture of the Median Nerve in the Young and the Elderly 123

8.1 Introduction and Objective 123

8.2 Materials and Methods 123

8.2.1 Study Design 123

8.2.2 Sample Size Estimation 124

8.2.3 Inclusion and Exclusion Criteria 124

8.2.4 Equipment and Software Used 124

8.2.5 Standardization of the Ultrasound System Setting 125

8.2.6 Preparation for Subjects 125

8.2.7 Scan Method 126

8.2.8 Image Acquisition and Transfer 126

8.2.9 Image Normalization 127

8.2.10 Echo Intensity Measurement 127

8.2.11 Cross Sectional Area Measurement 127

8.2.12 Echotexture Measurement 128

8.2.13 Reproducibility Testing 129

8.2.14 Statistical Analysis 131

8.3 Results 131

8.3.1 Demographic Data 131

8.3.2 Cross Sectional Area, Echo Intensity and Echotexture of the Median Nerve 132

8.3.3 Correlation between Echo Intensity and White Area Index of the Median Nerve 132

8.4 Discussion 133

8.4.1 Reproducibility of Measurements 133

8.4.2 Cross Sectional Area of the Median Nerve 134

8.4.3 Echo Intensity of the Median Nerve 135

8.4.4 Echotexture of the Median Nerve 135

8.5 Limitations 137

8.7 Conclusion 138

Chapter 9

Echogenicity of a Peripheral Nerve during Ultrasound Guided Nerve Blockade 140

9.1 Introduction and Objective 140

9.2 Material and Methods 140

9.2.1 Study Design 140

9.2.2 Sample Size Estimation 140

9.2.3 Inclusion and Exclusion Criteria 141

9.2.4 Equipment and Software Used 141
9.2.5 Preparation for Patient 142
9.2.6 Scan Method 142
9.2.7 Ultrasound Guided Sciatic Nerve Blockade 143
9.2.8 Image Acquisition and Transfer 144
9.2.9 Image Normalization 145
9.2.10 Cross Sectional Area Measurement 145
9.2.11 Echo Intensity Measurement 146
9.2.12 Reproducibility Testing 146
9.2.13 Statistical Analysis 147

9.3 Results 148
9.3.1 Demographic Data 148
9.3.2 Changes in Cross Sectional Area of the Sciatic Nerve 149
9.3.3 Changes in Echo Intensity of the Sciatic Nerve 149

9.4 Discussion 149
9.4.1 Reproducibility of Measurements 150
9.4.2 Reflection Coefficient and Echo Intensity 150
9.4.3 Posterior Acoustic Enhancement and Echo Intensity 151
9.4.4 Change in the Cross Sectional Area of the Sciatic Nerve 152
9.4.5 Echo Intensity after Local Anesthetic Injection 152

9.5 Limitations 153

9.6 Conclusion 153

Chapter 10

Summary 156

Bibliography 161

Appendices 185

LIST OF FIGURES

Figure 2-1. Illustrates the changes in the epineurial connective tissue of the sciatic nerve with age. (A) sciatic nerve of an 8-year-old child; (B) sciatic nerve of a 70-year-old-individual with increased adipose tissue; (C) sciatic nerve of a 93-year-old individual with predominant fatty tissue in the epineurium. (Reproduced from Sladjana et al, 2008)..... 24

Figure 2-2. Illustrates the correlation between the histological structure and the sonogram of a median nerve. (a) shows the photomicrograph of the histological specimen of a normal median nerve. The black arrow indicates a single fascicle ensheathed by a dense connective tissue layer, the perineurium. (b) shows a transverse sonogram of a normal median nerve with discrete hypoechoic fascicles (arrows). (Reproduced from Sturat. et al. 2003)..... 26

Figure 2-3. Illustration of the Heckmatt's Visual Scale. The Arrow indicates subcutaneous tissue; R=rectus femoris; V=vastus intermedius; F= femur. (Reproduced from Pillen 2006)..... 29

Figure 3-1. Equipment and software used during this project are shown. (a) US system with a high frequency transducer; (b) Commercial video recorder and SD card; (c) Adobe Premier Pro 2.0 software; (d) Site-Link Manager 3.4.1 software; (e) Adobe Photoshop CS2 software; (f) Image-Pro Plus 6.0 software; and (g) Laptop computer. 35

Figure 3-2. A typical US image of the median nerve in the mid-forearm. (a) A portion of the image is magnified 1600%, in which the individual pixels can now be seen as small squares; (b) illustration to demonstrate a "pixel" in the US image of the mid-forearm. "Square box" indicates one pixel. 39

Figure 3-3. Illustrates how spatial calibration was performed. (a) The spatial calibration tab in IPP was selected; (b) In the US image, a reference line (green) was set to match the depth scale (2.7cm). The spatial calibration of this image is 13.6 pixels mm^{-1}. 41

Figure 3-4. The "off-cart" measurement of distance (or length) and CSA using IPP software. The green colored numbers are the results of the measurements, which are also displayed in the measurement dialog box. 43

Figure 3-5. The Delta key, shown as a triangle indicates '*reset to factory defaults*' has been selected in the MicroMaxx US system. 44

Figure 3-6. A typical transverse sonogram of the median nerve in the forearm shows the two reference points, white text (GSM=255) and the black background (GSM=0). Inset showing the Curves Function for adjusting the entire gray-scale range of pixels in an image. 45

Figure 3-7. A typical transverse sonogram of the forearm is shown. A polygonal ROI has been placed around the outlines of the median nerve, and a square ROI box has been placed over the flexor muscle above the median nerve. The histogram palette (lower left) in the inset image shows the mean (SD) and median EI values of the median nerve in the US image. 46

Figure 3-8. Shows the filtering process using the median filter. (a) Filters tab in IPP. (b) ROI around the median nerve. 47

Figure 3-9. The thresholding process is shown on a typical transverse sonogram of the median nerve in the forearm. Inset shows the segmentation tab for selecting the threshold range. The threshold, gray-scale value selected in this image is 0-128. 49

Figure 3-10. A set of US images showing the different stages of the texture process. (a) An US image of the median nerve; (b) US image after normalization; (c) Noise Reduction-Median filtering; (d) Binary image after thresholding process..... 49

Figure 3-11. The process used to count the black and white area index in the ROI is illustrated. 50

Figure 4-1. A typical sagittal sonogram of the infraclavicular fossa. Distance from the skin to the axillary artery and the CSA of the axillary artery were measured using IPP. 57

Figure 4-2. A typical transverse sonogram of the mid-forearm. A polygonal ROI has been placed around the outlines of the median nerve. 59

Figure 5-1. (a) A *Select Series Nerve Block* US Blue Phantom is shown. (b) A typical transverse US image from the Blue Phantom. 66

Figure 5-2. System setup and preparation before the US scan. (a) General arrangement of the US system and the Blue Phantom; (b) LOGIQ® *e* US system; (c) US transducer and the blue phantom; (d) Cable suspended from an intravenous fluid stand; (e) High frequency linear-array transducer (12L-RS, 5-13MHz, 42 mm footprint) used in this study. 67

Figure 5-3. A typical transverse US image from the Blue Phantom. A circular ROI has been drawn around the outline of the simulated nerve. The histogram palette in the inset shows the mean (SD) and median EI values of the ROI in the US image. Scan settings are also shown on the top right corner of the image. B=B mode; Frq=US frequency; Gn=gain; E/A=enhance / average frame; Map=gray-scale map; D=depth; DR=dynamic range; FR=frame rate and AO=Acoustic (power) output. 69

Figure 5-4. Operation panel of a LOGIQ® *e* US system. The common function keys are labeled. TGC=time gain compensation. 71

Figure 5-5. The relationship between echo intensity and US system settings. (a) Positive correlation between the EI and gain setting; (b) Negative correlation between the EI and US frequency; (c) Negative correlation between the EI and dynamic range; (d) Negative correlation between the EI and depth setting and (e) Positive correlation between the EI and power output of an US system. 81

Figure 6-1. Shows the position of the patient in this study..... 85

Figure 6-2. A typical sagittal sonogram of the left infraclavicular fossa in (a) a male and (b) a female. The inset in (a) shows the position of the patient and the high-frequency linear-array transducer in the left infraclavicular fossa. Breast tissue in a female is encircled in (b). 87

Figure 6-3. Illustrates the "in-cart" measurements of various parameters on a typical sagittal sonogram of the left infraclavicular fossa. SA= vertical distance from the skin to the anterior wall of the axillary artery, SV= vertical distance from the skin to the anterior wall of the axillary vein, DA=maximum diameter of the axillary artery, DV= maximum diameter of the axillary vein, AA=CSA of the axillary artery, AV=CSA of the axillary vein and PM=width of the pectoral muscles..... 90

Figure 7-1. A typical transverse sonogram of the forearm in a young subject. The median nerve and the flexor muscles of the forearm are shown. Figure in the inset illustrates the position of forearm and location of the transducer. MN=Median nerve; FDS=Flexor digtorum superficialis; FDP=Flexor digitorum profundus and FPL= Flexor pollicis longus..... 111

Figure 7-2. A typical transverse sonogram of the forearm in (a) a young subject (a) and (b) an elderly subject. Note the polygonal region of interest (ROI) that has been placed around the outlines of the median nerve (MN) and the four ROI boxes with dimension 40X40 pixels that have been placed anterior, lateral, posterior and medial to the MN on the flexor muscles (FM) of the forearm. Inset showing the histogram of the echo intensity of the ROI over the MN..114

Figure 8-1. A typical transverse sonogram of the median nerve in the mid-forearm (a) in a young subject (male, 25 yrs old) (b) in an elderly subject (female, 85 yrs old). The region of interest (ROI) is placed around the outlines of the median nerve. Inset shows the normalized median nerve on the left, and the segmented median nerve magnified to 400% on the right in both images.....130

Figure 8-2. Correlation between the echo intensity (EI) and white area index (WI) of the median nerve in the 20 subjects studied..... 133

Figure 9-1. Position of the patient and the US transducer during an US-guided SNB at the subgluteal space. Also seen is an insulated nerve block needle being inserted in the long-axis (in-plane) of the US beam (reproduced with permission from (www.aic.cuhk.edu.hk/usgraweb).....144

Figure 9-2a. A typical transverse sonogram of the sciatic nerve is illustrated in the medial aspect of the subgluteal space before local anesthetic injection (reproduced with permission from www.aic.cuhk.edu.hk/usgraweb).....147

Figure 9-2b. A typical transverse sonogram of the sciatic nerve at the level of the greater trochanter and ischial tuberosity after 25 ml of local anesthetic injection. Note the distention of the subgluteal space and circumferential spread of local anesthetic around the sciatic nerve (reproduced with permission from www.aic.cuhk.edu.hk/usgraweb).....148

LIST OF TABLES

Table 2-1. The number of fascicles and the percentage of fascicular area in a nerve trunk of the brachial plexus. (Sunderland and Bradley, 1949)..... 22

Table 2-2. Heckmatt's Visual Scale..... 28

Table 4-1. Demographic data..... 62

Table 4-2. Intraobserver and interobserver reproducibility of the distance, CSA, EI, and WI measurements..... 63

Table 5-1. Baseline settings of the Customized "TEST" preset..... 69

Table 5-2.The ranges of system settings, for each parameter, that were studied..... 70

Table 6-1. Demographic data of the age-stratified groups..... 102

Table 6-2. Demographic data of the males and females subjects..... 103

Table 6-3. Correlation and comparison of "in-cart" and "off-cart" measurements.. 104

Table 6-4. Measured parameters at the left infraclavicular fossa in the male and female subjects..... 105

Table 6-5. Measured parameters at the left infraclavicular fossa in the age-stratified groups..... 106

Table 7-1. Echo-intensity of the median nerve (MN) and flexor muscles (FM) of the forearm, and the contrast between the nerve and muscle in the young and elderly subjects..... 122

Table 7-2. Echo-intensity of the flexor muscles of the forearm at the four region of interest (ROI) boxes around (anterior, lateral, posterior and medial) the median nerve..... 122

Table 8-1. Demographic data of the young and elderly subjects..... 139

Table 8-2. The cross sectional area, echo intensity, white area index and black area index of the MN in the young and the elderly..... 139

Table 9-1. Demographic data..... 154

Table 9-2. Echo Intensity and cross sectional area of the sciatic nerve during US guided SNB..... 155

LIST OF ABBREVIATIONS

2D	Two-dimension
AA	Area of axillary artery
AGC	Auto gain compensation
ANOVA	Analysis of variance
ASA	American Society of Anesthesiologists
AV	Area of axillary vein
AVI	Audio video interleave
AO	Acoustic output
BI	Black area index
BMI	Body mass index
CI	Confidence interval
cm	Centimeter
CSA	Cross sectional area
CT	Computerized tomography
CV	Coefficient of variance
DA	Diameter of axillary artery
dB	Decibel
DR	Dynamic range
DV	Diameter of axillary vein
EI	Echo intensity
F	Frequency
FDS	Flexor digtorum superficialis
FDP	FDP= Flexor digitorum profundus

FFM	Fat free mass
FPL	Flexor pollicis longus
FM	Flexor muscles
FR	Frame rate
GA	General anesthesia
GSM	Grey-scale median
HVS	Heckmatt's Visual Scale
Hz	Hertz
ICC	Intraclass correlation coefficient
IPP	Image-Pro Plus
LA	Local Anesthetic
Kg	Kilogram
LOR	Loss of resistance
MHz	Megahertz
MI	Mechanical index
mm	Millimeter
MN	Median nerve
MRI	Magnetic resonance imaging
MTH	Muscle thickness
NMD	Neuromuscular disease
P	Density
PM	Pectoral muscles
ROI	Region of interest
SA	Distance from the skin to the axillary artery
SD	Standard deviation

SM	Total skeletal muscle
SNB	Sciatic nerve blockade
SPSS	Statistical Package for the Social Sciences
SV	Distance from the skin to the axillary vein
TIFF	Tagged image file format
TGC	Time gain compensation
US	Ultrasound
v	Velocity
WI	White area index
yr	Year
Z	Acoustic impedance
α_R	Reflection coefficient
λ	Wavelength

Chapter1
Introduction

1.1 Introduction

Regional anesthetic procedures (peripheral and central neuraxial blocks) are frequently performed for anesthesia or analgesia during the perioperative period. Compared with systemic analgesia, regional anesthesia (RA) provided effective postoperative pain relief (Barron et al., 1999, Becchi et al., 2008, Hadzic et al., 2004, Hadzic et al., 2005b, Hadzic et al., 2005a, Karmakar et al., 2003) with reduced opioid requirements (Barron et al., 1999, Biboulet et al., 2004), which can decrease risk of nausea and vomiting (Hadzic et al., 2004, Hadzic et al., 2005b, Hadzic et al., 2005a), facilitate an earlier recovery of cognitive function in the elderly (Rasmussen et al., 2003, Sharrock et al., 2005) and a quicker discharge from hospital (Chan et al., 2001, Hadzic et al., 2004, Hadzic et al., 2005b, Hadzic et al., 2005a, Pavlin et al., 1998, Singelyn et al., 1998). However, compared with GA, which has close to near 100% success rate, RA has an inherent failure rate approximately 5-10% even in experienced hands (Nielsen and Steele, 2002). Success of any regional anesthetic technique depends on one's ability to accurately place the needle and, thereby, the local anesthetic drug can be injected as close as possible to the target nerve. Currently one has to rely on surface anatomical landmarks, fascial clicks, loss of resistance, eliciting paresthesia or nerve stimulation to position the block needle in the vicinity of the nerve (Broadbent et al., 2000, Choyce et al., 2001, Cousins et al., 2009, Franco et al., 2004, Hadzic, 2007, Neal, 2001, Perlas et al., 2006). Anatomical landmarks provide valuable clues to the position of the nerve but are surrogate markers, lack precision, can vary among patients (Broadbent et al., 2000, Orebaugh

and Williams, 2009, Royse et al., 2006, Wilson et al., 1998), and may be difficult to locate in obese patients (Nielsen et al., 2005). Even nerve stimulation, which has been recommended as the gold standard for nerve localization in regional anesthesia, may not always elicit a motor response (Assmann et al., 2007, Gurkan et al., 2008, Jan van et al., 2006, Plunkett et al., 2006, Sites et al., 2003, Urmey and Stanton, 2002). Moreover, one may not be able to predict the accuracy of needle placement prior to skin puncture with any of the above methods (Broadbent et al., 2000, Perlas et al., 2006). This often leads to multiple attempts at needle placement, pain and discomfort to the patient (Koscielniak-Nielsen et al., 2002, Koscielniak-Nielsen et al., 2004), an incomplete or failed block (Perlas et al., 2006), frustration for the anesthesiologist and possibly poor patient satisfaction (Fanelli et al., 1999, Koscielniak-Nielsen et al., 2002, Koscielniak-Nielsen et al., 2004). Furthermore, it also does not guarantee success and serious complications, such as systemic toxicity, intravascular injection, pneumothorax, and peripheral nerve injury (Crews et al., 2007, Gomez and Mendes, 2006, Long et al., 1989, Rosenblatt et al., 2006, Shah et al., 2005, Singelyn et al., 1998), although rare, still continue to occur. Various imaging modalities such as fluoroscopy (Nishiyama et al., 1999), computed tomography (CT) scan (Floch et al., 2003, McDonald and Spigos, 2000, Nishiyama et al., 1999), and magnetic resonance imaging (MRI) (Grau et al., 2002b, Klaastad et al., 1999, Klaastad et al., 2000, Marhofer et al., 2000, Wilson et al., 1998) have been used in an attempt to improve accuracy during block placement. However, this may involve transfer of the patient to the radiology suite, availability of a radiologist to interpret the image, exposure to radiation, and more importantly is not very practical in the operating room environment.

Recently there has been an increase in interest in the use of ultrasound (US) to guide peripheral and central neuraxial blocks in both adults and children (Gray, 2006, Marhofer et al., 2005). This has become possible due to improvements in US technology, better image processing capabilities of US system, and the availability of portable US devices that produce high resolution images comparable to the high-end cart based US systems. US guided regional anesthetic blocks have been shown to offer several advantages (Chan et al., 2003, Chan et al., 2007, Eichenberger et al., 2006, Kapral et al., 1994, Perlas et al., 2003, Perlas et al., 2006, Sandhu and Capan, 2002, Willschke et al., 2006, Yang et al., 1998). US imaging is non-invasive, simple to use and does not involve exposure to radiation. It allows the target peripheral nerve and the surrounding structures to be directly visualized during block placement, which is particularly advantageous in patients with difficult or variant anatomy, obesity or amputated limbs where evoked motor responses cannot be visualized (Assmann et al., 2007, Chan, 2003, Jan van et al., 2006, Orebaugh and Pennington, 2006, Orebaugh and Williams, 2009, Plunkett et al., 2006). It also helps to decide on the best possible site and maximum safe depth for needle insertion, allows real-time guidance of the needle and needle tip to the target site, avoid inadvertent vascular or pleural puncture and more importantly allows the operator to visualize the spread of the injected local anesthetic in real-time. This often results in reduced number of needle insertions during peripheral nerve (Casati et al., 2007b, Marhofer et al., 2004, Orebaugh et al., 2007, Sites et al., 2006) and central neuraxial blocks (Grau et al., 2002a, Grau et al., 2004). US guidance reduces the amount of local anesthetic required during the femoral nerve and brachial plexus block (Casati et al., 2007a, Marhofer et al., 1998, Sandhu et al., 2006). US also shortens the onset time of sensory block during brachial plexus (Chan et al., 2003, Marhofer et al.,

2004, Soeding et al., 2005, Williams et al., 2003) and sciatic nerve block (Domingo-Triado et al., 2007), and may also prolong the duration of the block in children (Marhofer et al., 2004, Oberndorfer et al., 2007). In addition, comparing with nerve stimulation US guidance reduces the accidental vascular puncture during stellate ganglion (Kapral et al., 1995) and axillary brachial plexus block (Liu et al., 2005). Also compared with landmarks-based methods US reduces the frequency of unintentional paraesthesia experienced by patients during the performance of interscalene and axillary blocks (Soeding et al., 2005) although complications can not be completely eliminated (Bigeleisen, 2006, Schafhalter-Zoppoth et al., 2004). Moreover, as the evidence is growing there are data which indicate that the use of US guidance may improve the quality of the block, and lead to higher success rates (Marhofer et al., 1998, Marhofer et al., 2004, Redborg et al., 2009, Schwemmer et al., 2006, Sites et al., 2006).

Currently majority of published data on US guided regional anesthesia have largely focused on the application and efficacy of US guidance for peripheral nerve blockade. The peripheral nerves are visualized using US, and qualitative sonographic characteristics of peripheral nerves are described in the literature (Demondion et al., 2003, Fornage, 1988, Sheppard et al., 1998, Silvestri et al., 1995, Yang et al., 1998). However, defining echogenicity by differentiating the gray-scale levels qualitatively is observer-dependent because the naked human eye is unable to distinguish all the 256 different gray-scale levels displayed in an US image (Russ, 2007a). The human eye is also extremely inaccurate at discerning differences in echogenicity when images have small or no difference in optical density (Smith-Levitin et al., 1997). Moreover, the naked human eye is not reliable in evaluating the brightness of an US image because of intra and inter-observer variability (Lamont et

al., 1990). In contrast, quantitative ultrasonographic methods have been used in radiology to evaluate the echogenicity and echotexture of musculoskeletal structures (Heckmatt and Dubowitz, 1987, Nielsen et al., 2000, Nielsen et al., 2006, Pillen et al., 2006b, Reimers et al., 1993b). Computer assisted image analysis is a sensitive, quantitative (Maurits et al., 2003, Nielsen et al., 2000), reproducible (Nielsen et al., 2000) and valid (Nielsen et al., 2000) method of analyzing and characterizing US images of skeletal muscles (Nielsen et al., 2000). It also achieves a higher interobserver agreement, than visual evaluation of skeletal muscle sonograms (Pillen et al., 2006b). However, to the best of our knowledge, there are no quantitative data on musculoskeletal structures during US guided regional anesthesia. Therefore, it seemed plausible to extend these methods to quantify US images during regional anesthesia.

1.2 Aims of the Project

The aims of this project were to:

1). Develop quantitative ultrasonographic methods to evaluate US images that were obtained during US guided regional anesthesia.

2). Test the reproducibility of the methods developed in above.

3). Investigate how US system settings affect the echo intensity of an US image.

4). Access the correlation between "off-cart" and "in-cart" measurements of distance and area made on US images.

5). Evaluate gender and age-related differences in the dimension of musculoskeletal structures at the infraclavicular fossa.

6). Study the echo intensity of the median nerve and the flexor muscles of the forearm using computer assisted gray scale analysis, and compare their differences in the young and the elderly.

7). Compare the cross sectional area of the median nerve and echotexture of the median nerve in the young and the elderly.

8). Quantify the changes in echo intensity of the sciatic nerve during US-guided sciatic nerve blockade.

1.3 Outline of the Thesis

This project used computer-assisted image analysis to quantitatively evaluate musculoskeletal images obtained during US-guided regional anesthesia.

Chapter 1 introduces the importance of US in current regional anesthesia practice and outlines the objectives of this project.

Chapter 2 outlines the history of medical US and its basic principles. Information on muscle and nerve measurements using US is also presented. Moreover, a detailed description of the anatomy, sonography of a normal peripheral nerve and its anatomic-echotexture correlation are discussed. Various quantitative methods that has been used to evaluate the echogenicity of an US image, particularly computer-assisted image analysis methods, are reviewed.

Chapter 3 describes in detail the methods and procedures that were used in the project. Detailed information is provided on the equipment and software, the process of image acquisition and transfer, the method of standardizing the US system, and how to normalize US images and measure echo intensity, and echotexture. The "off-cart" method used to measure dimensions is also described in detail.

Chapter 4 estimates the reproducibility of the quantitative ultrasonographic methods used in this project. US images of the infraclavicular fossa were obtained from volunteers and the following measurements were made: distance and cross-sectional area, echo intensity, and echotexture. The measurements were performed by two independent observers and they were also repeated on different days. The results show that the methods used are reproducible.

Chapter 5 establishes a relationship between echo intensity and the parameters of system settings which include frequency, gain, depth, dynamic range, and power output using a tissue-mimicking phantom. There is a positive linear correlation between the echo intensity and the amount of gain and power output used. Moreover, there is also a negative linear correlation between the echo intensity of the phantom and the frequency, dynamic ranges, and depth settings. These results show that it is essential to standardize the settings of an US system during quantitative ultrasonography.

Chapter 6 quantitatively describes the sonoanatomy of the left infraclavicular fossa of 98 patients (ASA I-III) using an "off-cart" measurement method. The US system settings were standardized and a high frequency (6-13MHz) linear-array transducer was used for the scan. A saggital scan of the musculoskeletal structure at the infraclavicular fossa was obtained. The distance from the skin to the axillary artery and vein, the diameter and cross-sectional area of the axillary artery and vein, and the width of the pectoral muscles were also measured. There was a good correlation between measurements made using the "in-cart" (electronic caliper) and the "off-cart" method that was developed for this study, indicating that "off-cart" measurements can substitute "in-cart" measurements for research purposes. Age and gender-related differences in the measurements of musculoskeletal structure at the infraclavicular fossa are also demonstrated.

Chapter 7 determines the echo intensity of the median nerve and flexor muscles of the forearm in the young and the elderly. The settings of the US system were standardized and a high frequency (6-13 MHz) linear-array transducer was used for the scan. Computer-assisted gray-scale analysis was performed on these normalized

images to determine the echo intensity of the median nerve and flexor muscles of the mid-forearm. The echo intensity of the median nerve and flexor muscles of the mid-forearm was significantly increased in the elderly. There was also a reduction in contrast between the median nerve and the adjoining flexor muscles in the elderly.

Chapter 8 compares the echotexture of the median nerve in the young and the elderly subjects. The median nerve at the mid-forearm was scanned using a standardized protocol. The cross-sectional area of the median nerve was measured using the "off-cart" method. US images were normalized. The echotexture of the median nerve image was determined using computer-assisted texture analysis, (i.e., gray-scale level and spatial distribution of pixels). Thereby, the cross sectional area, white area index, black area index, and echo intensity of the median nerve were obtained. There was an increase in the white area index and echo intensity, and a reduction in the black area index and cross sectional area of the median nerve in the elderly.

Chapter 9 reports the dynamic changes in the echo intensity of the sciatic nerve in 11 patients undergoing orthopaedic foot surgery under US-guided sciatic nerve blockade at the subgluteal space. A set of US images of the sciatic nerve were captured at three time points (before, during, and after local anesthetic injection). The echo intensity and cross sectional area of the sciatic nerve were measured. There was a significant reduction in the cross sectional area of sciatic nerve and an increase in echo intensity of the sciatic nerve after local anesthetic injection during the US-guided sciatic nerve blockade.

Chapter 10 summarizes the findings, discusses its clinical significance, and proposes future studies.

Chapter 2
Literature Review

2.1 History

Seeing is believing. In 1794, Lazzaro Spallanzani first demonstrated that blindfolded bats could navigate around obstacles in the dark but bumped against one another when their mouths were covered. He postulated that bats navigated using sound waves rather than light. In 1938, nearly 150 years after Spallanzani's demonstration, this scientific mystery, also called "Spallanzani Bat Problem" was solved by Griffin (Griffin, 1944) who recorded the sound emitted by bats using a Sonic Detector confirming that bats navigated using ultrasound (US) waves.

In 1880, French physicists Pierre and Jacques Curie discovered the piezoelectric properties of certain crystals (Newman and Rozycki, 1998), when they observed that an electric potential was generated when crystals were compressed. This was a major breakthrough in ultrasonic technology. The reverse effect was then demonstrated by the Curie brothers by showing that crystals could be made to deform when an electric field was applied to them. This was the backbone of the development of the US transducer. SONAR (Sound Navigation and Ranging), the use of sound to 'echo locate' underwater, played a vital role in World War I when it was used to detect submarines. After World War II, US equipment for medical imaging was developed. The use of US in medicine was initially confined to its use for therapy rather than diagnosis. In 1958, the first report on musculoskeletal ultrasonography was published by Dussik, et al., (Dussik et al., 1958) in their paper "Measurement of articular tissue with ultrasound" in the American Journal of Physical Medicine. In this work, Dussik et al. not only measured the speed and

attenuation coefficient of sound in bovine and human cartilage, but also described the ultrasonic artifact "acoustic fiber anisotropy" during the insonation of the US beam. In Glasgow, Donald et al. (Donald et al., 1958, Donald, 1962,Donald, 1963) carried out experiments with industrial ultrasonic metal flaw detectors on operated specimens of the uterus and ovary to differentiate between cysts, fibroids, and tumors. Using US, they diagnosed a woman, who at that time had been diagnosed with and was being treated for inoperable cancer of the stomach, as having a huge ovarian cyst instead. In 1958, they published a set of US images of abdominal mass in the Lancet (Donald et al., 1958). This was the beginning of medical diagnostic ultrasonography.

The use of US for regional anesthesia was reported more than 20 years later when in 1978 La Grange (la Grange et al., 1978) used a Doppler flow US detector to facilitate supraclavicular brachial plexus block in 61 patients by identifying the subclavian artery and vein before the block. However, La Grange was unable to visualize the brachial plexus nerves directly. A year later, Abramowitz (Abramowitz and Cohen, 1981) published a case report of a successful axillary brachial plexus block using the same method. In 1989, Ting and Sivagnanaratnam (Ting and Sivagnanaratnam, 1989) were the first to use US to facilitate the placement of a cannula into the axillary sheaths in 10 patients using a 3.5MHz US probe. The spread of local anesthetic solutions was also confirmed. The block was successfully performed on all cases without vascular punctures. Following this pioneering work, Kapral et al. (Kapral et al., 1994) performed real-time US-guided supraclavicular brachial plexus block on 40 patients in 1994. This was the first report to directly visualize a peripheral nerve using US in regional anesthesia. Kapral et al. visualized the brachial plexus using a 5 MHz probe and observed the spread of local anesthetic

in real time during the supraclavicular brachial plexus block. Lower limb nerve block under US guidance was reported by Marhofer et al. (Marhofer et al., 1997,Marhofer et al., 1998) in 1997 and 1998. The authors compared the onset time and quality of the block using US and peripheral nerve stimulation during a three-in-one nerve block. They demonstrated that US guidance significantly reduced the onset time and improved the quality of sensory blockade of the femoral nerve, the obturator nerve, and the lateral cutaneous femoral nerve and they were also able to avoid complications and demonstrated that US guided blocks required lesser dose of local anesthetic.

US imaging has also been used during central neuraxial blocks, either to preview the anatomy before needle puncture or to visualize the advancing needle in real time. In 1980, the first description of the neuroaxial structure, lumbar epidural space using US was presented by Cork et al. (Cork et al., 1980). In 1984 Currie (Currie, 1984) demonstrated a high degree of correlation between the US measured depth and the subsequent depth from the skin to the epidural space that was obtained after needle insertion. This finding was confirmed by Wallace and Currie (Wallace et al., 1992) in a study of 36 obese women using a 5 MHz transducer. This study showed that US allowed one to accurately determine the depth for needle insertion during central neuraxial blocks. Grau et al. (Grau et al., 2001b,Grau et al., 2001a,Grau et al., 2002a) have recently contributed significantly to this area of research. They showed that a preview scan prior to epidural puncture improved the success rate of epidural access on the first attempt, reduced the number of puncture attempts and the need to puncture multiple interspaces. Recently, the successful use of real-time US guidance in combination with loss-of-resistance (LOR) to saline for epidural access has been described by Karmakar et al. from the Department of Anesthesia and Intensive Care

of The Chinese University of Hong Kong (Karmakar et al., 2009). This technique which is performed by a single operator may extend the application of US to central neuraxial blocks.

2.2 Basis of Ultrasound

Sound is a form of mechanical energy that propagates through a medium as a wave of alternating pressure, causing local regions of compression and rarefaction. The number of cycles of oscillation per second made by a sound source and particles in the medium through which it moved is termed frequency (f), which is expressed in hertz (Hz, cycles/second). Sound waves propagate away from a source through a medium at a constant velocity (v), which is the speed of the sound waves in the medium. The wavelength (λ) of sound is the distance between wavefronts. The relationship between these variables is expressed as $v=\lambda \times f$. Frequency and wavelength are inversely related, such that as the frequency increases, the wavelength decreases. Amplitude refers to the strength of a sound wave and is expressed in dB. The velocity of sound in a medium depends on its acoustic impedance which is determined by the stiffness, elasticity, and density of that medium. It is also responsible for the varying velocity of sound transmission through different tissue in the human body. Average velocities of US of soft tissue, muscle, air, water and bone are 1,540, 1,580, 331, 1,498, and 3,360 m/sec, respectively (Hendee and Ritenour, 2002b). If the time taken by the US signal to return to the transducer is known, the distance (depth) from a transducer to a target can be calculated if the speed known. Human ear can detect sound between a frequency range of 20 and 20,000 Hz. US is sound with a frequency beyond 20,000 Hz. Medical US commonly uses a frequency range between 1 and 15 million Hz

(megahertz, MHz) (Hedrick et al., 2005,Pinkney, 1995b), and is produced by a piezoelectric crystal (element) in the transducer. A transducer acts both as a transmitter of the US beam and as a receiver of the echoes. The transducer element (crystals) can convert electrical to mechanical energy. Most ultrasonic transducers use artificial polycrystalline ferroelectric materials such as lead zirconate titanates (PZT), and the thickness of the elements determines the resonant frequency. When an electric field set up by a voltage is applied to a piezoelectric crystal, the crystal undergoes dimensional changes which cause it to vibrate and produce sound.

The emitted US signal while it travels through the tissue is reflected back when it encounters an interface. The major interaction of sound is reflection. The degree of the US reflected from an interface depends on the difference in acoustic impedance between two tissue interfaces (Merritt, 1998). Acoustic impedance (Z) is a ratio of acoustic pressure to acoustics volume flow, and Z is a measure of how US traverses that tissue and depends on density of the medium (ρ) and propagation velocity of US through the medium. The relationship between these variables is expressed as $Z=\rho \times v$. A large difference in acoustic impedance is referred to as acoustic impedance mismatch. The greater the acoustic mismatch the greater the amount of US reflected and less transmitted (Hedrick et al., 2005). The acoustic impedance of water, fat, muscle and soft tissue in human is approximately 1.50, 1.38, 1.70 and 1.63 MRayl (Hendee and Ritenour, 2002b). Specular reflection occurs at flat, smooth interfaces where the transmitted wave is reflected in a single direction depending on the angle of incidence, and when the US wavelength is smaller than the reflective structure. Scattering occurs if the US pulse encounters reflectors whose dimensions are smaller than its wavelength, and it also occurs when the incident wave encounters a nonspecular interface, i.e. red blood cell. After reflection and scattering,

when the speeds of US are different on each side of the tissue interface, the remainder of the incident beam is refracted with a change in the direction of the transmitted beam. The reflection, refraction, absorption and scattering of US cause attenuation of the US beam energy. Attenuation is measured in decibels per centimeter of tissue and is described by the attenuation coefficient. Attenuation varies between tissues and the attenuation coefficient for muscle, water and fat are 3.3, 0.0022, and 0.6dB/cm at 1MHz, respectively (Hendee and Ritenour, 2002b). The attenuation coefficient for fresh human peripheral nerve is 3.0dB/cm at 3.4 MHz (Goss et al., 1978b).

The main components of the imaging system include transducers, the US unit, the control panel, a monitor and a data storage device. The transducer acts both as a transmitter of the US beam and as a receiver of the echoes. The transducer emits pulse of high frequency US which travels through the tissue. Once it encounters an interface the US waves are reflected back towards the transducer. These reflected echoes are detected by the transducer and converted into electrical signals (piezoelectric effect). Theses signals are sent from the transducer to the US unit (receiver/processor) for processing. Since the US signal undergoes attenuation as it travels through tissue. The returning signals are of varying amplitude. The time gain compensation (TGC) compensates for the attenuation by amplifying the returning signals. Thereby, equally reflective structures from unequal depths are displayed as structure of equal brightness on the US monitor (Hendee and Ritenour, 2002a, Pinkney, 1995a,Pinkney, 1995b). After amplification, these signals are digitized from analog to digital format and sent to the signal processor. "Noise" in the electronics is reduced by filtering, and the compression process is performed to decrease the difference between the smallest and largest amplitudes of signals.

Hence, the amplitude of these signals can be limited to a narrow range for human senses (Kremkau, 2002). The ratio of the largest and smallest amplitude that can be handled by the US system is called "dynamic range". The signals are converted into an image by the image process. When this process is accomplished, the signals are displayed on the monitor as "dots" based on the strength of the signals. A strong signal is shown a brighter dot and weak signal as a dark dot. A combination of all these signals produces the final gray-scale image. The entire process is repeated very rapidly and thereby a real-time image is displayed. Real-time US images are displayed on a monitor and can be recorded on video tape, or saved on the hard disk of the US system (Merritt, 1998).

There are two basic modes for displaying the returning echo: A-mode and B-mode. A-mode (Amplitude) US provides an amplitude-modulated display. The echoes from the various depths are shown as vertical spikes on a horizontal line. The strength of the echo determines the amplitude of each spike. A-mode US image is seldom used today. B-mode (Brightness) US is more commonly used and provides a brightness-modulated display. The echoes from the various depths are shown as dots on the US monitor, which are discrete brightness levels. The brightness level is determined by the strength of returning echo. M-mode (Motion) US is a graphic B mode displayed against a single-dimension time axis. It is produced from US along a single scan-line and is commonly applied in echocardiography.

Three types of US transducer are commonly used and named according to the geometric arrangement of the piezoelectric elements in them. In a linear-array transducer the piezoelectric elements are arranged in parallel and a rectangular image is produced, which is as wide as the footprint of the transducer. A linear-array

transducer is commonly used to scan small part, muscle, peripheral nerves and superficial blood vessels. A curve linear-array transducer has a curved surface. A larger and deeper field of view is produced but lateral resolution is reduced compared with linear-array transducer. In a phased-array transducer US beams are emitted from a single point which diverges in a fan like manner. Thereby, although the transducer has a small footprint it can produce a sufficiently wide far filed of view. It is usually used for transthoracic echocardiography when the transducer is placed in the narrow space between the ribs.

The degree of image clarity is determined by spatial resolution. Resolution is the minimum reflector separation required to produce separate reflection in a pulse-echo system (Pinkney, 1995a,Pinkney, 1995b). Axial resolution is the ability to resolve objects that lie one above the other, and is determined by the pulse length of the US wave. A high frequency wave with a short pulse length produces better axial resolution than a low frequency wave. Lateral resolution is the ability to resolve objects that lie side by side, and is directly related to the transducers beam width. The lateral resolution can change with depth and can also improve when a higher-frequency transducer is used.

The brightness level of a structure in a US image is determined by the amplitude of the reflected echoes displayed. Strong reflections produce bright a dot (hyperechoic), whereas weak reflections produce gray a dot (hypoechoic). If no echo is received from structure it appears as a dark dot (anechoic). Moreover, when the US beam strikes a very strongly reflective interface, all the US beam is reflected back to the transducer producing a shadow beyond the structure. This is also referred to as posterior acoustic shadowing. Conversely, if the US beam passes through an object

which reflects little US, then deeper structures encounter a higher intensity of US which results in a greater reflection from the deeper tissues. This is referred to as posterior acoustic enhancement (Hendee and Ritenour, 2002a, Lin et al., 2002). When the angle of the insonation of an incident US beam is changed, the amplitude of reflected echo also changes which leads to a change in echogenicity of a structure. This is called "anisotropy" (angular dependence). A structure best visualized when the incident US beam is at right angles to the structure imaged. Therefore, small changes in the angle of incidence away from perpendicular can significantly affect their echogenicity of a structure.

2.3 Muscle and Nerve Dimension Measurements

US is frequently used to image musculoskeletal structures and high resolution US offers several advantages when used for this purpose. Compared with CT or MRI, US scanning is cheap, portable, can be quickly performed, and involves no radiation. In addition, an US examination can be performed at the bedside, in an operating room or in the intensive care unit. Ultrasonography has been used to measure the thickness and cross sectional area (CSA) of skeletal muscles and peripheral nerves in vivo (Abe et al., 1998, Cartwright et al., 2009,Sanada et al., 2006,Young et al., 1984,Young et al., 1985). This is commonly performed using an electronic caliper that is built into the US system, a method that is referred to as "in-cart" measurement.

2.3.1 Muscle Dimension Measurements

US is a reliable (Reeves et al., 2004) and valid (Sanada et al., 2006) method for measuring the thickness and CSA of human muscles. Reeves et al. (Reeves et al.,

2004) tested the reproducibility and validity of measuring the CSA of muscles using US against measurements made using MRI. They found that intraclass correlation coefficients (ICC) of the US and MRI measurements of the CSA measurement were 0.998 for reliability, and 0.999 for the validity. In addition, the coefficient of variance (CV) for the CSA measurement was 2.1% for images obtained using US. This showed that US was a valid and reliable tool for assessing the CSA of human muscles. Sanada et al. (Sanada et al., 2006) developed regression-based prediction equations for skeletal muscle mass using US. They measured the thickness of a muscle using US with a 5 MHz transducer. A strong correlation was found between the MRI and US measurements, this indicates that US-derived prediction equations were a valid method to predict skeletal muscle mass, and US was a simple alternative to MRI measurements. Young et al. (Young et al., 1984,Young et al., 1985) compared the CSA of the quadriceps muscle measured at the mid-thigh using US in the healthy young and the elderly subjects. They found that the CSA of the quadriceps in the elderly men was 25% smaller than that in the young men. Moreover, they also showed that the CSA of the quadriceps muscle was 33% less in the elderly women than that in the young women. These findings indicate that the thickness of muscle in the elderly is smaller than that in the young. Abe et al. (Abe et al., 1998) used US to compare the gender differences in muscle architectural structure and fat free mass between the young male and female athletes using a 5 MHz transducer. They found that the thickness of muscles in the male was markly larger than that in the female. Arts et al. (Arts et al., 2007) also measured thickness of the biceps muscle and the quadriceps muscle muscles in 194 subjects (0 to 90 yrs) using US. The authors demonstrated a good correlation between the thickness of the

muscles and age. Based on the data discussed one can conclude that US is a reliable method for measuring the thickness and CSA of skeletal muscles.

2.3.2 Nerve Dimension Measurements

US is also an accurate (Kamolz et al., 2001) and reproducible (Cartwright et al., 2009, Nakamichi and Tachibana, 2000,Tagliafico et al., 2008) method of measuring dimensions of a peripheral nerve. Kamolz et al. (Kamolz et al., 2001) evaluated the validation of measuring the diameter and CSA of the median nerve using US compared to measurements made directly from sectional wrists of unfixed human cadavers. They found that the two measurements of diameter and CSA were comparable. There was also correlation and the Pearson correlation coefficient for diameter measurement was 0.84, and for CSA measurement was 0.91. Cartwright et al. (Cartwright et al., 2009) assessed reproducibility of measuring the CSA of the median nerve using US. They found good correlation (ICC 0.70-0.98) of the CSA measurements of the median nerve between four different observers, and these CSA measurements were also comparable. Tagliafico et al. (Tagliafico et al., 2008) also demonstrated a good reproducibility by testing interobserver agreement (kappa coefficient=0.91) in the CSA measurements of the median and ulnar nerve. Nakamichi and Tachibana (Nakamichi and Tachibana, 2000) tested the reproducibility of the CSA measurement of the median nerve using US. They found that the coefficient of variation of the diameter (4.8%) and CSA (4.9%) of the median nerve in the amputated upper limb that obtained on different days were comparable. Based on these findings one can conclude that US is a reliable method for measuring dimension of peripheral nerves.

2.4 Anatomy of a Peripheral Nerve

A peripheral nerve consists of several fascicles that are bound together loosely by a connective tissue framework (Asbury, 1982). The endoneurium, perineurium and epineurium make up the connective tissue of a peripheral nerve. The fascicles are enclosed in a connective tissue sheath known as the epineurium. Each fascicle is in turn covered by a sheath of connective tissue (perineurium). The individual nerve fibers within the fascicle are enclosed by a sheath of connective tissue, known as endoneurium (Sunderland, 1965, Sunderland and Bradley, 1949, Sunderland and Bradley, 1952).

The neural fascicles varies at different levels along the same peripheral nerve (Bonnel, 1984,Moayeri et al., 2008,Sunderland and Bradley, 1949). The following investigations confirm the above. Sunderland and Bradley examined the number of fascicles and the percentage fascicular area of the entire nerve trunk in the brachial plexus nerve (**Table.1-1**) that were obtained from 20 fixed histological specimens from human cadaver (Sunderland and Bradley, 1949). They found that the number of fascicles was different at different locations in the brachial plexus. The number of fascicles tended to increase from a proximal location to distal location in the brachial plexus, but the percentage fascicular area of the nerve trunk tended to decrease. Similar results have been reported in the sciatic nerve (Sunderland and Bradley, 1949). Based on 100 brachial plexus nerve dissections in 50 adult cadavers, Bonnel observed an increase in the number of the fascicles and a decrease in diameter of the fascicles in the brachial plexus from a proximal part to distal location (Bonnel, 1984). Recently, Moayeri et al. compared the ratio of the CSA of the fascicles to the connective tissue at interscalene (45%), supraclavicular (48%), infraclavicular (34%)

and subcoracoid region (34%) in 3 cadavers. They found that the ratio of the CSA of the fascicles to connective tissue decreased significantly ($p<0.001$). The fascicular redistribution, dispersal, and intermingling of different branch fiber systems as they are traced along the nerve may explain this variations in the amount of the fascicles in a nerve.

Table 2-1. The number of fascicles and the percentage of fascicular area in a nerve trunk of the brachial plexus. (Sunderland and Bradley, 1949)

	Axilla (n/%)	Epicondyle (n/%)	Wrist (n/%)
Median Nerve	25 / 48%	50 / 40%	75 / 42%
Ulnar Nerve	7 / 48%	8 / 52%	17 / 40%
Radio Nerve	40 / 33%		29 / 39%

Data are presented as number/percentage. n= number of fascicles; %= percentage of fascicular area.

The amount of the connective tissue also varies in different locations along the course of a peripheral nerve (Bonnel, 1984, Moayeri et al., 2008, Sunderland, 1945). Based on the 100 dissections of the brachial plexus in embalmed adult cadavers, Bonnel (Bonnel, 1984) showed that in the trunks of the brachial plexus the percentage of connective tissue was 53 to 58%, and this increased to 78 % in the radial nerve, 73% in the median nerve, and 86% in the ulnar nerve, at the level of the divisions of the brachial plexus. Moayeri and colleagues (Moayeri et al., 2008) confirmed these findings from cadavers using cryomicrotomy high-resolution photography. They compared the amount of nonneural tissue (stroma and connective tissue) in the interscalene (201.5 mm^2), supraclavicular (222.7 mm^2), infraclavicular

(689.6 mm^2) and subcoracoid (706.3 mm^2) region of the brachial plexus, and found that the connective tissue increased along the course of the nerve ($P<0.02$). Sunderland also reported an increase in the amount of the connective tissue in sciatic nerve of cadavers from a proximal to distal location (Sunderland, 1945).

The peripheral nerve structures also change with advancing age (Jacobs and Love, 1985, Sladjana et al., 2008, Thierry Maisonobe, 1997, Tohgi et al., 1977). Tohgi et al. performed a histological study to quantify the changes that occur with aging in the peripheral nerve (Tohgi et al., 1977). The samples of nerves were obtained from 79 necropsies of acute death without any accompanying peripheral nerve diseases (age ranging from 1 week to 88 years). They found that there was a marked reduction in the number, diameter, and average density of the nerve fibers with age (Tohgi et al., 1977), particularly after the sixth decade (Jacobs and Love, 1985). The average density of the large myelinated fibers was greatest at the third decade, and thereafter decreased with age. The average density of large myelinated fibers at the nine decade was 54% of that at the third decade. Moreover, Tohgi et al. also showed that the average density of the small myelinated fiber also continued to decrease gradually with age, and the density of the small myelinated fiber at the eight decade was 74% of that at the second decade (Tohgi et al., 1977).

Furthermore, with advancing age, there also is an increase in connective tissue elements within a peripheral nerve (Cottrell, 1940, Sladjana et al., 2008). Cottrell (Cottrell, 1940) studied 30 cadavers (age ranging from 3 years to 81 years) and qualitatively evaluated the histological changes in the median, sciatic, femoral and the common peroneal nerves. Cottrell found that with age, particularly after the sixth decade, there is an increase in the connective tissue elements, a reduction of the

patency of the blood vessels and destruction of the nerve fibers. Recently, Slajana et al. (Sladjana et al., 2008) examined histological specimens of the sciatic nerve from 17 fixed human cadavers (age ranging from 8 years to 93 years) under light microscopy (**Fig.2-1**), and found that the number of fascicles in the young cadavers (age< 30 years) was greater than that in eight elderly cadavers (age> 60 years). In addition, Slajana et al. were able to demonstrate a negative correlation between age and the myelinated nerve fibers area (r^2=-1.25), and a positive correlation between age and the area of the connective tissue (r^2=1.25) in the sciatic nerve (Sladjana et al., 2008).

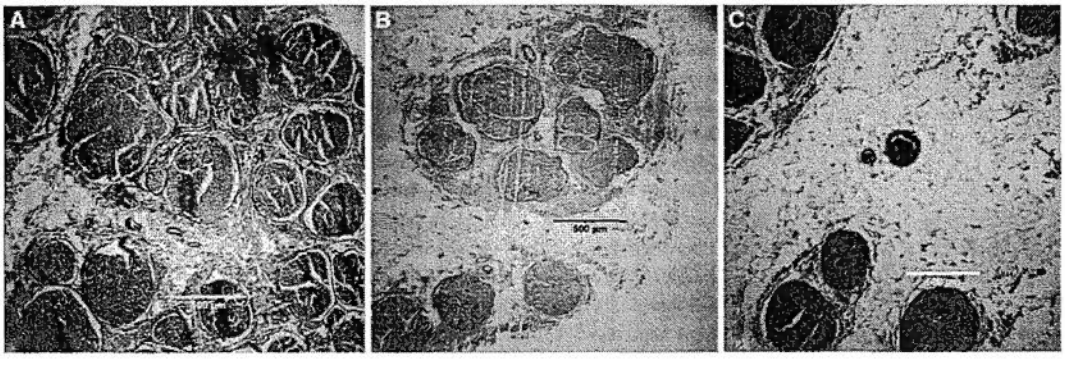

Figure 2-1. Illustrates the changes in the epineurial connective tissue of the sciatic nerve with age. (A) sciatic nerve of an 8-year-old child; (B) sciatic nerve of a 70-year-old-individual with increased adipose tissue; (C) sciatic nerve of a 93-year-old individual with predominant fatty tissue in the epineurium. (Reproduced from Sladjana et al, 2008)

2.5 Sonoanatomy of a Normal Peripheral Nerve

Sample et al. (Sample et al., 1978) were the first to delineate a minor 5mm neurovascular structure within the tracheoesophageal groove using US. Solbiati et al. (Solbiati et al., 1985) later demonstrated that the hypoechoic structure was a the recurrent laryngeal nerve. Thereafter, with the introduction of high-resolution

sonography, identifying peripheral nerves became a reality. Fornage (Fornage, 1988) imaged peripheral nerves in cadavers and healthy subjects using a high-resolution US and a 5-7.5 MHz linear-array transducer. He examined the median nerve (carpal tunnel and the forearm), the ulnar nerve (forearm and at the elbow), the sciatic nerve (thigh) and the popliteal nerve (fibular neck). He found that normal peripheral nerve was seen as echogenic tubular structures with parallel internal linear echoes on longitudinal scans. In a transverse scan those internal punctate echoes were in the oval, round echogenic sections. These findings have also been confirmed by other investigations (Graif et al., 1991,Martinoli et al., 1999,Peer et al., 2002,Peer, 2008,Silvestri et al., 1995,Stuart et al., 2004,Yang et al., 1998).

Nerves appear in different shapes, such as oval, round, triangular, lip shaped or even flat, and the shape of a nerve can change along the course of a nerve (Chan et al., 2003, Gruber et al., 2003, Karmakar et al., 2007, Karmakar et al., 2008, Retzl et al., 2001, Yang et al., 1998). When examined in the transverse axis using a high frequency US (13-15MHz), a nerve shows multiple round hyperechoic area in a homogenous hyperechoeic background (Martinoli et al., 1999, Silvestri et al., 1995). On longitudinal scan, the appearance of a nerve has been likened to a "tram track", that is, parallel hyperechoic lines are seen against a background of echo-poor space (Loewy, 2002).

2.6 Correlation between Anatomy and Qualitative Echotexture of a Peripheral Nerve

When a peripheral nerve is scanned in the transverse axis using a high-resolution US system, the hypoechoeic areas in a nerve correspond to the neuronal fascicles and

the hyperechoeic background corresponds to the connective tissue layer that binds the neuronal fascicles together (Silvestri et al., 1995).

Silvestri (Silvestri et al., 1995) and Martinoli (Martinoli et al., 1999) examined the correlation between the sonographic appearance and histology of a peripheral nerve in-vitro and in-vivo. Silvestri et al.(Silvestri et al., 1995) have also demonstrated that the number of fascicles in a peripheral nerve is underestimated on a sonogram, which may be due to anisotropy and lateral resolution. Thereafter, the anatomic-sonographic correlation has also been demonstrated in lower extremity nerves (Gruber et al., 2003,Peer et al., 2002) confirmed the findings of Silvestri et al.

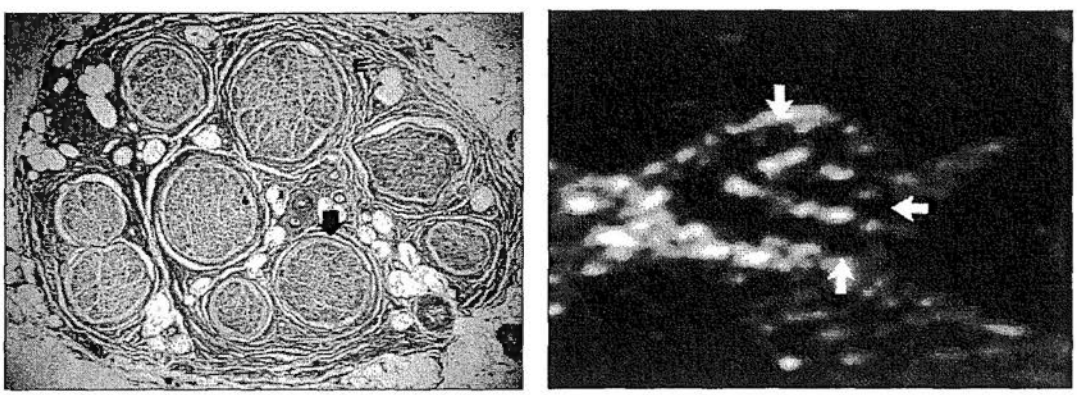

(a) (b)

Figure 2-2. Illustrates the correlation between the histological structure and the sonogram of a median nerve. (a) shows the photomicrograph of the histological specimen of a normal median nerve. The black arrow indicates a single fascicle ensheathed by a dense connective tissue layer, the perineurium. (b) shows a transverse sonogram of a normal median nerve with discrete hypoechoic fascicles (arrows). (Reproduced from Sturat. et al. 2003)

2.7 Limitations of Qualitative Ultrasonography in Assessing the Echotexture of a Peripheral Nerve

Qualitative ultrasonography of a peripheral nerve is based on the visibility of the naked human eyes, and terms such as isoechoic, anechoic, hypoechoic and hyperechoic are frequently used to describe the echogenicity (sonographic appearance) of a musculoskeletal structure (Karmakar and Kwok, 2009) in a sonogram.

However, defining echogenicity by differentiating the gray-scale levels qualitatively is observer-dependent particularly when the gray-scale levels between images are often very similar. The ranges of gray-scale levels in an US image (8 bit) are from 0 to 255 in most commercially available US systems, but the naked human eyes is unable to distinguish all the 256 different gray-scale levels that are displayed in an US image (Russ, 2007a). Levitin et al. (Smith-Levitin et al., 1997) have demonstrated that qualitative evaluation with human eyes is extremely inaccurate at discerning differences in echogenicity when images have small or no difference in optical density. Moreover, Lamont et al. (Lamont et al., 1990) have also shown that the naked eye is not reliable in evaluating the brightness of an US image because of intra and inter-observer variability. Therefore, it would be desirable to have a quantitative method to evaluate the echogenicity or echotexture of a peripheral nerve.

2.8 Quantitative Ultrasonographic Methods of Assessing the Echogenicity of Musculoskeletal Structures

2.8.1 Heckmatt's Visual Scale

Heckmatt's Visual Scale (HVS) as the name implies is a visual method of evaluating the echogenicity of a musculoskeletal structure according to a four-point grading scale. (Heckmatt et al., 1982) (**Table 2-2** and **Fig. 2-3.**)

Table 2-2. Heckmatt's Visual Scale

Grade	Ultrasound Appearance
Grade I	Normal muscle
Grade II	Increase in muscle echo while bone echo still distinct
Grade III	Marked increase in muscle echo and a reduced bone echo
Grade IV	Very strong muscle echo and a complete loss of bone echo

Heckmatt et al. (Heckmatt et al., 1982) compared 60 patients with neuromuscular diseases and 60 control children using HVS and diagnostic muscle biopsy. A good relationship was seen between the severity of pathological change in the muscle and HVS score. Children with normal muscle architecture had a normal HVS score, whereas children with markedly abnormal muscle architecture had a significant increase in the HVS score. This indicated that a high HVS score was associated with abnormal muscle architecture (Heckmatt et al., 1982). HVS has was a sensitivity of

67% to 78% and a specificity of 84% to 92% to detect neuromuscular disorders (NMDs) in children (Heckmatt et al., 1988,Zuberi et al., 1999). Recently, Brockmann et al. (Brockmann et al., 2007) has demonstrated an accuracy of 81%, sensitivity of 71%, and specificity of 92% for the HVS to identify alterations in the normal and abnormal muscle. These results suggest the HVS is a fairly reliable method of evaluating echogenicity of skeletal muscles in children.

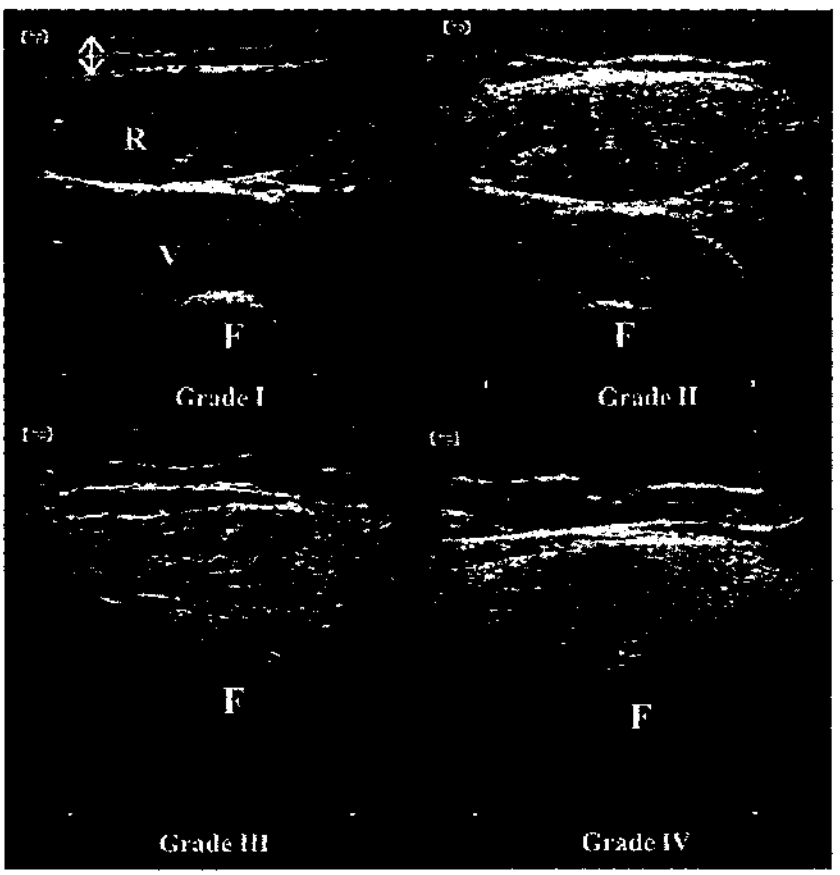

Figure 2-3. Illustration of the Heckmatt's Visual Scale. The Arrow indicates subcutaneous tissue; R=rectus femoris; V=vastus intermedius; F= femur. (Reproduced from Pillen 2006)

2.8.2 Computer Assisted Grey-Scale Analysis

Computer assisted gray-scale analysis is an objective method of gray-scale analysis that produce quantitative data, and is therefore suitable for statistical analysis and

research. Quantification of echo intensity has been used as a diagnostic tool in several clinical studies (Chikui et al., 2004, Lal et al., 2002, Mazziotti et al., 2003). This method has been used to differentiate symptomatic and asymptomatic plaques (Mazziotti et al., 2003), changes in the cancer tissue after radiotherapy and the thyroid gland of Hashimoto's throiditis (Mazziotti et al., 2003).

However, there are no published data evaluating the echo intensity (EI) of a peripheral nerve using computer assisted gray-scale analysis, and for musculoskeletal ultrasonography that are only data evaluating EI of skeletal muscles. Computer assisted grey-scale analysis is a sensitive (Maurits et al., 2004, Reimers et al., 1993a), reproducible (Nielsen et al., 2000, Pillen et al., 2006b) and validated method (Nielsen et al., 2000, Reimers et al., 1993b) for analyzing and characterizing the EI of skeletal muscles. This method has been used to differentiate normal from pathological muscles. Reimers et al. (Reimers et al., 1993a) have reported that the sensitivity of detecting neuromuscular disorder disease using computer assisted grey-scale analysis is 82.9% and the accuracy is 91.3%. Reimers et al. have also demonstrated a close correlation between the EI of a muscle and histological changes in the muscle (Reimers et al., 1993b), which was confirmed by Eisele et al. (Eisele et al., 1998). Maurits et al. (Maurits et al., 2004) have reported that EI measurement has a diagnosis sensitivity of 90% and a specificity of 91% in children with neuromuscular disease. Pillen et al. (Pillen et al., 2006b) have demonstrated that EI measurement also has a high interobserver agreement. They reported a kappa value 0.86 when computer assisted gray-scale analysis was used to evaluate the EI of the skeletal muscles, which was superior to the visual evaluation (kappa value 0.86 vs. 0.53; $p<0.001$) (Pillen et al., 2006b). Nielsen et al. (Nielsen et al., 2000) have also shown a good reproducibility of this method. They performed EI

measurements on the sonograms of the supraspinatus muscle of healthy subjects, and showed that coefficient of variation of the mean gray-scale value of 30 repeated EI measurements was 5-7%, and there were no significant differences in the EI measurements that were performed on the different days. These findings confirm that computer assisted gray-scale analysis is a reproducible of EI measurement. Other investigations using this method have also been reported (Maurits et al., 2003,Maurits et al., 2004,Scholten et al., 2003,Sipila and Suominen, 1991,Sipila and Suominen, 1996).

2.8.3 Computer Assisted Texture Analysis

Computer assisted texture analysis is a method of texture analysis used to evaluate the intensity, position and distribution of pixels in a digital image (Castellano et al., 2004, Lal et al., 2002, Nielsen et al., 2006). In contrast, the EI measurement is only a global measure of total brightness in an US image, and does not take into account the spatial arrangement of pixels in the US image.

There are no published data describing computer assisted texture analysis for evaluating the texture of a peripheral nerve, and very limited data on the texture of skeletal muscles. Nielsen et al. (Nielsen et al., 2006) used computer assisted texture analysis to compare the differences in the EI and texture measurements made on sonogram from the supraspinatus and vastus lateralis muscle in volunteers. They demonstrated significant differences in the EI and echotexture measurements between the two muscles, and suggested that combining gray-scale and texture analyses method may provide a more complete description of the tissue composition in the muscles than using the mean grey-scale value alone. Computer assisted texture analysis can also be used to detect alterations in skeletal muscle morphology.

Maurits, et al. compared US parameters (i.e., EI and white area index) in the muscles between volunteer and patients with neuromuscular disorders in the adults and children (Maurits et al., 2003, Maurits et al., 2004). They reported the computer assisted texture analysis has a diagnosis sensitivity of 92-100% and a specificity of 92-93% in adults with neuromuscular diseases, and can help in differentiating myopathy and neuropathy (Maurits et al., 2003). Similar findings were also found in children with neuromuscular diseases (Maurits et al., 2004).

However, there are no data evaluating the reproducibility or validity of computer assisted texture analysis for musculoskeletal sonography. Lal et al. demonstrated that there is a good correlation between the measurements of tissue components predicted with computer assisted texture analysis and the histologic measurements made on explanted carotid plaques (Lal et al., 2002). Therefore, future research should evaluate the reproducibility and validation of this method in musculoskeletal sonography.

2.9 Limitations of the Quantitative Ultrasonography Assessing the Echogenicity of Musculoskeletal Structures

The HVS is a relatively simple method of assessing the echogenicity of a musculoskeletal structure. However, since it is a visual scale it is highly dependent on the experience and judgment of its observer. Pillen et al. (Pillen et al., 2006b) have demonstrated that the HVS has a low interobserver (kappa value 0.53) and intraobserver agreement (kappa value 0.74) when used to evaluate the EI of a skeletal muscle. The EI of a skeletal muscle is affected by age, gender, weight, BMI (Maurits et al., 2003), whether the muscles are trained or not (Sipila and Suominen, 1993), difference muscles in the upper and lower limbs (Heckmatt et al., 1982,

Pillen et al., 2006b, Pohle et al., 1997, Zaidman et al., 2008), and the system settings of an US machine (Heckmatt and Dubowitz, 1985, Zaidman et al., 2008). These factors may explain why there are limitations using the HVS to analyze echogenicity in the US images.

In contrast, computer assisted image analysis, although more expensive and time-consuming, is a quantitative method with a good interobserver agreement, and it is also suitable for research. The system setting of an US machine can directly affect the quantitative measurements.

2.10 Summary

In conclusion, computer assisted image analysis is a sensitive, reproducible and validated method of analyzing and characterizing US images. Currently, there are no data on the EI or echotexture of a peripheral nerve in the literature, and evaluating them was the main objectives of this project.

Chapter 3
Methods Used for Quantitative Ultrasonography

3.1 Introduction and Objective

Quantitative Ultrasonography is an objective method using a computer assisted image analysis techniques for measuring the dimension, gray-scale level and texture of a region of interest (ROI) in an US image. All methods described in this chapter were used to quantitatively examine musculoskeletal sonograms in this project. The studies were approved by Joint The Chinese University of Hong Kong-New Territories East Cluster Clinical Research Ethics Committee 2007 (CREC Reference No.: **CRE-2007.213**), 2008 (CREC Reference No.: **CRE-2008.591**) and 2009 (CREC Reference No.: **CRE-2009.096**) (see Appendix).

3.2 Equipment and Software Used

3.2.1 Ultrasound Equipment

Two US systems with an appropriate transducer were used for the scan during this project (**Fig. 3-1 a**) including the MicroMaxx (Sonosite™ Inc., Bothell, USA) and LOGIQ e (GE Medical System, Milwaukee, Wisconsin USA).

The choice of a high or low frequency transducer for the US scan was dependant on the study protocol. The high frequency linear array transducers were the HFL38 (13-6 MHz, 38 mm footprint, Sonosite™ Inc., Bothell, USA) and 12L-RS (13-5 MHz, 42 mm footprint, LOGIQ e, GE Medical System, Milwaukee, Wisconsin USA). The low frequency transducer used was the C60e (5-2 MHz, 60 mm footprint, Sonosite™ Inc., Bothell, USA).

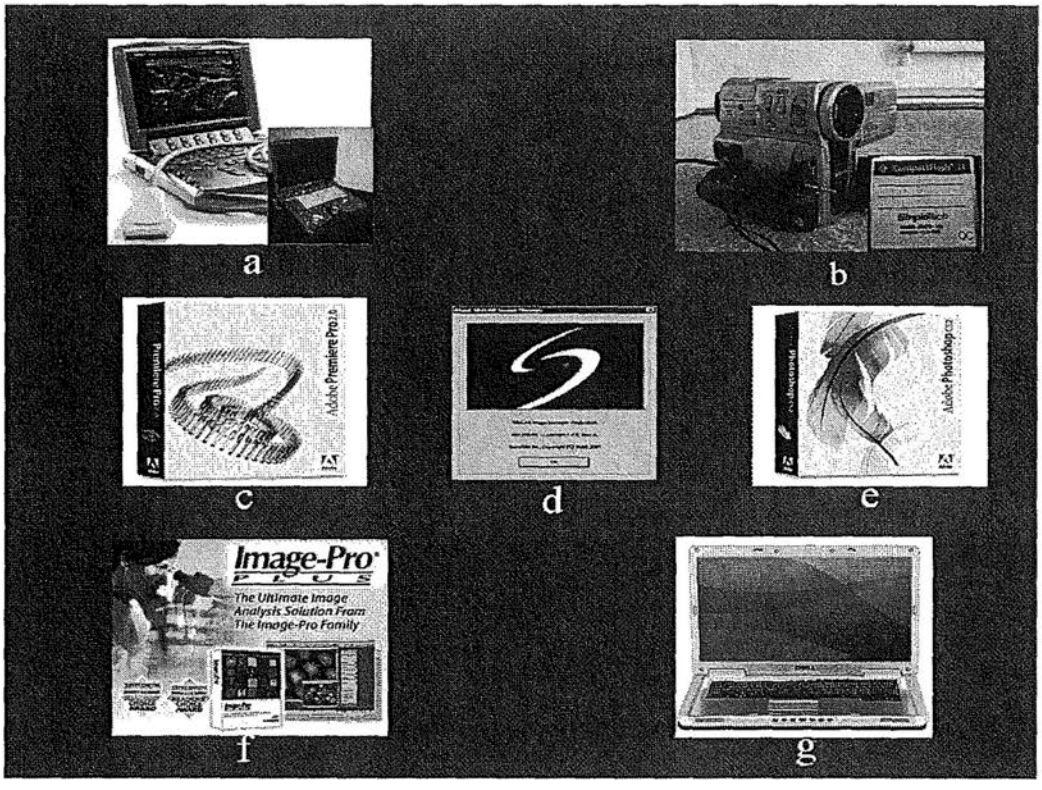

Figure 3-1. Equipment and software used during this project are shown. (a) MicroMaxx US system with a high frequency transducer and LOGIQ e US system; (b) Commercial video recorder and SD card; (c) Adobe Premier Pro 2.0 software; (d) Site-Link Manager 3.4.1 software; (e) Adobe Photoshop CS2 software; (f) Image-Pro Plus 6.0 software; and (g) Laptop computer.

3.2.2 Data Storage Device

The data from the US system was recorded on a tape (Sony Corporation, Ltd., Minato-ku, Tokyo, Japan) using a Sony video camera (Sony Corporation, Ltd., Minato-ku, Tokyo, Japan) via the video output terminal of the US system, or on to the Compact Flash SD card in the US system. (**Fig. 3-1 b**)

3.2.3 Image Process Software

Adobe® Premier Pro 2.0 (Adobe Systems Inc, San Jose, CA, USA) **(Fig. 3-1 c)** was used to capture a video loop from the tape. A still image in tagged image file format

(TIFF) was then captured for data analysis. For US image data that were saved on the Compact Flash SD card in the US machine, Site-Link Manager 3.4.1(Sonosite™ Inc., Bothell, USA) was used to transfer the data to a personal computer.**(Fig.3-1 d)**

Adobe® Photoshop CS2 (Adobe Systems Inc, San Jose, CA, USA) was used to normalize the captured still images and measure the Echo intensity (EI) of a region of interest (ROI) in the US image using the standard histogram function. **(Fig. 3-1 e)**

Image-Pro® Plus 6.2 (IPP, Media Cybernetics, Silver Spring, Maryland, USA) was used to perform "off-cart" measurements of distance (i.e., width, diameter), area (i.e. CSA), and determine the texture of a ROI in the US image. **(Fig. 3-1 f)**

All data download for processing or analysis were stored on a personal laptop computer (Dell Inspiron 6400, Dell Computer Corporation, Inc. USA). The same computer was also used for the image analysis. **(Fig. 3-1 g)**

3.3 Scanning Routine

After turning the US system's power on, B mode was selected for the scan. A high-frequency US transducer was used to image superficial structures such as median nerve and the infraclavicular fossa. A low-frequency US transducer was used to image more deep structures, such as the sciatic nerve. The scan preset, scan depth, frequency, dynamic range, and amount of gain were chosen based on the study protocol. All these settings on the US system were kept constant during the scan when the echogenicity was being evaluated. The position of the transducer head was marked on the subject skin with a skin marking pen to ensure that each set of scans was performed at the same site. The image was oriented to identify the anatomical relations of the various structures on the US screen. The orientation marker on the

transducer was directed toward the right side of the subject during a transverse scan, while it was oriented toward the head of the subject during a longitude (sagittal) scan. Liberal amounts of US gel were applied for acoustic coupling between the skin and the US transducer. Care was taken not to exert undue pressure over the area scanned because pressure can affect the gray-scale intensity of the pixels in the image. Moreover, to minimize anisotropy (angular dependence), the transducer was aligned (by tilting, sliding, or rotating the transducer) so that it was perpendicular to the target structure until maximum echogenicity of the underlying bones was achieved, a method that has previously been described. (Maurits et al., 2003,Maurits et al., 2004,Pillen et al., 2006b,Scholten et al., 2003)

3.4 Image Acquisition and Data Transfer

3.4.1 Image Recording

Once an optimal image was obtained, it was recorded on tape in Audio Video Interleave (AVI) format using a commercial video recorder, or saved to the SD card in the US system (**Fig. 3-1b**).

3.4.2 Video Data Transfer

The stored video recording on the tape was transferred to a personal computer using Adobe Premier Pro 2.0 (Adobe Systems Inc, San Jose, CA, USA). If the data were recorded on the SD card of the US system (MicroMaxx, Sonosite™ Inc., Bothell, USA), it was transferred to a personal computer using the Site-Link Manager 3.4.1 software (Sonosite™ Inc., Bothell, USA) (**Figs. 3-1c, d**).

3.4.3 Still Image Capture

Adobe Premier Pro 2.0 (Adobe Systems Inc, San Jose, CA, USA) was used to capture still images (3 per subject, TIFF format, 720×480 pixels and 8-bit gray levels) from the movie sequence and stored for data analysis. (**Fig. 3-1 c**)

3.5 Method for "off-cart" Measurements of Distance and Area

In digital imaging, the pixel (or picture element) is the smallest unit of information. It is normally arranged in a two-dimensional grid and represented by rectangles. The size of an object in an image is determined by the number of pixels in the image (Russ, 2007a) (**Fig. 3-2a**). The distance between two objects in an US imaging is determined by multiplying the edge length of a pixel by the number of pixels between the two objects, while the area is determined by multiplying the area of a pixel by the number of pixels within the object (**Fig. 3-2 b**). As a possible alternative to the "in-cart" method of measuring distance and area, in this project an "off-cart" method was developed and used for the measurements on the US images using Image-Pro® Plus 6.2 (IPP, Media Cybernetics, Silver Spring, Maryland, USA).

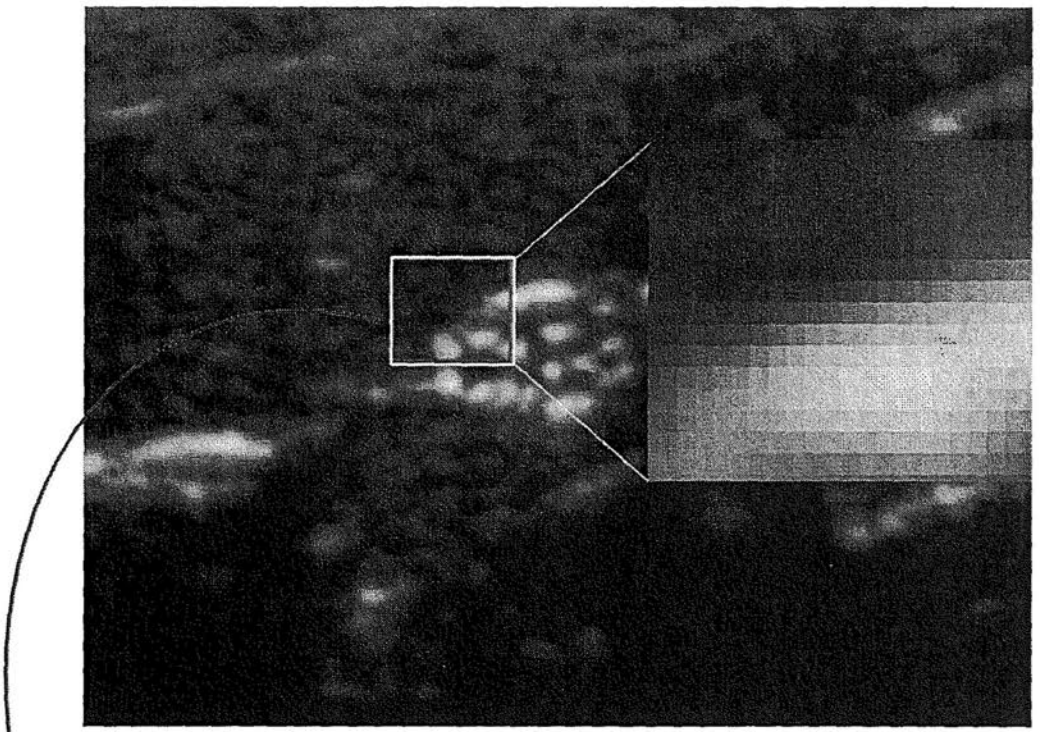

(a)

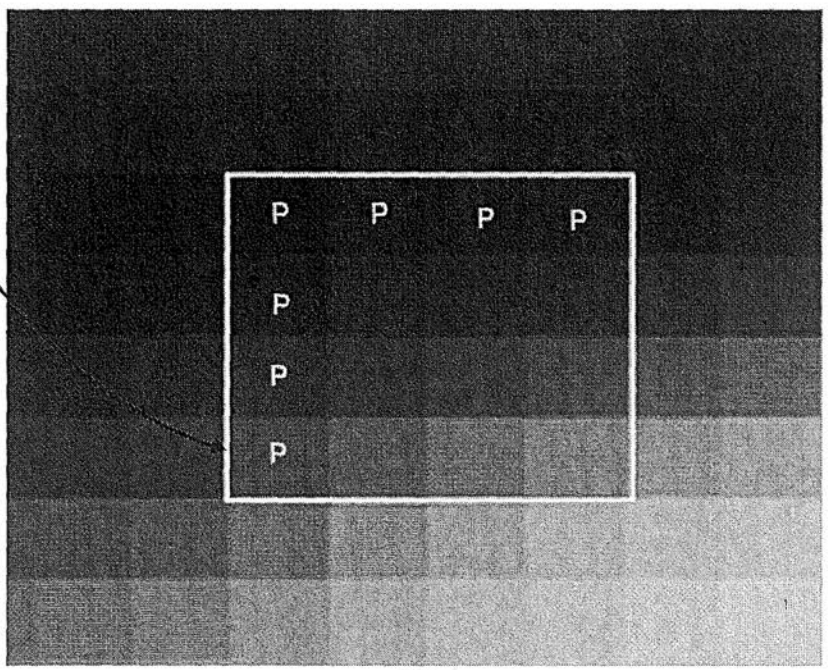

(b)

Figure 3-2. A typical US image of the median nerve in the mid-forearm. (a) A portion of the image is magnified 1600%, in which the individual pixels can now be seen as small squares; (b) illustration to demonstrate a "pixel" in the US image of the mid-forearm. "Square box" indicates one pixel.

3.5.1 Spatial Calibration

The size of an object in an image is determined by the number of pixels in the object. To measure distance and area in a digital image it is necessary to perform spatial calibration so that the number of pixels between two objects or in an area of a ROI in an US image can be translated into a physical unit of measurement (i.e., mm, cm). This was performed as follow:

A reference US image was imported into the IPP window. In the spatial calibration dialogue box of IPP, the "millimeter" (mm) unit was selected as the physical unit for measurement (**Fig.3-3a**). A reference line, calibration scale, was set to match the depth scale (object of known size) marked on the US image vertically (**Fig. 3-3b**). Thereafter, the number of pixels mm^{-1} in the horizontal (X) and vertical (Y) axes of the US image was determined (**Fig.3-3a**) and saved to the computer. Since different depth settings and two transducers were used in this project, specific calibration scales were made for each depth and each transducer.

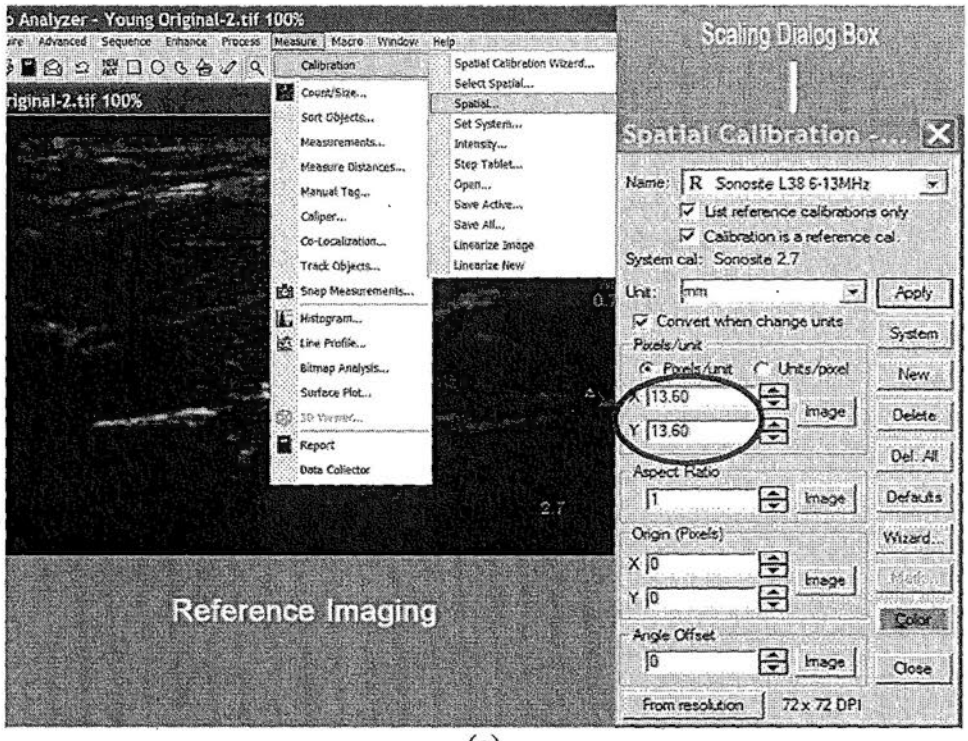

(a)

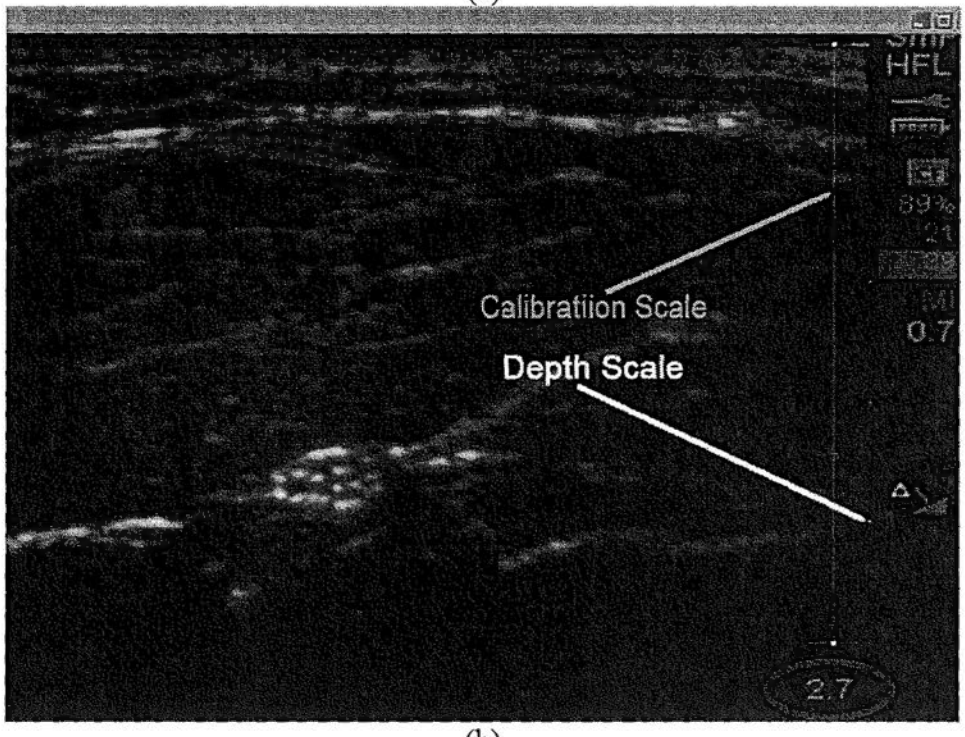

(b)

Figure 3-3. Illustrates how spatial calibration was performed. (a) The spatial calibration tab in IPP was selected; (b) In the US image, a reference line (green) was set to match the depth scale (2.7cm). The spatial calibration of this image is 13.6 pixels mm^{-1}.

3.5.2 Distance Measurement

The target image file was imported into the IPP window. Depending on the depth and the different transducer used, an appropriate spatial calibration scale previously saved on the computer was selected. To measure the distance, a straight colored line was stretched between two anatomical landmarks. The distance between these two points was expressed in mm (**Fig.3-4**).

3.5.3 Area Measurement

An appropriate spatial calibration scale, previously saved on the computer, was selected. A polygon ROI surrounding the outline of a ROI in the US image was created using the freehand polygon or best-fit circle tool. A closed color figure of the object was thereby produced (yellow in **Fig. 3-4**), and the result of the area was determined and displayed.

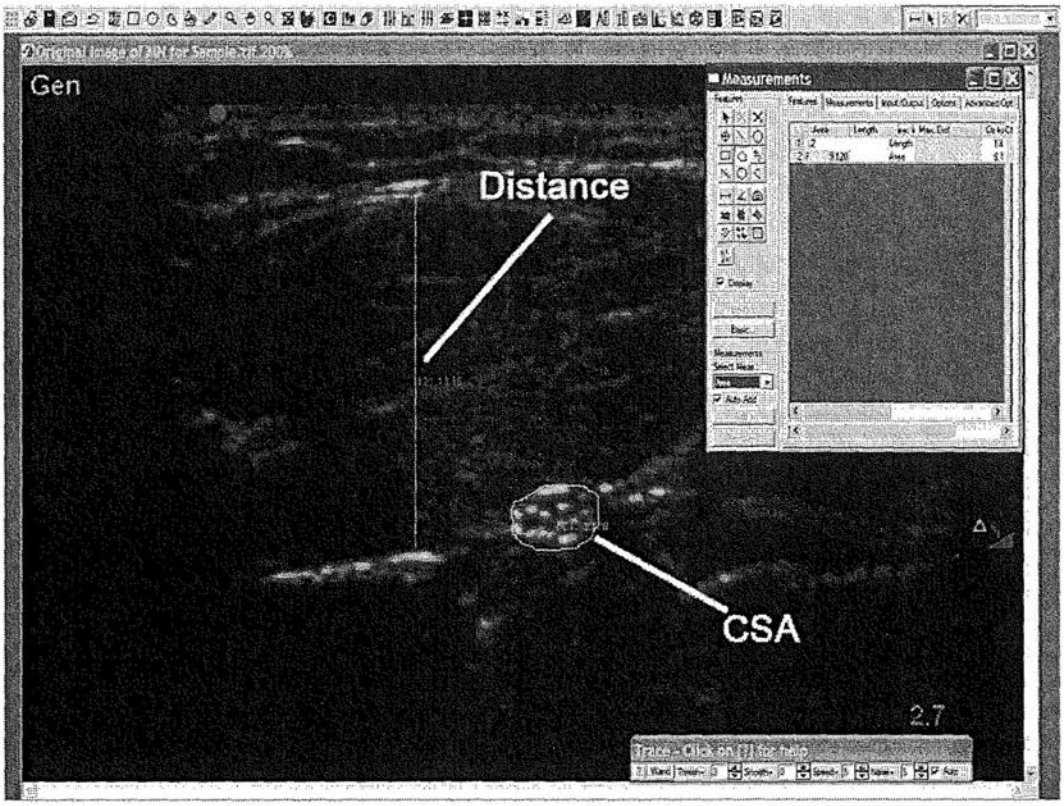

Figure 3-4. The "off-cart" measurement of distance (or length) and CSA using IPP software. The green colored numbers are the results of the measurements, which are also displayed in the measurement dialog box.

3.6 Method for Measuring Echo Intensity

3.6.1 Standardization of the Ultrasound System Setting

It is crucial to standardize system settings during quantitative sonographic studies because the echogenicity of an image can be affected by changes in system settings, which are discussed in **Chapter 5**. This was done by standardizing the scan preset, frequency, image optimization setting, amount of gain used, dynamic range and depth during each scan. As shown in the **Fig. 3-5**, in the MicroMaxx US system, the Delta key in the US system was set to 'reset to factory defaults' which ensured that the same setting was used in all subjects whenever an examination was commenced after booting the US machine.

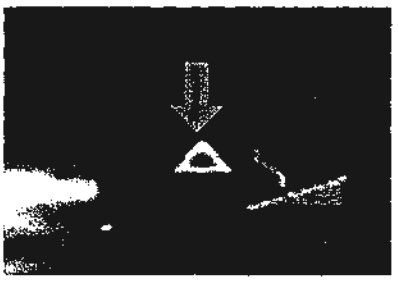

Figure 3-5. The Delta key, shown as a triangle indicates '*reset to factory defaults*' has been selected in the MicroMaxx US system.

3.6.2 Image Normalization

After US image acquisition (for more details, see **Section 3.4**), the still images were normalized (Adobe® Photoshop CS2) to ensure that the brightness and contrast of the whole image was at the same level before any gray-scale median (GSM) measurement was conducted. Normalization was performed by initially defining the GSM of two reference points in the 2D US image (TIFF), the one was the 'background' of the image and another was the text (i.e., Gen) in the US image (**Fig. 3-6**). Algebraic (linear) scaling (**Fig. 3-6**) was then performed using the "Curves Function" in Adobe Photoshop CS2, such that the GSM of the pure black equaled 0 and that of the pure white equaled 255 in the resultant image. This way, the gray-scale values of all the pixels in the image were adjusted according to the input and output values of the two reference points.

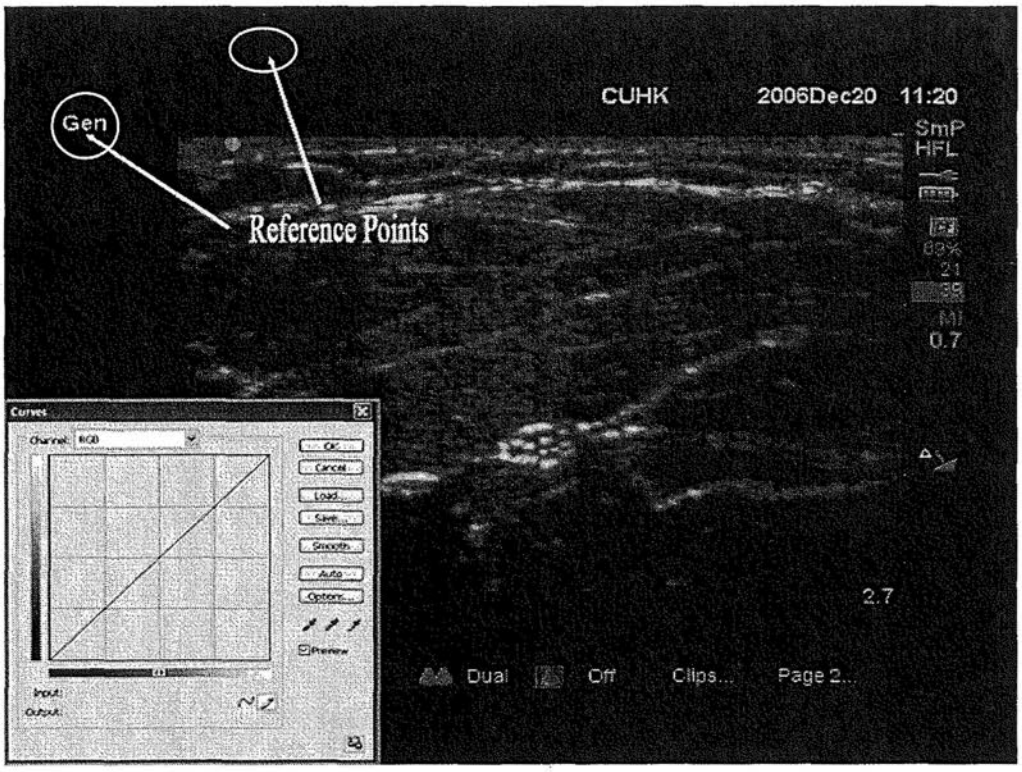

Figure 3-6. A typical transverse sonogram of the median nerve in the forearm shows the two reference points, white text (GSM=255) and the black background (GSM=0). Inset showing the Curves Function for adjusting the entire gray-scale range of pixels in an image.

3.6.3 ROI Selection and Echo Intensity Measurement

Computer assisted gray-scale analysis (Adobe® Photoshop CS2) was then performed on these images to measure the EI. A polygonal ROI was drawn around the outlines of the ROI (i.e., median nerve) using the freehand lasso tool in Adobe Photoshop CS2. The mean (SD) and median (range) EI of the ROI was determined using the standard histogram function in the Adobe® Photoshop software. The EI value of 0 represents 'pure black' and a value of 255 represents 'pure white'.

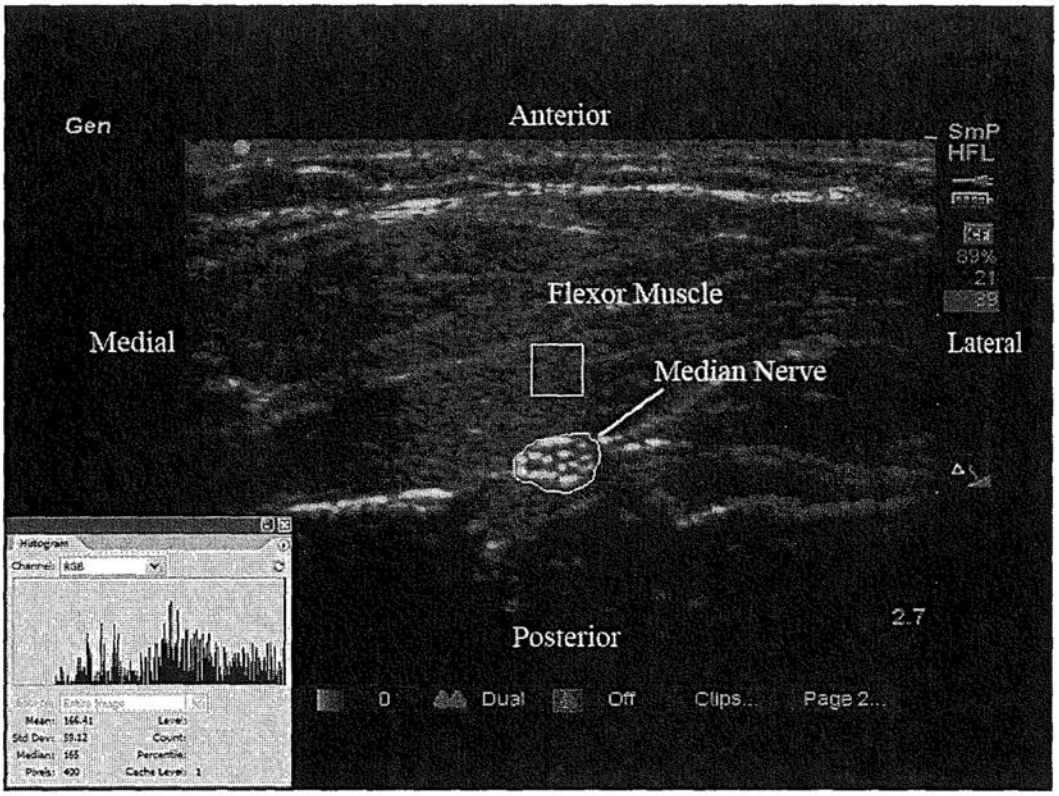

Figure 3-7. A typical transverse sonogram of the forearm is shown. A polygonal ROI has been placed around the outlines of the median nerve, and a square ROI box has been placed over the flexor muscle above the median nerve. The histogram palette (lower left) in the inset image shows the mean (SD) and median EI values of the median nerve in the US image.

3.7 Method for Measuring Texture

Texture in a digital image is attributed to the distribution of gray-scale values among the pixels in a given ROI in the image. Texture analysis is used to evaluate the position, intensity of pixels, and their grey-scale level intensity in the digital image (Castellano et al., 2004,Maurits et al., 2003,Russ, 2007a,Russ, 2007b). Computer assisted texture analysis was performed and results are presented as white area index (WI) and black area index (BI). (Please refer to **Section 3.7.5**)

3.7.1 Standardization of the Ultrasound System Setting

Details are outlined in **Section 3.6.1.**

3.7.2 Image Normalization

Details are outlined in **Section 3.6.2.**

3.7.3 Noise Reduction and ROI Selection

A normalized gray-scale US image (**Fig. 3-10b**) was imported into the IPP window. The US image was magnified to 200%. Spatial filtering was then performed using the median filter (3 X 3 kernel size) (**Fig. 3-8a**) to remove impulse noise from the US image without any reduction in the brightness difference and boundary shift (Russ, 2007b). After the filtering process ROI around the outlines of the object (i.e., median nerve) was carefully drawn with the freehand irregular ROI trace tool. This was then circumscribed with yellow color (**Fig. 3-8b**).

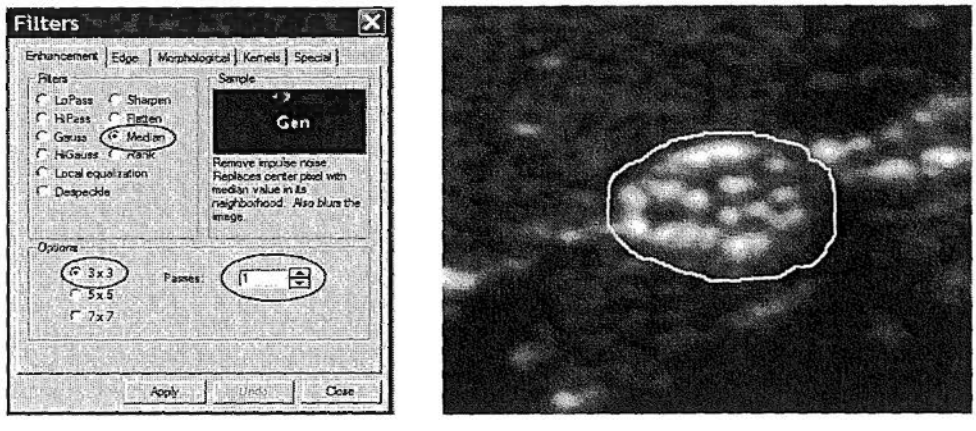

(a) (b)

Figure 3-8. Shows the filtering process using the median filter. (a) Filters tab in IPP. (b) ROI around the median nerve.

3.7.4 Thresholding

Threshold is defined as a range of gray-scale values in an image ranging from a minimum to maximum value. Thresholding is a process used to extract the regions within a defined gray-scale range as the foreground, and reject all of the other regions to the background. After thresholding, an input gray-scale image is transformed into a binary image using white and black color to distinguish two regions (Russ, 2007b). During the thresholding process, individual pixels in an US image are marked as a white object if their gray-scale value is greater than the set threshold value or as a black background otherwise. The thresholding process is illustrated in **Fig.3-9**. Thereafter, an input gray-scale US image was transformed into a segmented white and black color image **(Fig. 3-10)**.

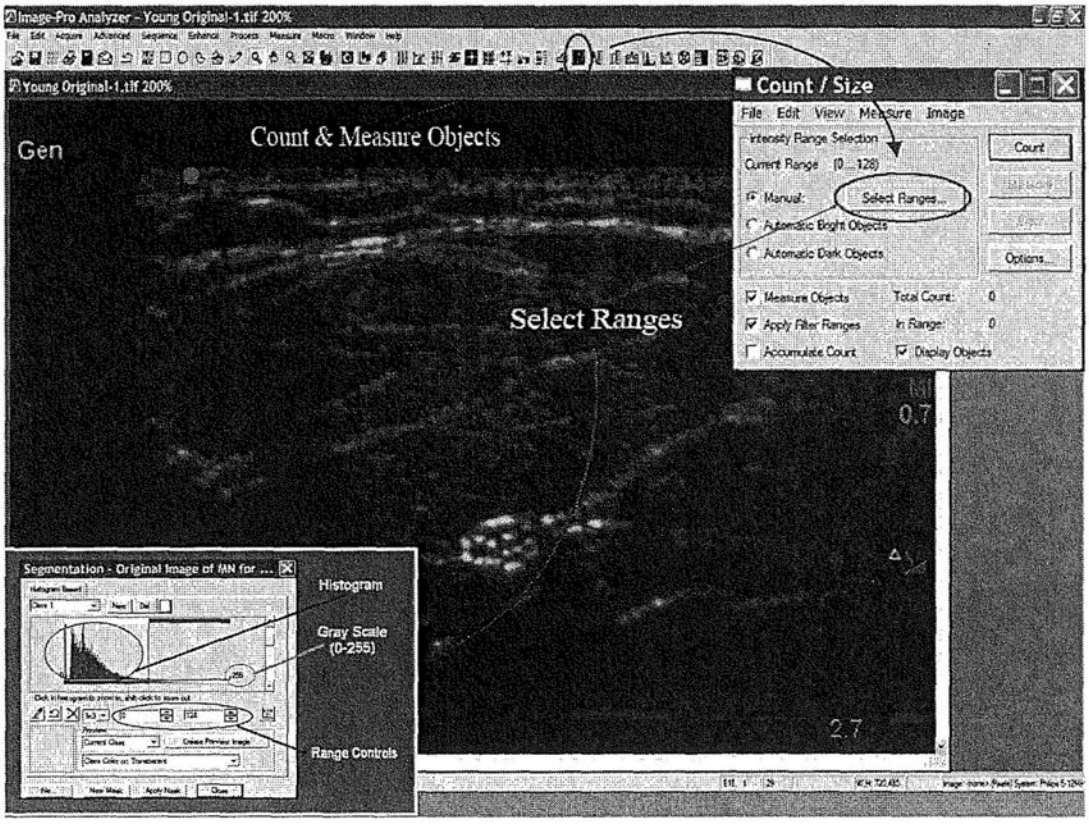

Figure 3-9 The thresholding process is shown on a typical transverse sonogram of the median nerve in the forearm. Inset shows the segmentation tab for selecting the threshold range. The threshold, gray-scale value selected in this image is 0-128.

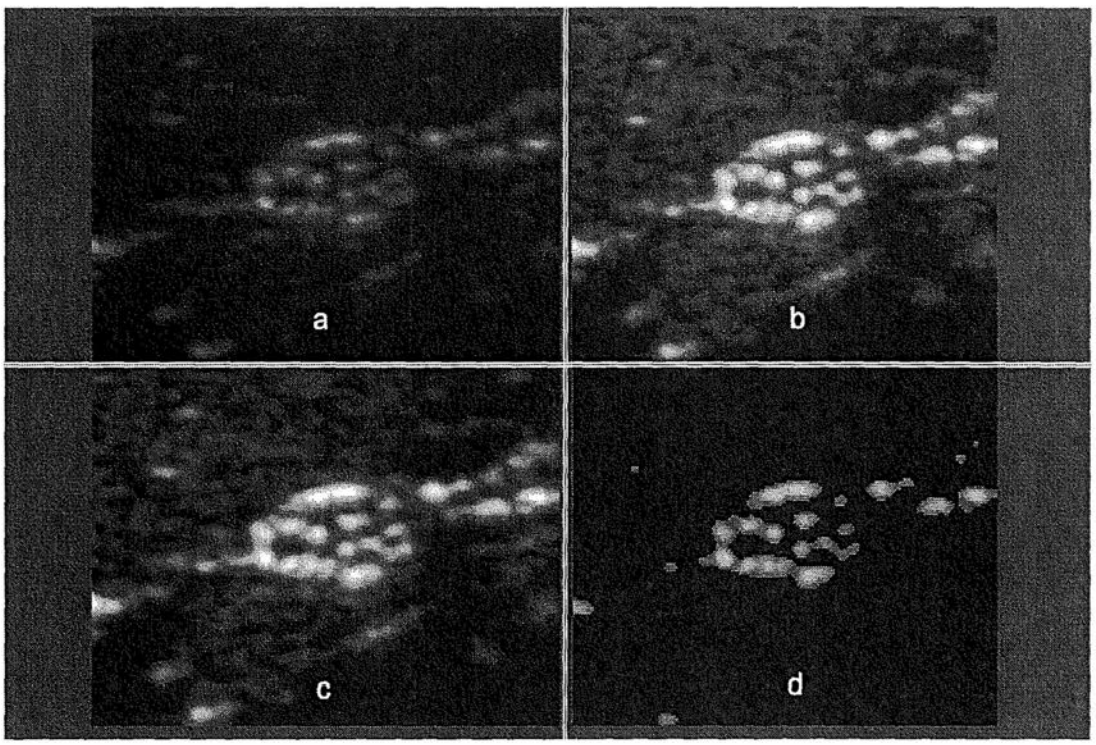

Figure 3-10. A set of US images showing the different stages of the texture process. (a) An US image of the median nerve; (b) US image after normalization; (c) Noise Reduction-Median filtering; (d) Binary image after thresholding process.

3.7.5 Black and White Area Index Measurement

During the thresholding process the pixels in the ROI within the threshold range (128-255) were overlaid and displayed as a reference color (white), the other pixels within the range (black: 0-128) were converted to the background color (black). As a consequence, a gray-level US image was segmented into a black and white binary image (**Fig. 3-10d**). In the resultant binary image, the white area was defined as a region which had at least three connected pixels (corresponding to a minimums area) with a gray-scale value within the defined threshold (white: 128-255). The white

area index (WI) was defined as the ratio of the white area to the total area of the ROI. The black area was defined as a region which had at least three connected pixels with a gray-scale value within the defined threshold (black: 0-128). The black area index (BI) was defined as the ratio of the black area to the total area of the ROI. The process used to count WI and BI in IPP is illustrated in **Fig.3-11.**

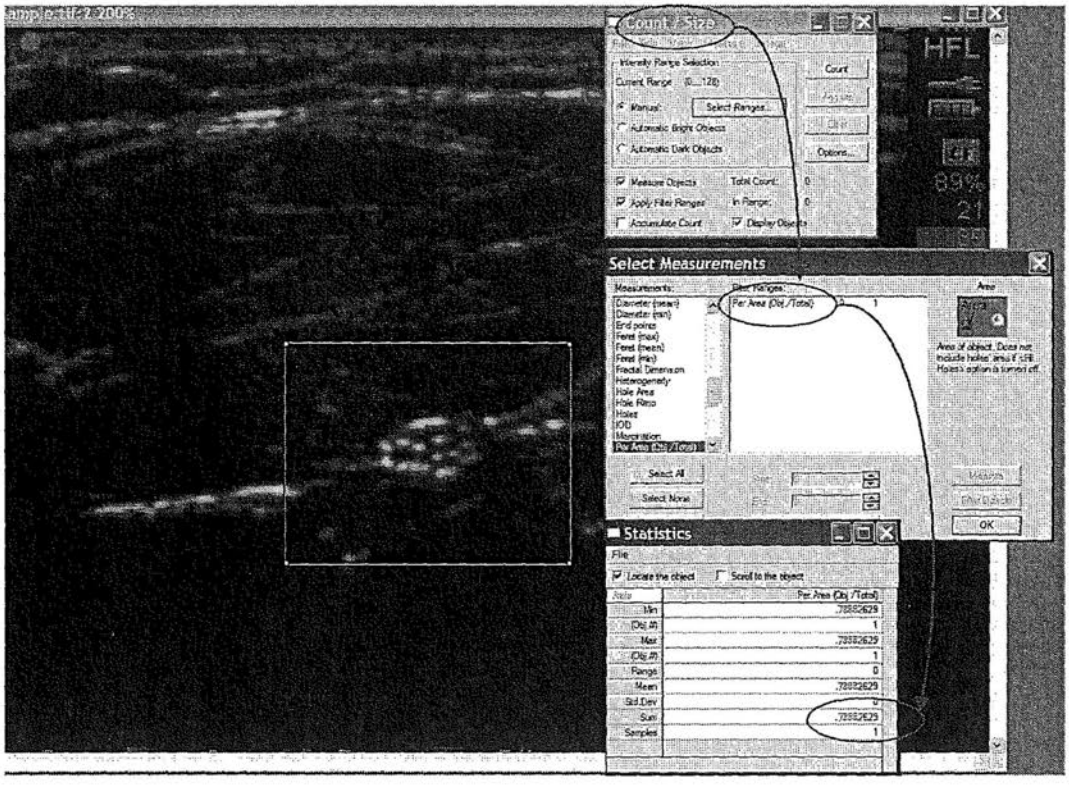

Figure 3-11. The process used to count the black and white area index in the ROI is illustrated.

3.8 Summary

The steps used for quantitative ultrasonography are illustrated in the flow chart below.

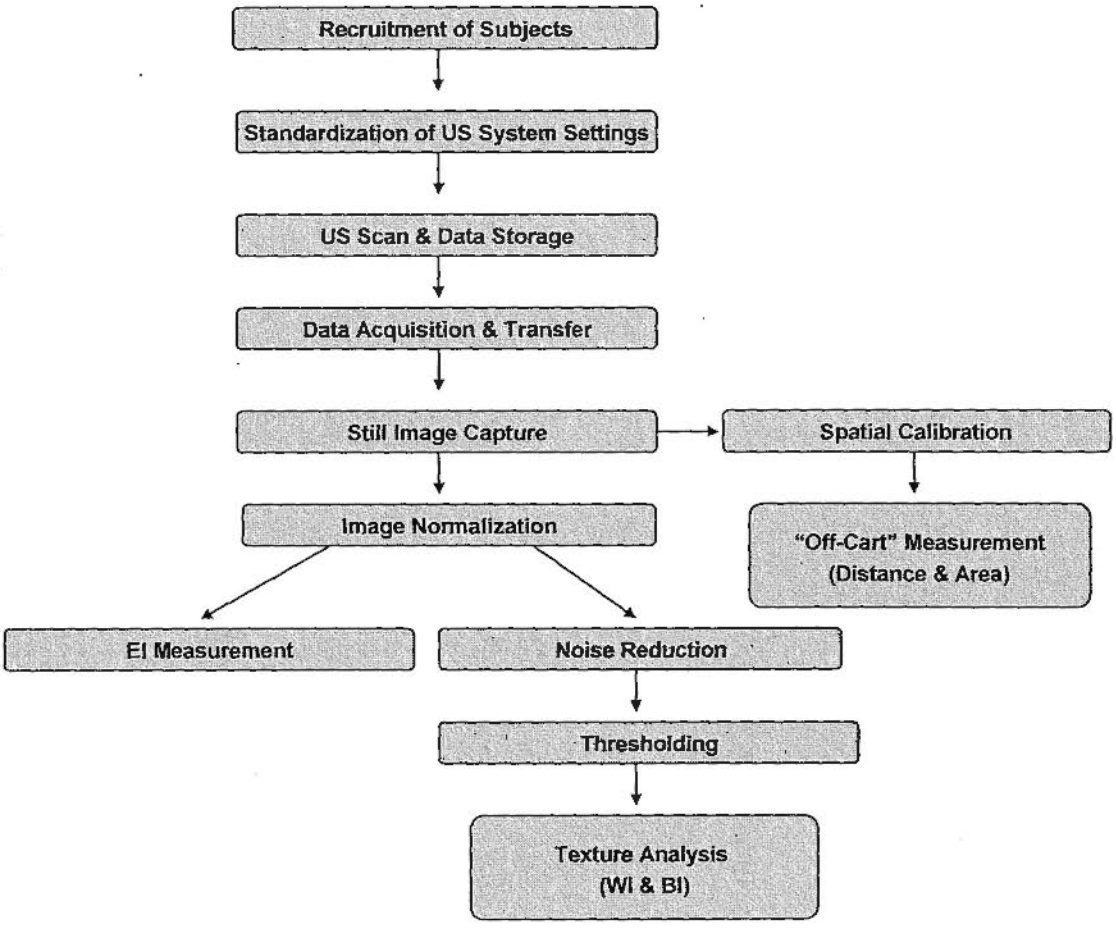

Chapter 4

Reproducibility of Quantitative Ultrasonography

4.1 Introduction and Objective

The methods used for quantitative ultrasonography in this project are described in the previous section. There are no data on the reproducibility of the EI and texture measurements of a peripheral nerve in the literature, and there are also no published data assessing the reproducibility of "off-cart" measurement of distance (width) and area (CSA) in the musculoskeletal structures using Image-Pro® Plus, which were evaluated in this study.

4.2 Materials and Methods

4.2.1 Study Design

This was a non-randomized observational study.

4.2.2 Inclusion and Exclusion Criteria

Two groups of subjects were recruited for the study. Group 1 comprised of 10 adult volunteers who were recruited from the Faculty of Medicine of the Chinese University of Hong Kong for the EI and texture measurement. Group 2 comprised of 30 adult patients from the Prince of Wales Hospital who were undergoing orthopedic lower limb surgery for the "off-cart" distance and area measurement. Subjects with the following criteria were excluded from the study:

1). No informed consent

2). Presence of infection, trauma or injury at the site of scan

3). Diabetes, advance tumors, neuropathy or musculoskeletal disorders

4). American Society of Anesthesiologists (ASA) physical status>III.

4.2.3 Equipment and Software Used

The US scans were performed using the MicroMaxx US system (Version V 3.1, ARM 30.80.301.014 with no auto-gain or compound imaging facilities) and a high frequency linear array transducer (HFL38, 13-6 MHz, 38 mm footprint) (**Fig. 3-1a**). A Compact Flash card in the US machine was used to record all image data from the US system (**Fig. 3-1b**). All US images from the SD card of the US machine were transferred to a personal computer using the Site-Link Manager 3.4.1 software (**Fig. 3-1d**). Adobe® Premier Pro 2.0 software was used to capture a still image from the video loop and was stored as a TIFF image for data analysis (**Fig. 3-1c**). Adobe® Photoshop CS2 software was used to normalize the image and determine the EI using the standard histogram function (**Fig. 3-1d**). Image-Pro® Plus 6.2 was used to perform measurements of distance and CSA and determine the texture of the US image (**Fig. 3-1 f**). All data downloaded for processing or analyses were stored on a personal laptop computer.

4.2.4 System Settings

When US scan was performed in the infraclavicular fossa, the default, "Small Parts" preset, "General" image optimization setting was used for each scan. Dynamic range was set to a preset level, equal to 0, and depth was set to 4.9 cm which was considered adequate for imaging the infraclavicular fossa. Gain was manually adjusted to optimize the US image. However, when the US scan was performed in the mid-forearm, the settings of US system were standardized for every subject. This was done by setting the Delta key in the US system to '*reset to factory defaults*', at

the advice of the manufacturer. This ensured that the same set of settings of US system was used for every subject whenever an examination was commenced after booting the US machine. The "small parts" preset, "general" image optimization setting, "dynamic range" (preset = 0) was chosen before every scan and the MN was focused so that it was in the centre of the image. The "depth-setting" was also standardized to 2.7 cm, which was considered adequate for imaging the MN in the mid-forearm. These standardized scan settings were used in every subject studied. More details of the system settings are presented in **Section 6.2.4** of **Chapter 6** and **Section 7.2.5** of **Chapter 7**.

4.2.5 Preparation for Subjects

The US scan in the Group 1 was performed on the left mid-forearm with the volunteers lying comfortably in the supine position. The left arm was abducted and externally rotated, with the palm of the hand facing the ceiling, and resting on a padded arm rest. The US scan in the Group 2 was performed preoperatively and before the induction of anesthesia. The patient was positioned in the supine position with the head turned away from the side scanned. The left arm was abducted to 90 degrees, and externally rotated such that the palm of the hand was facing the ceiling, and positioned at the same level as the heart. The arm was also placed on a padded arm rest.

4.2.6 Scan Methods

The US scans were performed by a single investigator, the project supervisor (M.K), who is experience in US imaging, using the MicroMaxx US system and a high frequency linear array transducer (HFL38, 13-6 MHz, 38 mm footprint). In the Group 1, the median nerve in the mid-forearm was selected for the scan because it is

a relatively superficial structure and is readily accessible for US imaging. Liberal amounts of US gel was applied for acoustic coupling between the skin and the US transducer and it was positioned midway between the flexor crease of the elbow joint and the distal flexor crease of the wrist joint. A transverse scan of the MN was thereby obtained. Care was taken not to exert undue pressure over the area scanned because pressure can affect the grey-scale intensity of the pixels in the image. Moreover to minimize anisotropy (angular dependence) the transducer was aligned such that it was perpendicular to the forearm bones. This was done by gently tilting the transducer during the scan until maximum echogenicity of the bones was visualized, a method that has previously been described. (Maurits et al., 2003,Maurits et al., 2004,Pillen et al., 2006b,Scholten et al., 2003)

In the Group 2, the coracoid process was identified in the infraclavicular fossa and marked. After skin preparation a high-frequency 13-6MHz linear-array transducer was positioned infero-medial to the coracoid process underneath the clavicle in a parasagittal plane to obtain the best saggital view of the axillary artery. Liberal amounts of US gel was applied for acoustic coupling between the skin and the US transducer. The transducer was aligned so that it was perpendicular to the axillary artery. Care was taken not to exert undue pressure over the scanned area because pressure can affect the measurements of the musculoskeletal structures. Thereby, a saggital image of the infraclavicular fossa was obtained. Structures that were imaged included the skin, subcutaneous tissue (and breast tissue in females), pectoralis major and minor muscles, axillary artery and vein (2^{nd} part), and cords of the brachial plexus.

4.2.7 Image Acquisition and Transfer

Please refer to **Section 3.4** in **Chapter 3** for more details on image data collection, transfer, and still image acquisition. Ten transverse US images of the median nerve at the mid-forearm were obtained from the young volunteers. These images were used to test the reproducibility of the EI and texture measurements of the median nerve using Photoshop and IPP, respectively. Moreover, a total of 30 sagittal images of the left infraclavicular fossa were obtained from the 30 patients. These images were used to test the reproducibility of the "off-cart" measurements of distance and area using IPP.

4.2.8 "Off-cart" Measurement of Distance and Area

The "off-cart" measurements of the distance from the skin to the axillary artery and CSA of the axillary artery were performed on the US images obtained from Group 2. In brief, an appropriate reference spatial calibration scale (9.3 pixels /mm) previously saved on the computer was selected. To measure distance from the skin to the axillary artery a straight color line was stretched between these two structures in the US image (**Fig. 4-1**). To measure CSA of a polygon ROI surrounding the outline of the axillary artery was then drawn with the freehand polygon irregular tool of IPP. Thereby, a closed figure covering the axillary artery was obtained (**Fig. 4-1**). The results of the distance and CSA were then displayed. The "off-cart" measurement of the CSA of the MN was performed on the US images obtained from Group 1. An appropriate reference spatial calibration scale (13.6 pixels /mm) previously saved on the computer was selected. For CSA measurement of a polygon ROI, surrounding the outlines of the MN in the US image, was created using the freehand polygon feature irregular tool. A closed figure covering the MN (**Fig.4-2**) was thereby

obtained. Thereafter, the result of CSA was determined using IPP and results were expressed in mm. More details are outlined in **Sections 3.5.1 to 3.5.3** of **Chapter 3**.

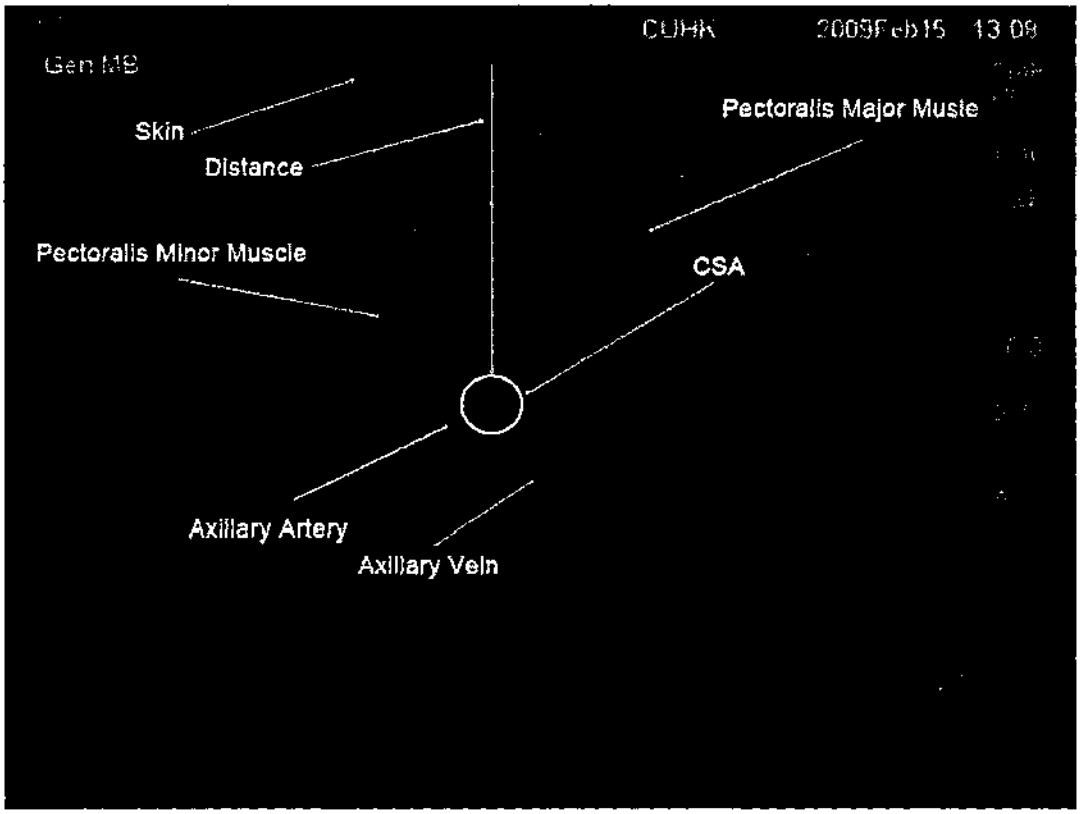

Figure 4-1. A typical sagittal sonogram of the infraclavicular fossa. Distance from the skin to the axillary artery and the CSA of the axillary artery were measured using IPP.

4.2.9 Echo Intensity and Texture Measurements

The EI and texture measurements were performed on the US images obtained from Group 1. In this study the median nerve in the US image was chosen as the ROI (**Fig. 4-2**). The EI and texture of the median nerve were determined using Adobe Photoshop and Image-Pro® Plus software. Details of the standardization and normalization of US image are outlined in **Sections 3.6** of **Chapter 3**. The mean (SD) and median (range) EI of the median nerve were determined by the standard histogram function in the Adobe® Photoshop software. For the echotexture measurement method please refer to **Section 3.7** of **Chapter 3**. In brief, the median

value of the gray-scale level (128) was chosen as the threshold value. The noise of the image was reduced by the median filter. The gray-scale US image was converted to a black and white color binary image by thresholding. The white area index (WI) of the median nerve was then determined using IPP.

4.2.10 Repeated Measurements

In order to test for interobserver agreement, the first set of measurements of distance, CSA, EI and WI in the US images were performed by the author (observer 1) in isolation. The second set of measurements were performed by an independent observer 2 (T.L, computer technician) in the same department, on the same US images using the same methodology. Moreover, in order to test for intraobserver consistency the same set of measurements were repeated on the US images by the author (LX) a month later.

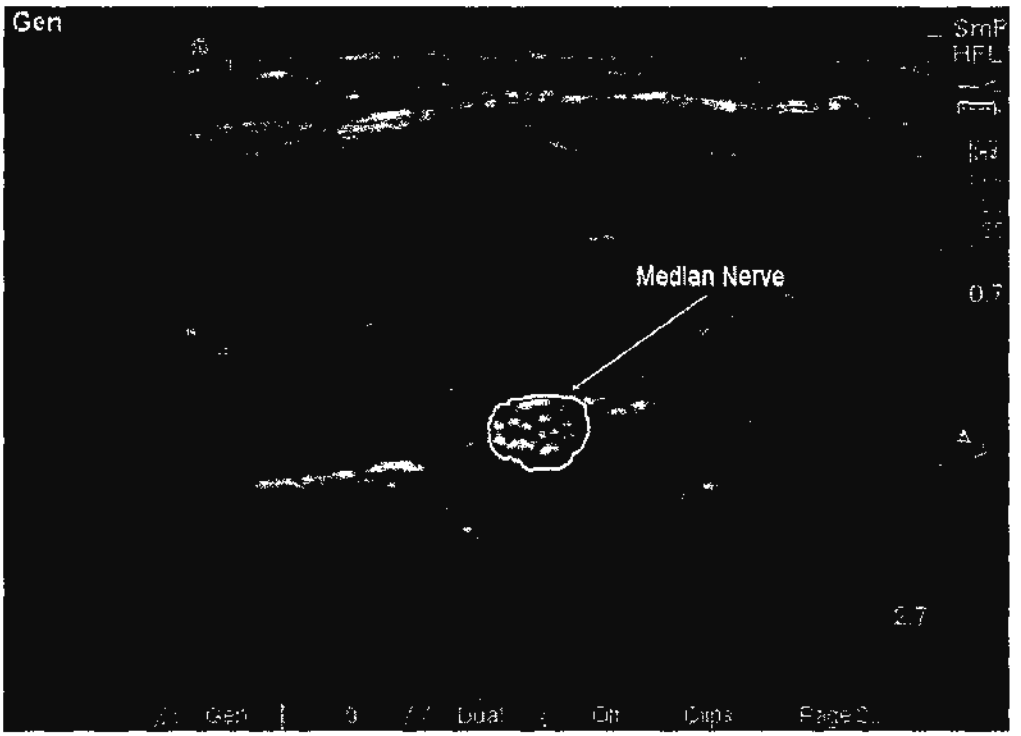

Figure 4-2. A typical transverse sonogram of the mid-forearm. A polygonal ROI has been placed around the outlines of the median nerve.

4.2.11 Statistical Analysis

Statistical Package for the Social Sciences (SPSS) for Windows 14.0 (SPSS Inc, Chicago, IL, USA) was used for the statistical analysis. The Kolomogorov-Smirnov test was applied to test the normality. The mean measurements (distance, CSA, EI and WI) from the three images from each subject were averaged one mean result for statistical analysis. Interobserver and intraobserver variability was tested using the intraclass correlation coefficient. The paired samples t-test was used to compare the differences in the results obtained by the two observers and on the two days that the measurements were made. A p-value less than 0.05 was considered statistically significant.

4.3 Results

Demographics data for the two study groups are presented in **Table 4-1**. There were no significant differences in the measurements of each parameter made by the two observers, and on the two days (**Table 4-2**) when these measurements were made. The intraclass correlation coefficients (ICC) of all the measurements of each parameter by the two observers and on the different days were greater than 0.75, which indicates that there was good interobserver agreement and intraobserver consistency (Portney and Watkins, 2000) for all measurements made in this study.

4.4 Discussion

In this study, we have demonstrated a good reproducibility of the quantitative ultrasonographic methods used to measure the distance, CSA, EI and WI on the musculoskeletal sonogram.

There were good intraobserver and interobserver correlations between the "off-cart" measurements of the distance and CSA in the US image. The measurements of the distance and CSA made on different days, and that made by the two observers were comparable. The "off-cart" measurement of the CSA of the MN in the US image using computer software has a good reproducibility, which is in agreement with Nakamichi et al. (Nakamichi and Tachibana, 2000). Although we are not aware of any comparable data evaluating the reproducibility of the "off-cart" measurement of distance (i.e., diameter or width) and CSA of an artery in the literature, "off-cart" measurement using computer software has also been shown to be a valid and reliable method used in skeletal muscles (Reeves et al., 2004,Sanada et al., 2006). Based on

our findings, we believe that the "off-cart" method used in this study is valid and reproducible.

There were also good intraobserver and interobserver correlations between the EI and WI measurements in the US image, and these measurements were comparable between different observers and on the different days. Currently, there are no data on the reproducibility of EI measurements of a peripheral nerve. However, the EI measurement using computer assisted gray-scale analysis in skeletal muscle has been shown to have a good reproducibility (Maurits et al., 2003,Nielsen et al., 2000,Pillen et al., 2006b) and is valid (Nielsen et al., 2000). Moreover, there are no comparable data on the WI of a peripheral nerve in the literature. However, there was a good correlation between the measurements of tissue components predicted with computer assisted texture analysis (IPP) and histologic measurements made on the explanted carotid plaques (Lal et al., 2002). These findings indicate that computer assisted texture analysis is a valid and reproducible method. We, therefore, believe that the same is applicable when computer assisted image analysis is used to evaluate the EI and WI of the MN in the forearm.

4.5 Conclusion

We have demonstrated that the quantitative, computer assisted methods that were used to measure distance, area, EI and texture of musculoskeletal structures in this study are reproducible, and can be applied to the rest of the work in this thesis.

Table 4-1. Demographic data.

Group	Gender (n)	Age (yr)	Weight (kg)	Height (cm)	BMI
1	5M/5F	25.8 (3.77; 20-30)	60.3 (8.77; 48-76)	166 (6.23; 156-173)	22.0 (2.92;17.0-26.8)
2	11M/19F	46.5 (18.4;18-82)	65.0 (12.4.; 47.5-100)	165 (6.47; 155-180)	23.7 (3.84; 18.1-36.7)

Data are presented as mean (SD; range). M=male, F=female, BMI=body mass index, and n=frequency.

Table 4-2. Intraobserver and interobserver reproducibility of the distance, CSA, EI, and WI measurements.

Parameter	Number of Subjects (n)	Interobserver Agreement		Intraobserver Consistency	
		ICC(95% CI)	*p*-value(t-test)	ICC(95% CI)	*p*-value(t-test)
Distance	30	0.96(0.95-0.99)	0.76	0.99(0.98-0.99)	0.71
CSA (Artery)	30	0.95(0.89-0.97)	0.22	0.98(0.96-0.99)	0.26
CSA (MN)	10	0.76(0.33-0.93)	0.26	0.86(0.53-0.96)	0.16
EI	10	0.80(0.55-0.95)	0.89	0.92(0.72-0.98)	0.55
WI	10	0.97(0.89-0.99)	0.72	0.96(0.85-0.99)	0.06

The intraclass correlation coefficient (ICC; 95% CI) is presented. Distance=distance from skin to axillary artery; CSA=Cross sectional area of the axillary artery; Artery=axillary artery; MN=median nerve; EI=echo intensity; WI=white area index and n= frequency. The p-value is the probability of two measurements assessed using paired-sample t-test. $p<0.05$ is considered statistically significantly.

Chapter 5

Effect of Ultrasound System Settings on the Echo Intensity of an Ultrasound Image: An In-Vitro Phantom Study

5.1 Introduction and Objective

Computer assisted gray-scale analysis is a quantitative method for evaluating the echogenicity of a tissue and has a good reproducibility. However, when the echogenicity of a musculoskeletal structure (i.e., muscle) is analyzed quantitatively, it is crucial that all the system settings in the US system are standardized before the measurement because the echogenicity of a ROI in the US image may vary with changes in the system. (Heckmatt and Dubowitz, 1985, Zaidman et al., 2008) There are limited quantitative data demonstrating how changes in US system settings can affect the EI of an US image, which this study was designed to investigate.

5.2 Materials and Methods

This was an in vitro study using a tissue-mimicking US phantom that was conducted at the Department of Anesthesia & Intensive Care of The Chinese University of Hong Kong at the Prince Wales Hospital, Shatin, Hong Kong.

5.2.1 Ultrasound Phantom

All tests were conducted using a tissue-mimicking US phantom (Blue Phantom's™ Select Series Nerve Block US Phantom, Advance Medical Technologies, LLC, Kirkland, WA 98033, USA). The Blue Phantom is made up of a proprietary tissue-simulating material that has acoustic properties comparable to human tissue. A tissue-mimicking phantom can provide highly reproducible US images, and is thus

an ideal medium to test the effects of US system settings on the EI of a structure. The Blue Phantom is approximately 16 cm x 11 cm x 4cm (length x width x height) and contains a simulated "nerve" structure that is embedded in the material. This simulated structure has higher acoustic impedance than the surrounding tissue, and produces a brighter acoustic signal than the surrounding tissue. There are also two simulated "blood vessels" filled with fluid which results in areas with lower acoustic impedance and appears hypoechoic when imaged with US. (**Fig. 5-1**)

5.2.2 Equipment and Software Used

The LOGIQ® *e* US system with a high frequency linear array transducer (12L-RS, 5-13MHz, 42 mm footprint) was used to scan the phantom (**Fig. 5-2 a, b,** and **e**). The US image data were recorded on tape (AVI format) using a video camera (Sony Corporation, Ltd., Minato-ku, Tokyo, Japan). Adobe® Premier Pro 2.0 (Adobe Systems Inc, San Jose, CA, USA) **(Fig. 2-1 c)** was used to capture the video loop and stored as a still image (TIFF format) for data analysis. Adobe® Photoshop CS2 (Adobe Systems Inc, San Jose, CA, USA) was used to normalize the US image and measure the EI of a ROI in the US image using the standard histogram function **(Fig. 3-1 e).** All data downloaded for processing or analysis were stored on a personal laptop computer (Dell Inspiron 6400, Dell Computer Corporation, Inc., USA). The same computer was also used for the image analysis in the project **(Fig. 3-1 g).** Details are outlined in **Section 3-2** of **Chapter 3**.

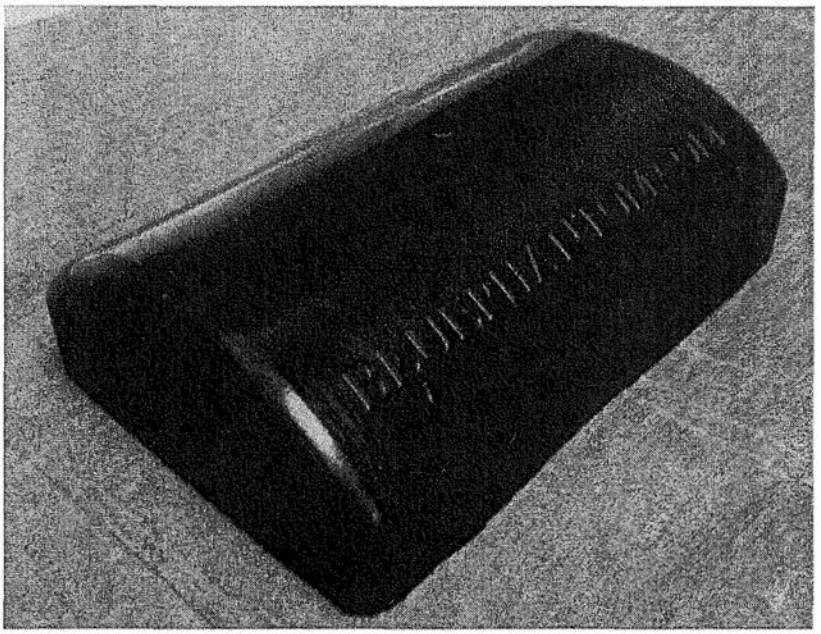

(a)

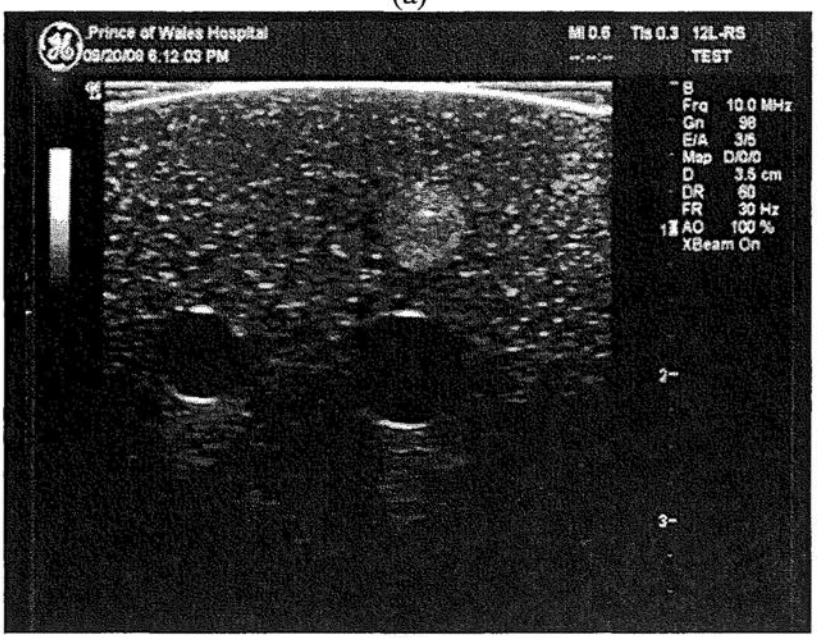

(b)

Figure 5-1. (a) A *Select Series Nerve Block* US Blue Phantom is shown. (b) A typical transverse US image from the Blue Phantom.

5.2.3 Preparation before the US Scan

The US phantom was placed on a flat surface (**Figs. 5-2a, c, and d**). A liberal amount of US gel (Schiller Ultrasonic Gel, Bucher Medical, CH-8105 Regensdorf, Switzerland) was applied for acoustic coupling between the surface of the Blue Phantom and the US transducer. Care was taken not to exert undue pressure over the

area scanned because pressure can affect the gray-scale intensity of the pixels in the image. The transducer was positioned midway and perpendicular to the phantom (**Fig. 5-2c**). The cable of the transducer was suspended from an intravenous fluid stand (**Fig. 5-2d**) to ensure that very little pressure was exerted on the phantom and to minimize movement of the transducer and thereby avoid anisotropy during the experiment.

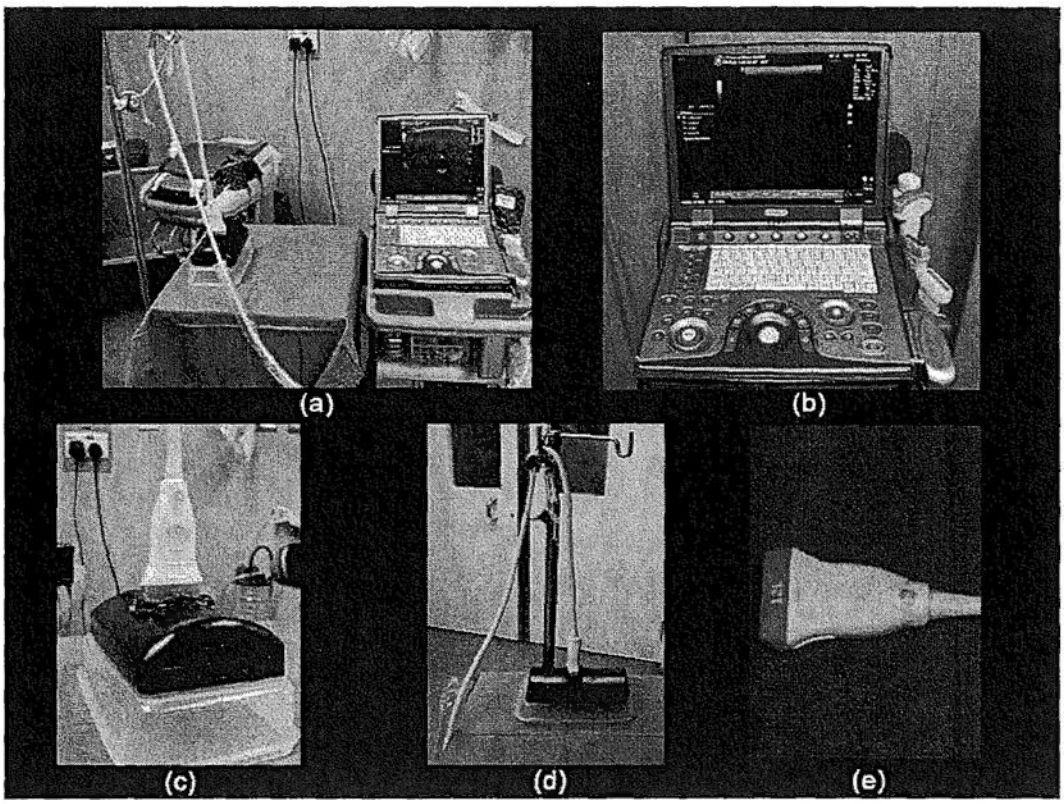

Figure 5-2. System setup and preparation before the US scan. (a) General arrangement of the US system and the Blue Phantom; (b) LOGIQ® *e* US system; (c) US transducer and the blue phantom; (d) Cable suspended from an intravenous fluid stand; (e) High frequency linear-array transducer (12L-RS, 5-13MHz, 42 mm footprint) used in this study.

5.2.4 Standardization of the Ultrasound System Settings

Before starting the US examination, the scan settings were standardized to a default value. These default values were used as a startup baseline before each experiment

and were used to investigate the effects of changing system parameters on EI measurements. Standardization of the US system (GE Medical System, Milwaukee, Wisconsin 53201, USA) was performed as follows:

After powering on the US system, B mode was selected for the scan. A high-frequency broadband linear-array transducer (12L-RS, 5-13 MHz, and 42mm footprint) was chosen for this experiment because of the relatively shallow scan depth in the phantom. The factory default preset was then selected and a transverse scan of the Blue Phantom was performed. The image was then optimized through adjustments on the gain (overall), depth, focus, frequency, and dynamic range. Time gain compensation (TGC) slide rulers were also set to the neutral (middle) position and the auto gain compensation (AGC) was disabled (**Fig. 5-4**). The focal zone was placed at the center of the ROI, which was the hyperechoic simulated nerve structure in the Blue Phantom. Once the image was optimized, the system setup window was activated. All optimized settings were saved as a customized preset and named as "TEST" preset (**Fig. 5-3**). The baseline settings of this customized preset were then determined from the system, which are presented in **Table 5-1**. Therefore, whenever the "TEST" preset was chosen after booting the US system, it ensured that the system settings were the same before the US examination.

Table 5-1. Baseline settings of the Customized "TEST" preset.

Preset	
US Mode	B-Mode
Frequency	10.0MHz
Gain	98dB
Enhance/Average Frame	3/5
Map	D
Depth	3.5cm
Dynamic Range	60dB
Frame Rate	30 Hz
Acoustic (Power) Output	100%

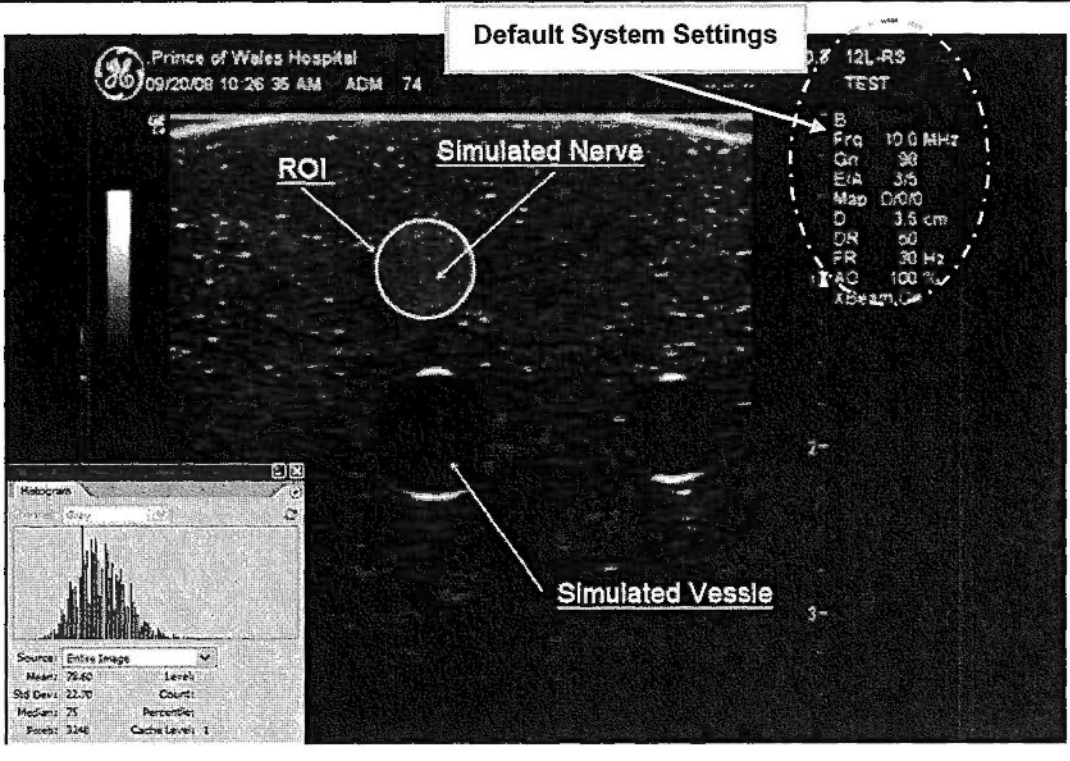

Figure. 5-3. A typical transverse US image from the Blue Phantom. A circular ROI has been drawn around the outline of the simulated nerve. The histogram palette in the inset shows the mean (SD) and median EI values of the ROI in the US image. Scan settings are also shown on the top right corner of the image. B=B mode; Frq=US frequency; Gn=gain; E/A=enhance / average frame; Map=gray-scale map; D=depth; DR=dynamic range; FR=frame rate and AO=Acoustic (power) output.

5.2.5 Image Acquisition and Transfer

Based on the default preset, the effects of five different system settings on EI measurement were investigated. The systems settings evaluated included frequency, depth, gain, dynamic range, and power output because they are the parameters that are commonly adjusted to optimize an US image in the clinical setting. When the effect of a given parameter was studied the other parameters were kept constant. The range of parameter settings that were studied are listed below:

Preset	Value
Frequency (MHz)	7, 8, 10, 12
Gain (dB)	40, 50, 60, 70, 80, 90, 98
Depth (cm)	0.5, 1.0, 1.5, 2.0, 2.5, 3.0
Dynamic Range (dB)	30, 45, 60, 75, 90, 105, 120
Power Output (%)	20, 30, 40, 50, 60, 70, 80, 90, 100

Table 5-2.The ranges of system settings, for each parameter, that were studied.

When studying the effect of the depth on EI measurement, a same sized ROI was used at different depths.

The US images were recorded on a tape (in AVI format) using a commercial video recorder. The stored video data from tape was transferred to a personal computer using Adobe Premier Pro 2.0. Still images (five per subject, TIFF, 720×480 pixels, and 8-bit gray levels) were captured from the movie sequence using Adobe Premier Pro 2.0 for data analysis.

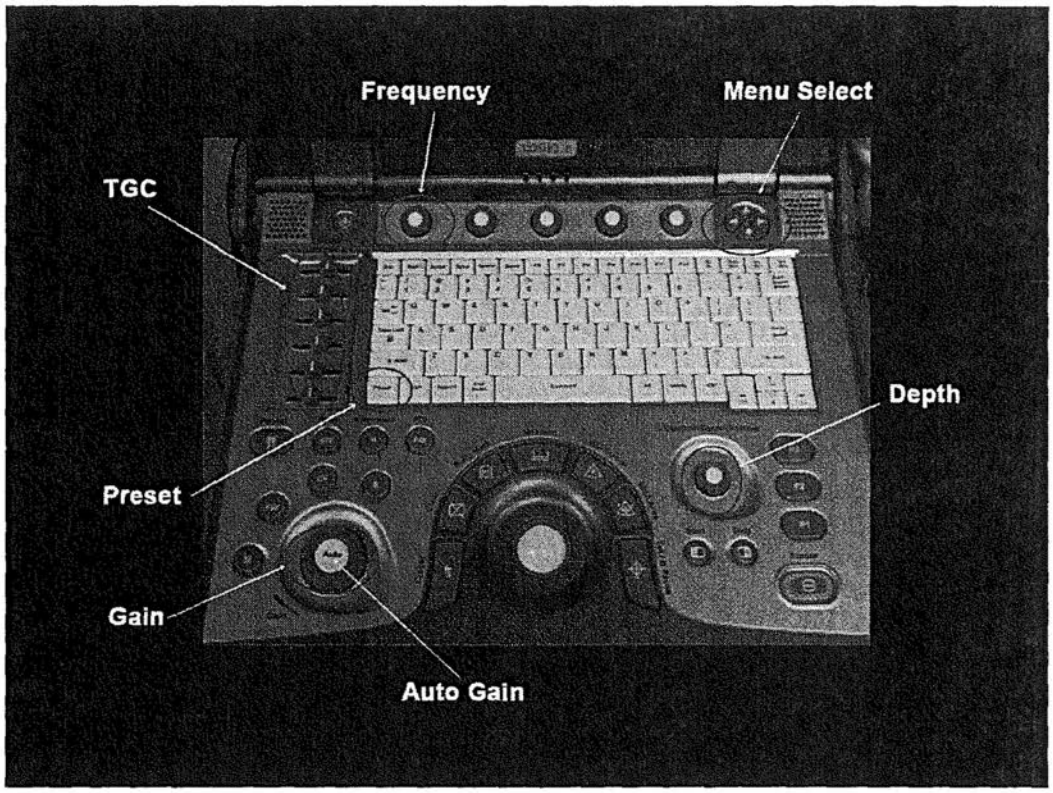

Figure 5-4. Operation panel of a LOGIQ® *e* US system. The common function keys are labeled. TGC=time gain compensation.

5.2.6 Image Normalization

The digital images were normalized using Adobe Photoshop CS2. Details are outlined in **Section 3.6.2**. During normalization, the gray-scale values of all pixels in the image were adjusted according to the values of two reference points (pure black=0; pure white=255) and this was done to allow a comparison of the EI of individual images in the same gray-scale range.

5.2.7 ROI Selection and Echo Intensity Measurement

Computer assisted gray-scale analysis (Adobe® Photoshop CS2) was then performed to measure the EI. A polygonal ROI was drawn around the outlines of the simulated nerve using the elliptical marquee tool in the Adobe Photoshop CS2. The mean (SD)

and median (range) EI of the ROI was determined using the standard histogram function in Adobe® Photoshop CS2.

5.2.8 Statistical Analysis

Statistical Package for the Social Sciences (SPSS) for Windows 14.0 (SPSS Inc., Chicago, IL, USA) was used for the statistical analysis. Pearson correlation coefficient was calculated to assess the strength and direction of the linear relationship between all paired variables; the probability of a given Pearson correlation coefficient (r) was also determined. A simple linear regression model analysis was used to explore the relationship between the dependent variable (EI) and five independent variables (system settings). Otherwise, curve estimation procedure was used to estimate regression statistics and produce related plots for the relationship if it was not necessarily linear. A p-value less than 0.05 was considered statistically significant.

5.3 Results

A total 165 still US images were obtained and analyzed from the Blue Phantom in this study. All EI measurements were determined using the standard histogram function of Adobe Photoshop CS 2.

5.3.1 Gain

Figure 5-5a shows the relationship between the EI measurement and gain settings. Each scatter plot in the figure represents an EI measurement of the ROI. Regression analysis demonstrates a linear relationship between the EI and the gain setting. Seven gain settings from 98 to 40 dB were used to test its effect on EI measurements. A positive correlation (Pearson's $r = 0.99$; $p<0.0005$) was seen between the EI and gain.

5.3.2 Frequency

Four frequency settings were studied (7, 8, 10, 12 MHz) using the 12L-RS transducer (5-13 MHz, 42 mm footprint). The lowest frequency was 7 MHz while the highest one was 12 MHz. The relationship between the EI measurement and the US frequency are presented in **Fig. 5-5b**. Regression analysis demonstrates that the EI decrease with an increase in US frequency. Moreover, there was a negative correlation (Pearson's $r=-0.845$; $p<0.0005$) between the EI measurement and the US frequency.

5.3.3 Dynamic Range

Six different sets of dynamic range settings, from 120 dB to 20dB, were used to investigate its effect on EI. **Figure 5-5c** illustrates there is a decease in the EI measurement with an increase in dynamic range. There was also a negative correlation (Pearson's $r=-0.91$; $p<0.0005$) between the EI measurement and the dynamic range.

5.3.4 Depth

Six different depth settings (0.5-3cm) were used to study the effect of depth on EI measurement. There was a decrease in the EI with an increasing depth (**Fig. 5-5d**). There was a negative correlation (Pearson's $r=-0.96$; $p<0.0005$) between the EI measurement and the depth.

5.3.5 Power Output

Five power output settings were used to study the effect of power output on EI measurement (**Fig. 5-5e**). There was an increase in the EI with an increase in the

power output. A positive correlation (Pearson's r= 0.95; p<0.0005) was seen between the EI and power output.

5.4 Discussion

In this in-vitro study, using computer-assisted gray-scale analysis we have demonstrated that changes in the system settings of an US system can affect the EI measurements in an US image.

5.4.1 Effect of Gain on the Echo Intensity

There was a positive correlation between the EI and the amount of gain used. Our finding is in agreement with results previously published by Zaidman et al. (Zaidman et al., 2008) who also demonstrated a positive correlation between the gray-scale level and gain. They found that an increase in the overall gain setting (from 0 to 40 dB) result in an increase in gray-scale levels (from 0 to 255) of the US image. This indicates that a change in the gain can affect the gray-scale level of an US image. Returning signals from a tissue produce voltage pulses in the transducer, which are then sent to the US unit for processing. The small voltages of the electric signals are amplified (Hendee and Ritenour, 2002a, Pinkney, 1995a, Pinkney, 1995b). Gain is the ratio of the amplifier output to the input electric power, and determines how much amplification is accomplished in the amplifier (Kremkau, 2002). When the gain is increased, the smaller voltages of the signal are amplified to larger ones, which result in an increase in the brightness of an object. This explains our finding.

5.4.2 Effect of Frequency on the Echo Intensity

The EI of the ROI in the phantom decreased with an increase in the frequency of US. We are not aware of any comparable data directly evaluating the relation between US

frequency and EI measurement. The amplitude of reflected echoes is dependent on the attenuation of the US energy as it travels through tissue, so greater the attenuation of the US signal, less is reflected back to the transducer (Hedrick et al., 2005). Knipp et al. (Knipp et al., 1997) have shown that when the US frequency is increased from 2.5 MHz to 7MHz, the attenuation increased from approximately 2dB/cm to 7dB/cm, which suggests a positive correlation between the attenuation and frequency of US beams. Theoretically, the amount of attenuation of an US beam can be calculated using the equation (Hedrick et al., 2005).

$$Intensity(loss) = \mu \times f \times z \quad (5.1)$$

where *Intensity (loss)* means intensity (dB) loss by attenuation, μ means attenuation coefficient of the medium, f means the frequency of the US beam, and z means the distance traveled in the medium. With a constant μ, the attenuation of the US beam is directly proportional to both the US frequency and the depth it travels through the tissue. Therefore, an increase in the US frequency results in an increasing attenuation of US beam, and may explain the decrease in the EI with an increase in the US frequency that we have demonstrated.

5.4.3 Effect of Dynamic Range on the Echo Intensity

The EI of the ROI decreased with an increase in the dynamic range. Using an US phantom, Scorza (Scorza, 2009) demonstrated that the mean gray-scale level of a ROI (10 x 10 pixels, placed at 80mm depth) in the US image was approximately 100, 150, 200 and 250 when the dynamic range setting was 90dB, 60dB, 40dB and 20dB, respectively. These results suggest that lower dynamic range setting results in higher gray-scale level in an US image. In theory, dynamic range in decibels can also be

calculated by the equation: (Hedrick et al., 2005,Hendee and Ritenour, 2002a,Hendee and Ritenour, 2002b,Kaplan and Qinglin Ma, 1994)

$$DR = 20 \log \frac{A}{a} \quad (5.2)$$

In the **equation (5.2)**, DR equals dynamic range, A equals the strongest allowable signal and a equals the weakest signal. Dynamic range is the ratio of the largest signal to the smallest signal that an US system can handle. This function is used to determine how the gray-scale range of an US image is displayed after the gray-scale range of echo signals are compressed by the processing unit (Hedrick et al., 2005,Kremkau, 2002). When the dynamic range is reduced, the weaker portion of the strength of echo signals is set to a lower brightness level (blacker), and the stronger portion of the echo signals is set to a higher brightness level. This explains why the EI of the hyperechoic simulated nerve (**Fig. 5-3**) in the US image from the phantom decreased with an increase in dynamic range in this study.

5.4.4 Effect of Depth on the Echo Intensity

The EI of the ROI also decreased with an increase in the depth. This is in agreement with the results published by Knipp et al, (Knipp et al., 1997) who also demonstrated in an "in-vitro" model that mean gray-scale levels decreased when the depth was increased. Lefebvre et al. (Lefebvre et al., 2000) have also demonstrated that a change in depth setting results in 10-20% variation in the gray-scale level in the phantom image. When an US beam travels through a medium, it gradually attenuates because of absorption, reflection and scattering. There is a positive relation between the attenuation of US and the distance (depth) it travels in a medium (Hedrick et al., 2005,Hendee and Ritenour, 2002b). Therefore, attenuation explains the decrease in the EI with increasing depth of scan that we have demonstrated in this study.

5.4.5 Effect of Power Output on the Echo Intensity

We also found that there was a relation between EI and the power output used for the scan. To the best of our knowledge, there are no comparable data. Jaffe and Harris (Jaffe and Harris, 1980) have reported that different power outputs (22dB vs.16dB) from an US system result in a visible difference in the appearance of US images of the liver. However, this was only a subjective visual evaluation. Forsberg et al. (Forsberg et al., 2005) state that when the mechanical index (MI) is decreased from 0.7 to 0.3, the video intensity is reduced up to 32%. The power output of an US system controls the strength of the US beam emitted from the transducer. If the ROI is located at the same depth in a medium, then the stronger the US emitted from the transducer, the greater is the amplitude of the reflected US beam from the ROI, which results in an increase in the brightness of the image displayed on the US screen. This explains why an increase in power output results in an increase in the EI of a ROI in the US image.

5.5 Limitations

Our results must be interpreted after considering that this was an in-vitro study using a tissue-mimicking phantom. By doing so we were unable to simulate the conditions of musculoskeletal structures in-vivo. Therefore, our results may not translate to the same effects during clinical US imaging. Future research evaluating the effect of US system setting on the echo intensity of musculoskeletal structures in-vivo is warranted.

5.6 Conclusion

In conclusion, using a tissue-mimicking phantom we have demonstrated a positive linear relation between the echo intensity and the amount of gain and power output used, and a negative linear relation between the echo intensity and the frequency, dynamic ranges and depth. Therefore, it is crucial to standardize the settings of an US system during quantitative ultrasonography.

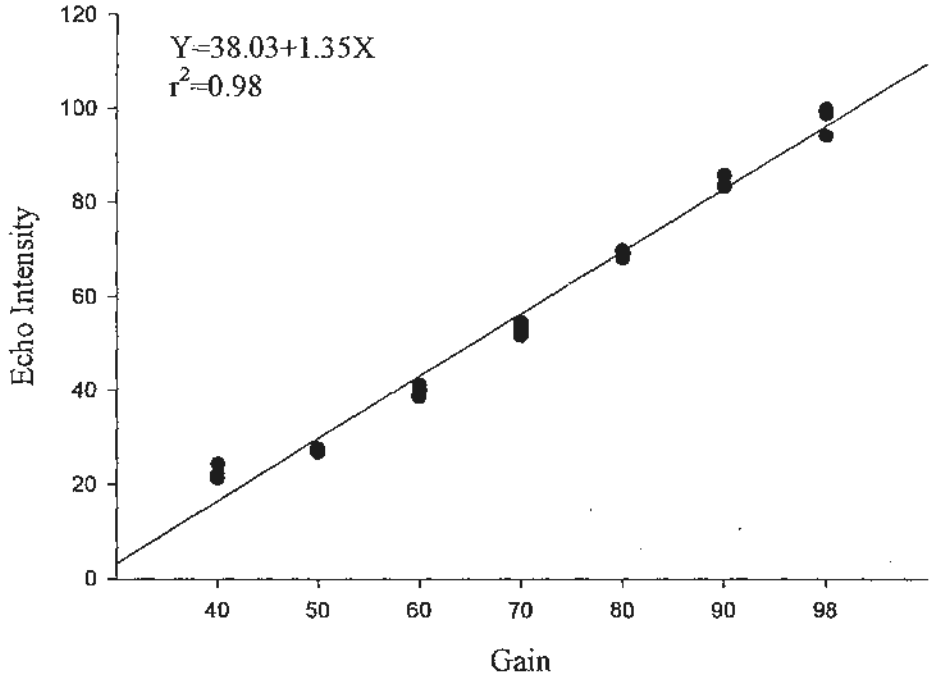
Y=38.03+1.35X
r²=0.98
Echo Intensity
Gain
0
20
40
60
80
100
120
40
50
60
70
80
90
98

(a)

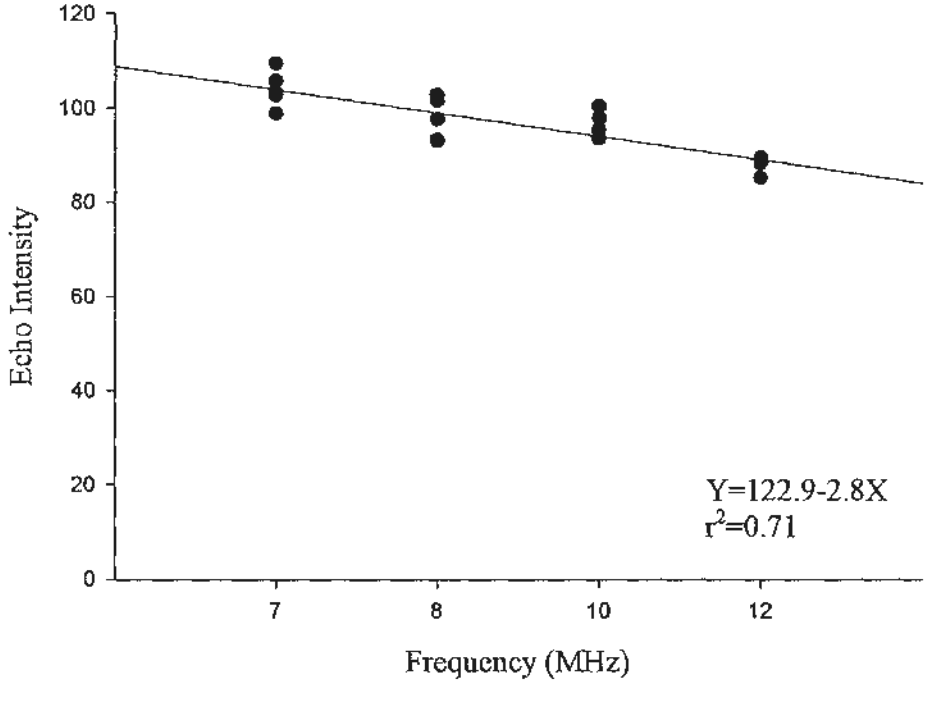
Y=122.9-2.8X
r²=0.71
Echo Intensity
Frequency (MHz)
0
20
40
60
80
100
120
7
8
10
12

(b)

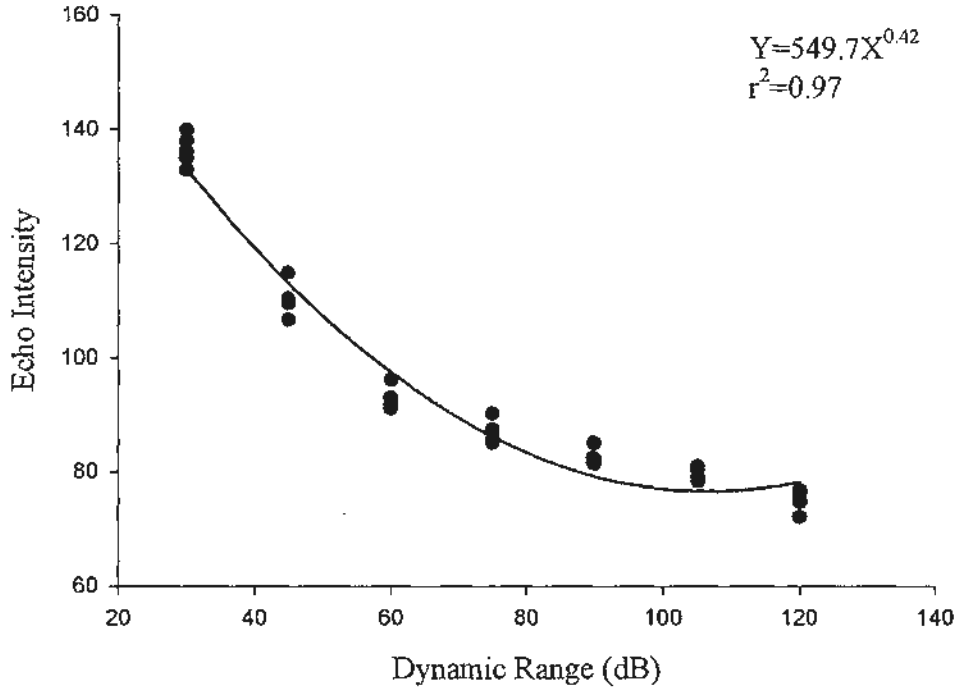
Y=549.7X^0.42
r²=0.97
Echo Intensity
Dynamic Range (dB)
160
140
120
100
80
60
20
40
60
80
100
120
140

(c)

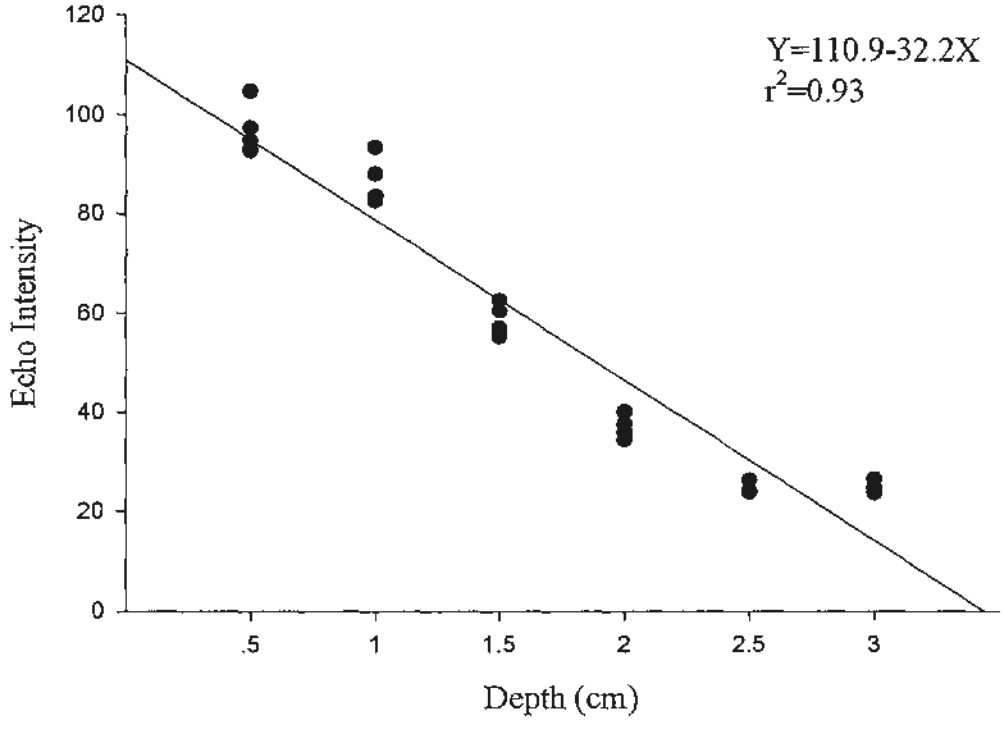
Y=110.9-32.2X
r²=0.93
Echo Intensity
Depth (cm)
120
100
80
60
40
20
0
.5
1
1.5
2
2.5
3

(d)

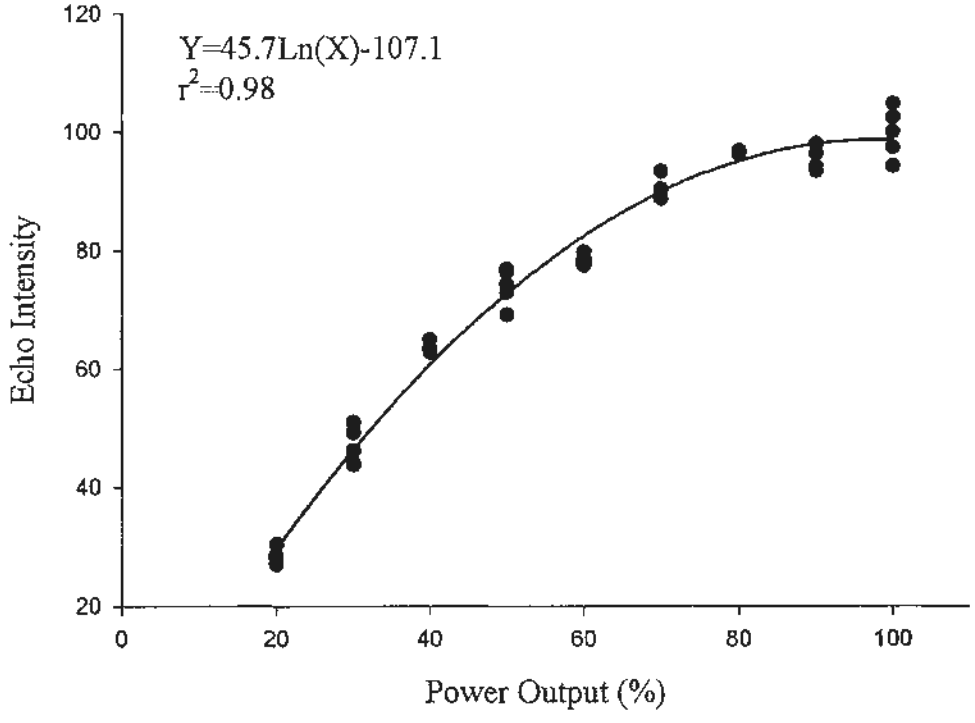

(e)

Figure 5-5. The relationship between echo intensity and US system settings. (a) Positive correlation between the EI and gain setting; (b) Negative correlation between the EI and US frequency; (c) Negative correlation between the EI and dynamic range; (d) Negative correlation between the EI and depth setting and (e) Positive correlation between the EI and power output of an US system.

Chapter 6

"Off-cart" Measurements of Musculoskeletal Structures at the Infraclavicular Fossa

6.1 Introduction and Objective

During US imaging, measurements of distance and area are performed using an electronic caliper that is built into the US system, which is also referred to as "in-cart" measurement. Such measurements have been performed before US guided peripheral nerve (Greher et al., 2002, Kuo et al., 2007, Ootaki et al., 2000, Perlas et al., 2003, Wang et al., 2007) and central neuraxial (Cork et al., 1980, Grau et al., 2002a) blocks to decide on the best possible site and maximum safe depth for needle insertion. However, this process is relatively time-consuming and also interrupts the scan. In contrast, "off-cart" measurements are made on US image using image analysis software at a later stage, and several methods have been described in the literature (Karmakar et al., 2009, McCartney et al., 2007, Morita et al., 2007, Nakamichi and Tachibana, 2000). However, there are no data comparing the accuracy of these methods, which this study was designed to evaluate. A secondary goal of this study was to evaluate any gender or age-related differences in the dimensions of musculoskeletal structures at the infraclavicular fossa using the "off-cart" method that was developed for this study.

6.2 Material and Methods

6.2.1 Study Design

This was a non-randomized observational, cohort study which was approved by the Joint The Chinese University of Hong Kong-New Territories East Cluster Clinical Research Ethics Committee 2009 (**CREC Reference No.: CRE-2009.096**) (See Appendix). The study was conducted in the Department of Anesthesia and Intensive Care of The Chinese University of Hong Kong at the Prince Wales Hospital, Shatin, Hong Kong.

The musculoskeletal structure at the left infraclavicular fossa was selected for the US scan because they are relatively superficial structures and are readily accessible for US imaging.

6.2.2 Inclusion and Exclusion Criteria

98 consenting Hong Kong, Chinese adult patients at the Prince of Wales Hospital who were due to undergo surgery were recruited for this study. The following patients were excluded:

1). No informed consent

2). Presence of infection, trauma, or injury in the left infraclavicular fossa

3). Patients with diabetes, advanced tumors, neuropathy, or musculoskeletal disorders

4). ASA physical status > III.

6.2.3 Equipment and Software Used

The US scans were performed by a single investigator, the project supervisor (MK), who is experienced in US imaging, using a single US system with a high-frequency linear array transducer (HFL38, 13-6 MHz, 38 mm footprint). Once an optimal image was obtained, the data from the US system were recorded on a tape using a Sony video camera via the video output terminal. Adobe® Premier Pro 2.0 **(Fig. 3-1c)** was used to capture the video loop from tape and store it as a still in TIFF for data analysis. Image-Pro® Plus 6.2 was used to perform the "off-cart" measurements of distance (or width) and CSA **(Fig. 3-1f)**. All data download for processing or analysis were stored on a personal laptop computer **(Fig. 3-1g).**

6.2.4 System Setting

The US scan of the left infraclavicular fossa and "in-cart" measurements were independently performed by the project supervisor (M.K.). The default, "Small Parts" preset, "General" image optimization setting was used for each scan. Dynamic range was set to a preset level equal to 0, and depth was set to 4.9 cm. Gain was manually adjusted to optimize the US image.

6.2.5 Preparation for the Patient

All scan and measurements were performed preoperatively and before the induction of anesthesia. The patient was positioned in the supine position with the head turned away from the side scanned. The left arm was abducted to 90 degrees, and externally rotated such that the palm of the hand was facing the ceiling, and positioned at the same level as the heart. The arm was also placed on a padded arm rest. **(Fig.6-1)**

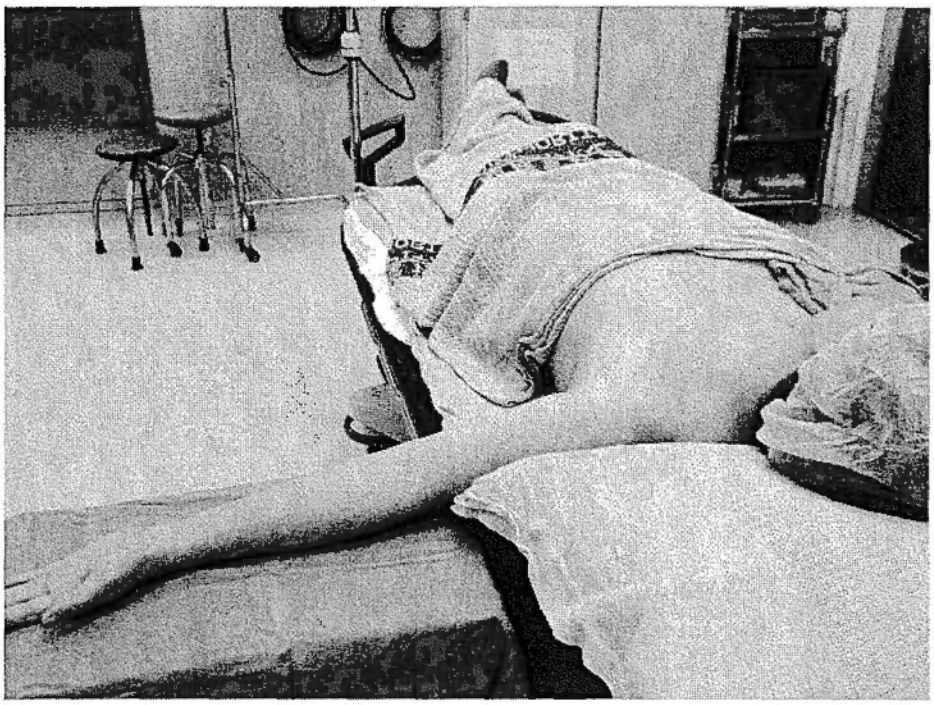

Figure 6-1. Shows the position of the patient in this study.

6.2.6 Scan Method

The coracoid process was identified in the infraclavicular fossa and marked. After skin preparation a high-frequency 13-6MHz linear-array transducer was positioned infero-medial to the coracoid process underneath the clavicle in a parasagittal plane to obtain the best saggital view of the axillary artery (**Fig. 6-2**). Liberal amounts of US gel was applied for acoustic coupling between the skin and the transducer. The transducer was aligned so that it was perpendicular to the axillary artery. Care was taken not to exert undue pressure over the scanned area because pressure by distorting the tissue, can affect the measurements of the musculoskeletal structures. Thereby a saggital image of the infraclavicular fossa was obtained (**Fig. 6-2**). Structures that were imaged included the skin, subcutaneous tissue (and breast tissue in females), pectoralis major and minor muscles, axillary artery and vein (2^{nd} part), and cords of the brachial plexus. (**Figs. 6-2; 6-3**)

6.2.7 Infraclavicular Fossa Sonoanatomy

The pectoralis major muscle is situated at the upper and anterior part of the chest wall, and makes up the bulk of the chest wall muscles in males (**Fig. 6-2a**) and lies under the breast in females. (**Fig. 6-2b**) As illustrated in **Fig. 6-2**, the pectoralis major muscle is deep to the skin and subcutaneous tissue, and the smaller and thinner pectoralis minor muscle lies deep to the former. In females the breast tissue is seen as lobulation overlying the pectoral muscles in a sonogram (Gilda, 2004). The pectoralis minor muscle also tapers superiorly toward the coracoid process. In addition, a bright hyperechoic fascial layer separates the two hypoechoic muscles. The axillary artery and vein (2^{nd} part) lie under the pectoralis minor muscle and fascia. The axillary artery is located superior and medial to the axillary vein in the infraclavicular fossa. The three cords of the brachial plexus are arranged around the axillary artery. The lateral cord lies superior and lateral, the posterior cord lies posterior and the medial cord lies posterior and medial to the axillary artery (Demondion et al., 2003,Galloway and Bodenham, 2003,Gilda, 2004,Greher et al., 2002,Karmakar and Kwok, 2009,Ootaki et al., 2000,Wang et al., 2007).

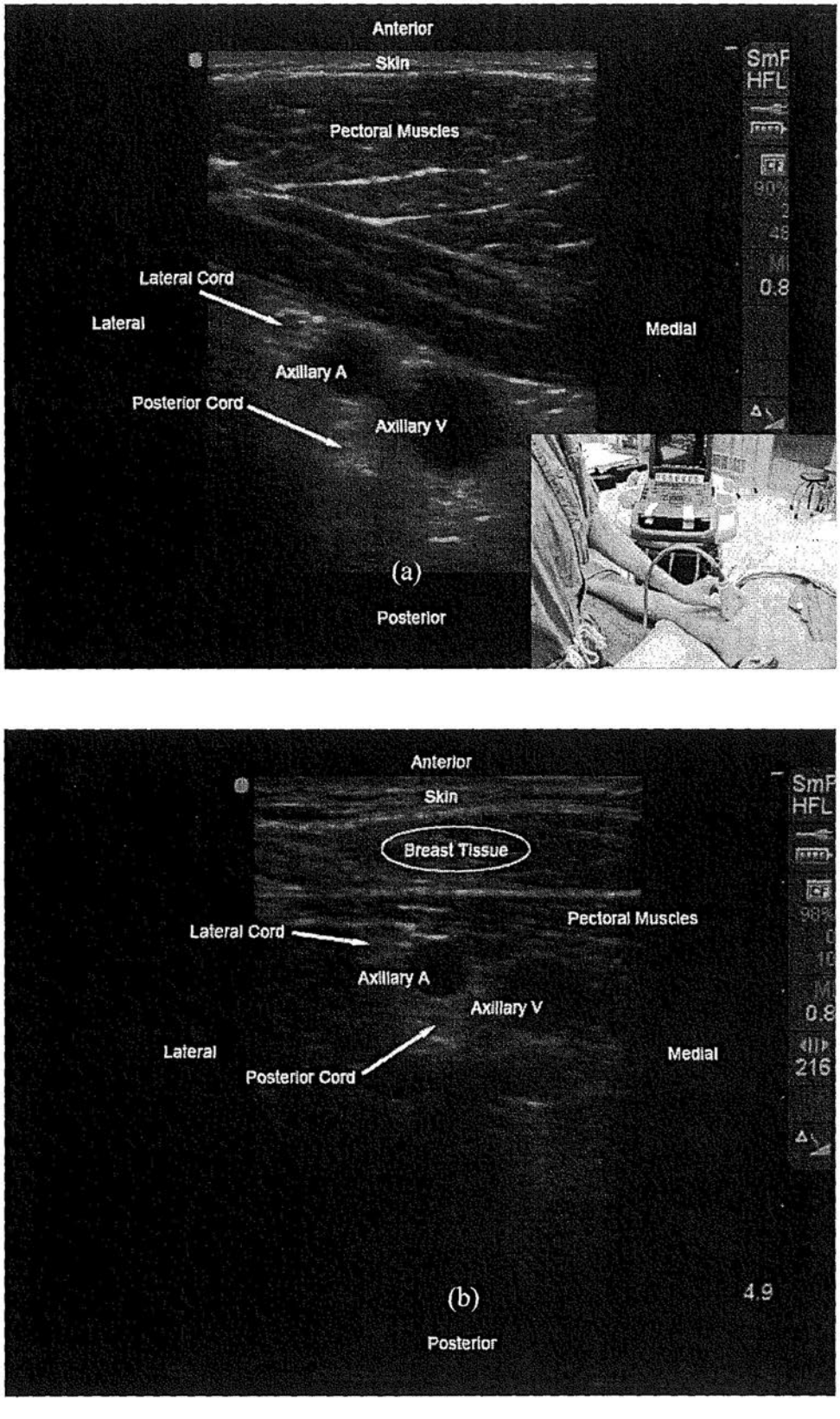

Figure 6-2. A typical sagittal sonogram of the left infraclavicular fossa in (a) a male and (b) a female. The inset in (a) shows the position of the patient and the high-frequency linear-array transducer in the left infraclavicular fossa. Breast tissue in a female is encircled in (b).

6.2.8 "In-cart" Measurements

Once an optimal image was obtained, the image was frozen on the monitor, and "in-cart" measurements of distance (or width) and area (CSA) were performed using the electronic caliper that is built into the US system. The parameters that were measured included:

1). Vertical distance from the skin to the anterior wall of the axillary artery (SA) and vein (SV) (**Figs. 6-3a, b**)

The first point of the caliper was positioned on the skin surface in the US image, and the other caliper was positioned on the anterior wall of the axillary artery and vein.

2). Maximum diameter of the axillary artery (DA) and vein (DV) **(Figs. 6-2c, d)**

3). Cross sectional area (CSA) of the axillary artery (AA) and vein (AV) **(Figs. 6-2e, f)**

4). Width of the pectoral muscles (PM, pectoralis major and minor muscle) **(Fig. 6-1b)**

In this study, the width of the pectoralis major and minor muscles could not be measured separately because it is often difficult to accurately delineate the interface between the two muscles in an US image.

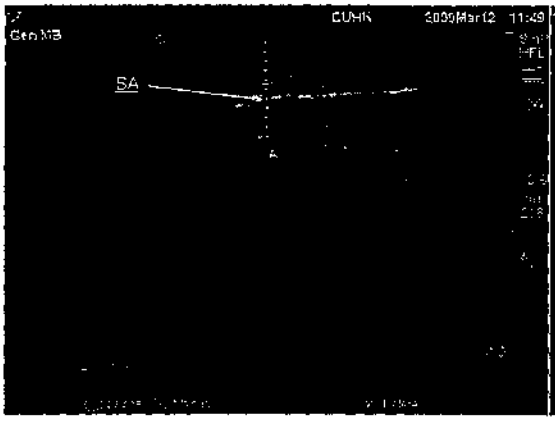
CUHK
2009Mar12 11:49
Gen MB
SA

(a)

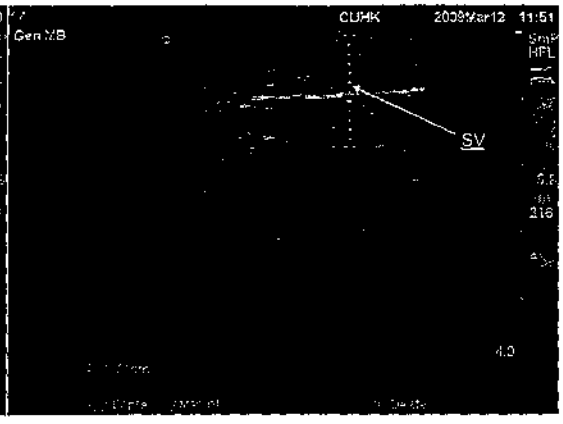
CUHK
2009Mar12 11:51
Gen MB
SV

(b)

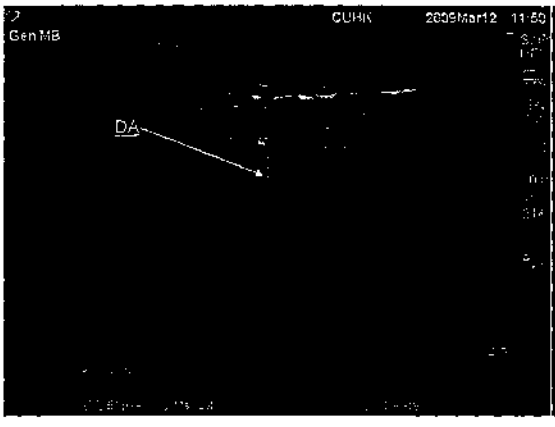
CUHK
2009Mar12 11:50
Gen MB
DA

(c)

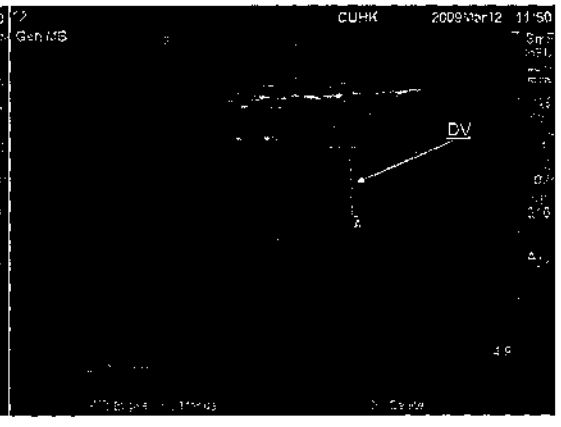
CUHK
2009Mar12 11:50
Gen MB
DV

(d)

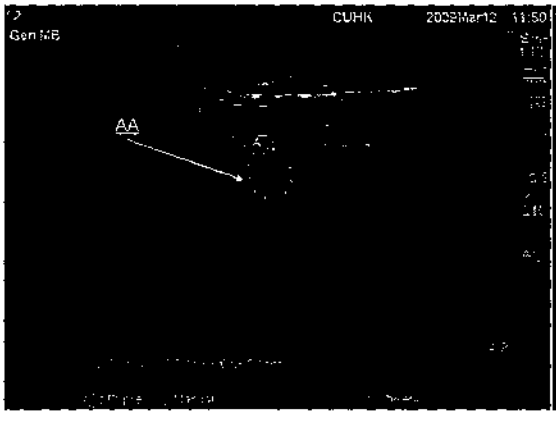
CUHK
2009Mar12 11:50
Gen MB
AA

(e)

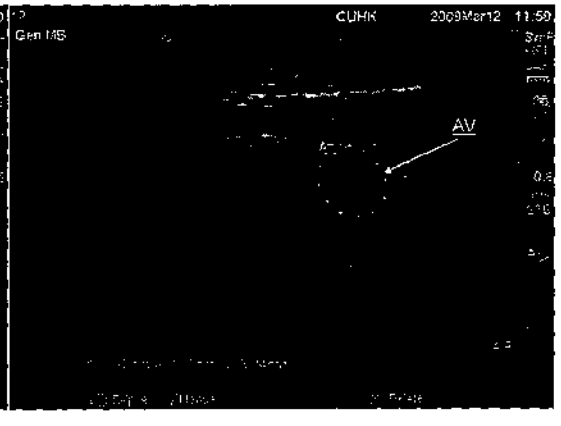
CUHK
2009Mar12 11:50
Gen MB
AV

(f)

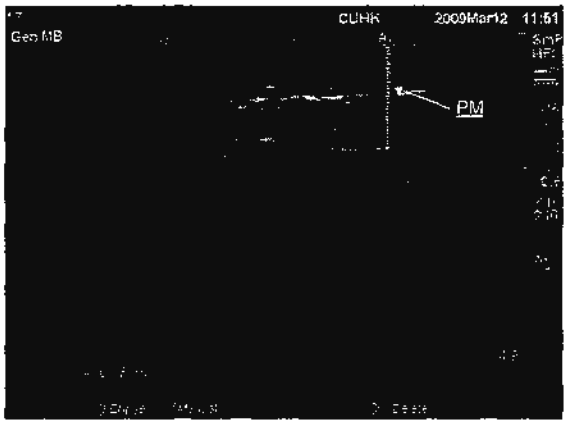

(g)

Figure. 6-3 Illustrates the "in-cart" measurements of various parameters on a typical sagittal sonogram of the left infraclavicular fossa. SA= vertical distance from the skin to the anterior wall of the axillary artery, SV= vertical distance from the skin to the anterior wall of the axillary vein, DA=maximum diameter of the axillary artery, DV= maximum diameter of the axillary vein, AA=CSA of the axillary artery, AV=CSA of the axillary vein and PM=width of the pectoral muscles.

6.2.9 Image Acquisition and Data Transfer

Once an optimal image was obtained, US images were recorded on tape (in AVI format) using a commercial video recorder (Sony Corporation, Ltd., Minato-ku, Tokyo, Japan) via the video output terminal. The stored video from the tape was transferred to a personal computer using Adobe Premier Pro 2.0 (Adobe Systems Inc, San Jose, CA, USA) and still images were captured (3 per subject, TIFF format, 720×576 pixels and 8-bit gray levels) from the movie sequence and stored for data analysis. More details are outlined in **Section 3-4** of **Chapter 3**.

6.2.10 Spatial Calibration

A reference US image was imported into the IPP 6.2 (Media Cybernetics, Silver Spring, Maryland, USA) window. A reference line, calibration scale, was set to match the depth scale (4.9 cm) marked on the US image vertically. Thereafter, the

spatial calibration, 93 pixels /cm in the horizontal (X) and vertical (Y) axes of the US image was determined. Since the depth setting was standardized in this study, the spatial calibration scale was valid for all the US images in which "off-cart" measurements were made.

6.2.11 "Off-cart" Measurements

The appropriate spatial calibration scale described above saved was selected in IPP. To measure the distance (SA and SV), diameter (DA and DV) and width of PM, a straight line was stretched between two anatomical landmarks. To measure CSA of the artery and vein (AA and VA), a polygon ROI surrounding the outline of the axillary artery and vein in the US image was created using the freehand polygon tool. A closed figure of the vessels was thereby obtained. Results of SA, SV, DA, DV, AA, AV and PM were expressed in mm (or mm^2). More details are outlined in **Sections 3.5.1-3.5.3** of **Chapter 3**.

6.2.12 Reproducibility Testing

Please refer to **Sections 4.2.8** and **4.4.1** in **Chapter 4**.

6.2.13 Statistical Analysis

G Power for Windows 3.0.10 (Franz Faul, University Kiel, Germany) was used to determine the sample size of this study. Prospective power analysis based on pilot data showed that 24 subjects per group would have an 80% power to detect a mean difference of 5mm in the distance from skin to axillary artery between the young (age< 40 years) and the elderly group (age≥ 60 years), assuming that the common standard deviation was 6mm using a two group t-test with a 0.05 two-sided significance level.

Data were analyzed using SPSS for Windows 14.0 (SPSS Inc., Chicago, IL, USA). The mean measurements from the three images from each subject were transformed into one mean result for statistical analysis. The Kolmogorov-Smirnov test was used to test the normality of the data recorded. If the data were normally distributed, they are presented as a mean (SD; 95% CI); otherwise, they are presented as a median (range). The difference in the demographic data of three age-stratified groups (**Table. 6-1**) was tested using One-way analysis of variance (ANOVA), and the difference in the demographic data of the males and females (**Table. 6-2**) was tested using two independent sample t-test. Chi-square test was used to compare the number of males and females in the three age-stratified study groups. The variability of the results obtained using the two measurement methods, "off-cart" and "in-cart" measurements, was tested using the intraclass correlation coefficient (ICC). The paired samples t-test was also used to compare the systematic differences in the results obtained using the two measurement methods. This allowed us to determine the consistency of the measurements methods. In addition, these 98 patients were divided into age-stratified groups or gender-related groups, respectively, to investigate age and gender related differences in the dimension of musculoskeletal structure at the infraclavicular fossa using "off-cart" measurement method. An independent two samples t-test was used to test the difference in the sonoanatomy parameters between the male and female groups. Patients were divided into three age-stratified groups, Group 1 (<42 years old), Group 2 (42-58 years old), and Group 3 (>59 years old) using the Visual Binning function of SPSS to produce approximately equal number of patients each group for statistical comparison. Two-way ANOVA was used to determine the impact of gender and age on all measured parameters of musculoskeletal structures. When the analysis of variance was significant, the Bonferroni Post-hoc test was

performed. A probability value of $p<0.05$ for two-sided tests was considered statistically significant.

6.3 Results

6.3.1 Demographic Data

98 patients were recruited for this study. The demographic data of the three age-stratified groups are presented in **Table 6-1**. The mean (SD; range) height ($p=0.06$), weight ($p=0.41$) and BMI ($p=0.89$) were comparable between the three groups, and the number of male and female patients in each group was also comparable ($p=0.11$).

The demographic data of the gender-related groups are presented in **Table 6-2**. The mean (SD; range) age between the male and female groups was comparable, $p=0.52$. However, as expected, the weight and height in the male group was greater than that in the female group, $p<0.0005$, but the BMI ($p=0.24$) was comparable.

6.3.2 Correlation between "In-cart" and "Off-cart" Measurements

As presented in **Table 6-3,** there were no significant difference in the various parameters measured using the "off-cart" and "in-cart" methods. Furthermore, the ICC of all the measurements made using the "off-cart" and "in-cart" methods were greater than 0.75. This proves that there was good consistency between the two methods used to measure distance and CSA in this study (Portney and Watkins, 2000).

6.3.3 Parameter Measured at the Infraclavicular Fossa

Parameters that were measured at the infraclavicular fossa using the "off-cart" method are presented in **Tables 6-5** and **6-6**.

6.3.3.1 Distance from the Skin to the Axillary Artery and Vein

The mean SA and SV was comparable in the male and female subjects, p=0.93 and p=0.54, respectively. The mean SV in Group 1 was significantly greater than that in Group 3 (p=0.003). No significant difference in mean SA was found between the three age-stratified groups (p=0.15).

6.3.3.2 Diameter of the Axillary Artery and Vein

The mean DA in the male group was significantly larger than that in the female group (p<0.0005). The mean DV in the males was also significantly larger than that in the females (p=0.006). The mean DA in Group 3 was also significantly larger than that of Group 2 (p=0.03) and Group 1 (p=0.009). The mean DV was comparable between the three age-stratified groups (p=0.66).

6.3.3.3 Cross Sectional Area of the Axillary Artery and Vein

The mean CSA of the AA and AV in the males were significantly larger than that in the females (p<0.0005). The mean CSA of the AA in Group3 was also significantly larger than that in Group 2 and Group 1 (p<0.0005). The mean CSA of the AV in the three age-stratified groups were comparable, p=0.96.

6.3.3.4 Width of the Pectoral Muscles

The mean width of the PM in the males was significantly larger than that in the females, $p<0.0005$. The mean width of the PM in Group 2 and Group 3 was significantly smaller than that in Group 1, $p<0.0005$, but it was comparable between Group 2 and Group 3, $p=0.16$

6.4 Discussion

In this study we have demonstrated that there is a good correlation between measurements made by "off-cart" and "in-cart" methods. Using the "off-cart" method we also found age-stratified and gender related differences in measurements of musculoskeletal structures made at the infraclavicular fossa.

6.4.1 Reproducibility of "Off-cart" Measurement

The method used for "off-cart" measurement of distance and area in this study is valid, reliable and reproducible.(Please refer to **Section 4.3.2** and **4.4.1**) Our results are in agreement with previously published data (Nakamichi and Tachibana, 2000,Reeves et al., 2004,Sanada et al., 2006). Please refer to **Section 4.3.2** and **Section 4.4.1** in **Chapter 4** for details.

6.4.2 Correlation between "In-cart" and "Off-cart" Measurements

We have demonstrated that there is a good correlation between the "in-cart" and "off-cart" measurement of distance (or diameter and width) and CSA in a sonographic image. There are no comparable data in the literature. Normally, the distance and area measurements are performed using an electronic caliper that is built into the US system. Such "in-cart" method has been used to measure the distance or area of a

ROI in a muscle, (Abe et al., 1998,Maurits et al., 2003,Young et al., 1984,Young et al., 1985) blood vessel, (Galloway and Bodenham, 2003, Greher et al., 2002) peripheral nerve (Greher et al., 2002, Kuo et al., 2007, Ootaki et al., 2000, Perlas et al., 2003, Wang et al., 2007), and central neuraxial structure (Cork et al., 1980, Grau et al., 2002a). The "off-cart" measurement of distance and area in a sonographic image using computer software has a good reproducibility (Nakamichi and Tachibana, 2000), and is also valid and reliable (Reeves et al., 2004,Sanada et al., 2006). However, to the best our knowledge, there are not data comparing the two methods. We believe the present study may be the first study to compare "off-cart" and "in-cart" methods of measuring dimension in musculoskeletal sonogram using image analysis software. Based on our findings, we believe the "off-cart" method that was used in this study, can substitute the "in-cart" method of measurement for research purposes.

6.4.3 Distance from the Skin to the Axillary Vessels

The distance from the skin to the axillary vein in Group 1 (<42 years old) was significantly greater than that in Group 3 (>59 years old). There are no comparable data in the literature. The reduced distance from the skin to the vessel in our elderly patients may be due to age-related changes in the musculoskeletal structures, particularly in the muscles. With aging there is a loss of skeletal muscle mass (Rosenberg, 1989). Arts et al. found that the peak muscle thickness occurs between 25-50 years old, thereafter it starts to decrease with advancing age (Arts et al., 2007). Therefore, the thickness of the skeletal muscles is smaller in the elderly than that in the young (Frontera et al., 2000a,Young et al., 1984,Young et al., 1985), which may explain the reduced distance from the skin to the axillary vein at the infraclavicular fossa in our elderly subjects.

6.4.4 Dimensions of the Axillary Vessels

The axillary artery in males was larger than that in females. Our finding is in accordance with published studies (Bjarnegard et al., 2003, van der Heijden-Spek JJ et al., 2000). Bjarnegard (Bjarnegard et al., 2003) showed that the mean diameter of the brachial artery was significantly larger in males (6.1mm) than in females (5.3 mm), $p<0.001$. van der Heijden-Spek, et al. also observed that the brachial artery diameter increased with age, and the diameter of the brachial artery in males (4.55 mm) was larger that that in females (3.65mm), $p<0.001$(van der Heijden-Spek JJ et al., 2000).

The axillary vein in males was also larger than that in females. There are no published data using US to quantify gender-related differences in the size or dimension of the axillary vein in the infraclavicular area. However, our findings are similar to that of Rominger, (Rominger, 1958) who described the diameter of the axillary vein in 100 adults using a venogram. During a venogram, renografin (contrast material) was injected into the veins and radiography was performed. The average diameter of the axillary veins at the lateral scapular border was 10 mm (range: 8-16 mm) in males and 8mm (range: 6-16 mm) in females, and at the first rib was 13 mm (range: 8-19 mm) in males and 11 mm (7-14 mm) in females. The documented difference (15-20%) in the diameter of the axillary vein between the male and female groups is comparable to the difference (16%) in the present study. Difference in the diameter of the common femoral vein (male 9.6 mm vs. female 7.4 mm) has also been demonstrated (Jeanneret et al., 1999).

The diameter and CSA of the axillary artery also increased with age. This is consistent with previously published data (Bjarnegard et al., 2003, Bjarnegard et al.,

2004, Kawasaki et al., 1987). Bjarnegard et al. have demonstrated that there is a slight positive correlation between the diameter of the brachial artery and age, and also showed that the diameter of the brachial artery in the elderly group (69 ± 2 years) was significantly larger than that in the young (25 ± 2 years). (Bjarnegard et al., 2003,Bjarnegard et al., 2004) Increase in the diameter of the brachial artery (Kawasaki et al., 1987), common carotid artery (Benetos et al., 1993), abdominal aorta (Kawasaki et al., 1987) and femoral artery (Kawasaki et al., 1987) with age have also been reported. These results suggest that age contributes to an increase in the diameter and CSA of the axillary artery.

The reason for the gender-related and age-stratified differences in the dimension of the axillary artery and vein is still poorly understood. With age there is an increase in the dilation of an artery (Bader, 1967, Sonesson et al., 1993), which may be due to degeneration of the elastic fibers and a parallel increase in the collagen tissue in the arterial wall. This leads to remodeling of the arterial wall (Dobrin and Mrkvicka, 1994, Watanabe et al., 1996), and may explain our findings. Moreover, the size of blood vessels is also related to the body size (Schroeder et al., 2000). As expected, in this study the height and weight of females were smaller than that in the males, which may explain the smaller dimension of the vessels in our female subjects.

6.4.5 Width of the Pectoral Muscles

The width of the PM in the males was significantly larger than that in the females. This is in agreement with Abe et al. (Abe et al., 1998, Abe et al., 2003). They measured the FFM and regional and total skeletal muscle (SM) using contiguous whole body magnetic resonance imaging (MRI), which demonstrated that the skeletal muscles of the chest and shoulder in males (288 cm^2) had a greater CSA than

that in the females (161cm^2) (Abe et al., 2003). Abe et al. also compared muscle architectural structure and fat free mass (FFM) between the young male and female using US, and they found that the mean muscle thickness (MTH) ratio of young females to young males was 62.8% (Abe et al., 1998). Moreover, Maurits et al. have demonstrated that the size of the muscles are larger in males than in females for all weight classes (Maurits et al., 2003). However, the reason of the gender-related difference is still not clear. As expected, the average height and weight in males is larger than that in females. There is a also positive strong relationship between the weight, height and the size of the muscle (Gallagher et al., 1997, Proctor et al., 1999), which may explain the gender-related differences in the width of the PM in this study.

The width of PM was larger in the young than in the elderly. There are no comparable data in the literature. This reduction in the width of PM may also be related to the age-related change in the human body composition. In the elderly there is a reduction in skeletal muscle mass (Evans, 1992, Gallagher et al., 1997) and a replacement of the contractile elements in the muscle by fat and connective tissue (Maurits et al., 2003) which is also called sarcopenia. (Rosenberg, 1989) Muscle thickness progressively increases until the age of 20 years, and peak muscle thickness is reached between the ages of 25-50 years old. Thereafter, it starts to decrease (Arts et al., 2007). An average adult can expect to gain approximately one pound of fat every year between ages 30 to 60, and lose about a half a pound of muscle over that same time span (Forbes, 1999, Gallagher et al., 1997). Marked reduction in the CSA of the muscles is also found in the elderly (Frontera et al., 2000a, Young et al., 1984, Young et al., 1985) because of atrophy in the aging muscle (Forbes, 1999, Frontera et al., 2000a, Frontera et al., 2000b, Gallagher et al., 1997).

These imaging and histological findings described above may explain the reduction in the width of the PM in the elderly of this study as expected.

6.5 Limitations

Our results must be interpreted after considering the following facts. This was a non-randomized observation cohort study. The population in the present study comprised of patients undergoing surgery with relatively good health, so they may not be representative of the general population. A previous investigation (Ko et al., 2001) was performed in the Prince of Wales Hospital on the 3718 Hong Kong Chinese subjects (Female: 3003 and Male: 715), who were examined and correlated with smoking habit. These subjects had known risk factors (i.e. a positive family history of diabetes, a history of gestational diabetes mellitus, obesity, and a previous history of impaired glucose tolerance) for glucose intolerance and were referred to the Diabetes and Endocrine Center to be screened for diabetes. Mean (range) age was 38.4 (12-88) years in these Chinese subjects, it was reported that 21.1% of subjects had diabetes, In addition, of the 715 male, 24.5% were smokers and 19.2% drank alcohol (Ko et al., 2001). Thus these potential confounding factors need be taken into account in future studies.

Another potential source of error is when too much pressure is applied over the area scanned when one can compress the underlying muscle, especially in thin individuals. Moreover, it is common knowledge that a patient's position may contribute to variation in the size of a vessels, for instance, the diameter of the axillary vein is increased by a head-down tilt due to increased venous pressure. Therefore, minimal pressure should be applied during musculoskeletal scan and same position should be maintained during US scan, which was done during this study.

6.6 Conclusion

In conclusion, in this study we have demonstrated that there is a good correlation between "in-cart" and "off-cart" measurements of dimension in musculoskeletal sonograms. The "off-cart" measurement that was performed at the infraclavicular fossa also demonstrated significant age and gender related differences in the size of musculoskeletal structures.

Table 6-1. Demographic data of the age-stratified groups.

Parameter	Group1 (n=33)	Group2 (n=34)	Group3 (n=31)	p-value
Gender (Male/Female)	M 20/ F 13	M 12/ F 22	M 16/ F 15	0.11
Age (yr)	< 42	42-58	>59	
Height (cm)	166.7 (6.4; 156-180)	164.0 (4.1;155-174)	163.8 (4.10; 152-173)	0.06
Weight (kg)	64.0 (13.2; 45-100)	61.6 (8.70; 47.5-81.5)	62.1 (10.4; 45-100)	0.41
BMI (kg/m^2)	22.9 (4.1; 17.1-36.7)	22.9 (2.8; 18.1-28.4)	22.8 (3.3; 16.9-36.7)	0.89

Data are presented as mean (SD; range). BMI=body mass index, n=frequency. $p < 0.05$ is considered statistically significantly.

Table 6-2. Demographic data of the male and female subjects.

Parameter	Both (n=98)	Male (n=48)	Female (n=50)	p-value
Age (year)	48.8 (18.1;18-85)	47.7 (21.2; 18-85)	49.9 (14.6; 23-82)	0.52
Height (cm)	164.9 (4.10; 152-180)	168.6 (4.5; 158-180)	161.3 (3.6; 152-172)	<0.0005
Weight (kg)	62.1 (10.4; 45-100)	66.0 (10.5; 46-100)	58.4 (8.9; 45-92)	<0.0005
BMI (kg/m^2)	22.8 (3.3; 16.9-36.7)	23.2 (3.6; 16.9-36.7)	22.4 (3.0; 18.0-31.1)	0.24

Data are presented as mean (SD; range). $p<0.05$ is considered statistically significantly. n=frequency.

Table 6-3. Correlation and comparison of "in-cart" and "off-cart" measurements

Parameter	Number of Subjects (n)	ICC (95%CI)	p-value (t-test)
SA	98	0.99 (0.993-0.997)	0.08
SV	98	0.98 (0.981-0.991)	0.06
DA	98	0.87 (0.811-0.911)	0.60
DV	98	0.97 (0.948-0.976)	0.30
AV	98	0.96 (0.934-0.970)	0.05

The intraclass correlation coefficient (ICC; 95% CI) is presented. The p-value is the probability of two measurements assessed using the paired-sample t-test. n=frequency. $p<0.05$ is considered statistically significantly. SA= vertical distance from the skin to the anterior wall of the axillary artery, SV= vertical distance from the skin to the anterior wall of the axillary vein, DA=maximum diameter of the axillary artery, DV= maximum diameter of the axillary vein, AA=CSA of the axillary artery, AV=CSA of the axillary vein.

Table 6-4. Measured parameters at the left infraclavicular fossa in the male and female subjects.

Parameter	All (n=98)	Male (n=48)	Female (n=50)	p-value
SA (cm)	2.41 (0.50;1.26-3.87)	2.43 (0.53; 2.25-2.54)	2.39 (0.47; 2.26-2.55)	0.93
SV (cm)	2.50 (0.53; 2.40-2.61)	2.49 (0.55; 2.31-2.60)	2.51 (0.52;2.37-2.67)	0.54
DA (cm)	0.62 (0.13; 0.27-0.95)	0.68 (0.12; 0.65-0.72)	0.57 (0.11; 0.53-0.60)	<0.0005
DV (cm)	0.92 [0.50-2.09]	0.99 (0.27; 0.92-1.06)	0.84 (0.18; 0.78-0.92)	0.006
AA (cm^2)	0.28 [0.11-0.89]	0.33 (0.14; 0.32-0.37)	0.26 (0.09; 0.23-0.29)	<0.0005
AV (cm^2)	0.69 [0.22-1.83]	0.76 (0.30; 0.73-0.89)	0.58 (0.22; 0.52-0.68)	<0.0005
PM (cm)	0.91 [0.40-3.15]	1.88 (0.62; 1.74-1.97)	0.71 (0.21; 0.59-0.84)	<0.0005

Data are presented as mean (SD; 95%CI) if the data is normally distributed, otherwise as median [range], n=frequency. $p < 0.05$ is considered statistically significantly. SA= vertical distance from the skin to the anterior wall of the axillary artery, SV= vertical distance from the skin to the anterior wall of the axillary vein, DA=maximum diameter of the axillary artery, DV= maximum diameter of the axillary vein, AA=CSA of the axillary artery, AV=CSA of the axillary vein and PM=width of the pectoral muscles.

Table 6-5. Measured parameters at the left infraclavicular fossa in the age-stratified groups.

Parameter	Group1 (n=32)	Group2 (n=39)	Group3 (n=27)	p-value
SA (cm)	2.54 (0.54; 2.35-2.73)	2.34 (0.40; 2.20-2.49)	2.32 (0.51; 2.13-2.52)	0.15
SV (cm)	2.70 (0.55; 2.50-2.89)	2.47 (0.47; 2.31-2.63)	2.32 (0.50; 2.14-2.51)	0.019
DA (cm)	0.59 (0.11; 0.55-0.62)	0.61 (0.10; 0.58-0.65)	0.67 (0.16; 0.61-0.73)	0.01
DV (cm)	0.96 (0.28; 0.86-1.06)	0.89 (0.17; 0.83-0.95)	0.90 (0.25; 0.81-0.99)	0.66
AA (cm^2)	0.24 (0.08; 0.21-0.27)	0.28 (0.07; 0.25-0.30)	0.38 (0.16; 0.32-0.44)	<0.0005
AV (cm^2)	0.73 (0.30; 0.62-0.84)	0.67 (0.27; 0.58-0.76)	0.68 (0.29; 0.57-0.78)	0.96
PM (cm)	1.63 (0.87;1.31-1.93)	1.13 (0.66; 0.89-1.36)	1.09 (0.55; 0.89-1.29)	0.002

Data are presented as mean (SD; 95%CI). Bonferroni Post-hoc test was performed between each group for multiple comparisons. The SV in Group 3 vs. Group 1 $p=0.003$; The DA in Group 3 vs. Group 2 $p=0.03$, Group 3 vs. Group 1 $p=0.009$; The AA in Group3 vs. Group 2 $p< 0.0005$, Group3 vs. Group 1 $p< 0.0005$; The PM in Group 3 vs. Group 1 $p< 0.0005$, Group 3 vs. Group 1 $p< 0.0005$, n=frequency, and $p< 0.05$ is considered statistically significantly.

Chapter 7

Echogenicity of the Median Nerve and the Flexor Muscles of the Forearm in the Young and the Elderly

7.1 Introduction and Objective

Recently there has been an increase in interest in the use of US to guide peripheral nerve blocks (Karmakar et al., 2007, Karmakar et al., 2008, Marhofer et al., 2005). We have demonstrated that there is significant age and gender-related differences in the dimension of musculoskeletal structure at the infraclavicular fossa (Please refer to **Chapter 6**). It is also our observation during US guided regional anesthesia that musculoskeletal structures appear significantly brighter in the elderly, which often makes it difficult to accurately delineate a peripheral nerve with US in this age group. There are published data showing that the echo intensity (EI) of skeletal muscles is significantly increased in the elderly (Maurits et al., 2003). However there are no data comparing the EI of a peripheral nerve in the young and the elderly which this study was designed to evaluate.

7.2 Material and Methods

7.2.1 Study Design

This was a non-randomized, case series. This study was approved by the Joint The Chinese University of Hong Kong-New Territories East Cluster Clinical Research Ethics Committee 2007 (**CREC Reference No.: CRE-2007.213**) (See Appendix), and it was conducted in the Department of Anesthesia and Intensive Care of The Chinese University of Hong Kong at the Prince Wales Hospital, Shatin, Hong Kong.

7.2.2 Sample Size Estimation

G Power for Windows 3.0.10 (Franz Faul, University Kiel, Germany) was used to estimate the sample size of this study. Prospective power analysis based on pilot data showed that 9 subjects per group would have an 80% power to detect a mean difference of 60 in the EI of the MN, the primary outcome variable of this study, assuming that the common standard deviation was 40 using a two group t-test with a 0.05 two-sided significance level. 24 Hong Kong Chinese subjects were recruited for this study.

7.2.3 Inclusion and Exclusion Criteria

13 healthy young volunteer (<30 years old, Group Y) and 11 elderly (>60 years old, Group E) patients who were presenting for orthopedic lower limb surgery at our hospital were recruited for the study. The median nerve (MN) and the adjoining flexor muscles (flexor digtorum superficialis, flexor pollicis longus and flexor digitorum profundus), in the mid-forearm were selected for the US scan because they are relatively superficial structures and readily accessible for US imaging.

The following patients were excluded from the study:

1). No informed consent;

2). Presence of infection and fracture on the forearm scanned;

3). Patients with diabetes, advanced tumors, neuropathy or musculoskeletal disorders;

4). ASA physical status >III.

7.2.4 Equipment and Software Used

The US scans were performed by a single investigator, the project supervisor (MK), who is experienced in US imaging, using the same US system (Version V 3.1, ARM 30.80.301.014 with no auto-gain or compound imaging facility) and a high frequency linear array transducer (HFL38, 13-6 MHz, 38 mm footprint). (**Fig. 3-1a**) A Compact Flash card of the US machine was used to record all image data from the US system. (**Fig. 3-1b**) All US images from the SD card of the US machine were transferred to a personal computer using the Site-Link Manager 3.4.1 software (**Fig. 3-1d**). Adobe® Premier Pro 2.0 was used to capture a still image which was stored in TIFF for data analysis. (**Fig. 3-1c**) Adobe® Photoshop was used to normalize the image and calculate the EI using the standard histogram function. (**Fig. 3-1d**)

7.2.5 Standardization of the Ultrasound System Setting

The system settings of an US system can significantly affect the EI of an US image (For details please refer to **Chapter 5**). Therefore the settings of the US system were standardized for every subject. This was done by setting the Delta key in the US system to 'reset to factory defaults' (**Fig. 3-5**), at the advice of the manufacturer. As a result, the same set of settings of US system was used for every patient whenever an examination was commenced after booting the US machine. The "small parts" preset, "general" image optimization setting, "dynamic range" (preset = 0) was chosen before every scan and the MN was focused so that it was in the centre of the image. The "depth-setting" was also standardized to 2.7 cm, which was considered adequate for imaging the MN and the flexor muscles (FM) in the mid-forearm. These standardized scan settings were used in every subject studied.

7.2.6 Preparation for Subjects

The US scans were performed on the left mid-forearm with the subject lying comfortably in the supine position. The left arm was abducted and externally rotated, with the palm of the hand facing the ceiling, and resting on a padded arm rest.

7.2.7 Scan Method

The US scans were performed on the left mid-forearm. Liberal amounts of US gel was applied to the skin over the area scanned for acoustic coupling and US transducer was positioned midway between the flexor crease of the elbow joint and the distal flexor crease of the wrist joint. A transverse scan of the MN and the FM of the forearm were thereby obtained (**Fig. 7-1**). Care was taken not to exert undue pressure over the area scanned because pressure can affect the grey-scale intensity of the pixels in the image. Moreover to minimize anisotropy (angular dependence) the transducer was aligned such that it was perpendicular to the forearm bones was visualized. This was done by gently tilting the transducer during the scan until maximum echogenicity of the bones, a method that has previously been described (Maurits et al., 2003, Maurits et al., 2004, Pillen et al., 2006b, Scholten et al., 2003).

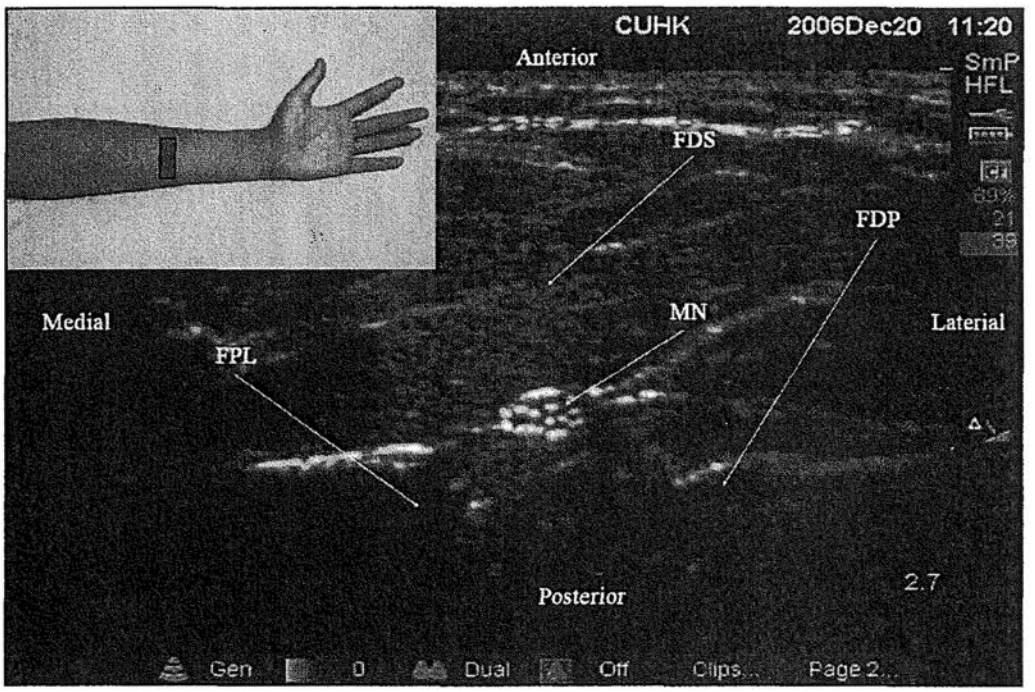

Figure 7-1. A typical transverse sonogram of the forearm in a young subject. The median nerve and the flexor muscles of the forearm are shown. Figure in the inset illustrates the position of forearm and location of the transducer. MN=Median nerve; FDS=Flexor digtorum superficialis; FDP= Flexor digitorum profundus and FPL= Flexor pollicis longus.

7.2.8 Image Acquisition and Transfer

Once an optimal image of the MN and FM was obtained three video loops (AVI format, 6 seconds each) were recorded on to the Compact Flash card of the US machine in each subject for analysis at a later date. SiteLink Image Manager 3.4.1 software was used to transfer the video loops from the US system to a laptop computer. Still images (3 per subject, TIFF, 720×480 pixels and 8-bit gray levels) were then captured from the video loops using Adobe Premier Pro 2.0. More details are outlined in **Section 3-4** of **Chapter 3**.

7.2.9 Image Normalization

The still images were then "normalized" (Adobe® Photoshop CS2) to ensure that the brightness and contrast of the whole image was at the same level before any grey-scale median (GSM) measurement. Normalization was performed by initially defining the GSM of 2 reference points (background and text) in the 2D (TIFF) image. Algebraic (linear) scaling was then performed using the" Curves Function" in Adobe Photoshop CS2 such that the GSM of the pure black equaled 0 and that of the pure white equaled 255 in the resultant image. This way, the grey-scale values of all the pixels in the image were adjusted according to the input and output values of the two reference points.

7.2.10 ROI Selection

A polygonal region of interest (ROI) was drawn around the outlines of the MN using the freehand lasso tool in Adobe Photoshop CS2.

Four ROI boxes with dimension 40X40 pixels were placed anterior, lateral, posterior and medial to the MN on the FM (**Figure 7-2a and b**). Four small ROI boxes, as opposed to a single large ROI box, were used to measure the EI of the FM because the MN is located between the FM in the forearm, which made it difficult to include the FM without the MN. We also hoped that this would minimize selection bias and intraobserver variability. While placing the ROI boxes on the muscles care was taken to include only muscle in the ROI box and exclude any fascia or bone.

7.2.11 Echo Intensity Measurement

Computer assisted grey-scale analysis (Adobe® Photoshop CS2) was then performed on these images, to measure the EI of the MN and the FM. The grey-scale intensity

or echo intensity [mean (SD) and median (range)] values of the pixels inside the ROI, MN and FM, were determined separately using the standard histogram function in Adobe® Photoshop CS2. EI value of 0 represents 'pure black' and a value of 255 represents pure white.

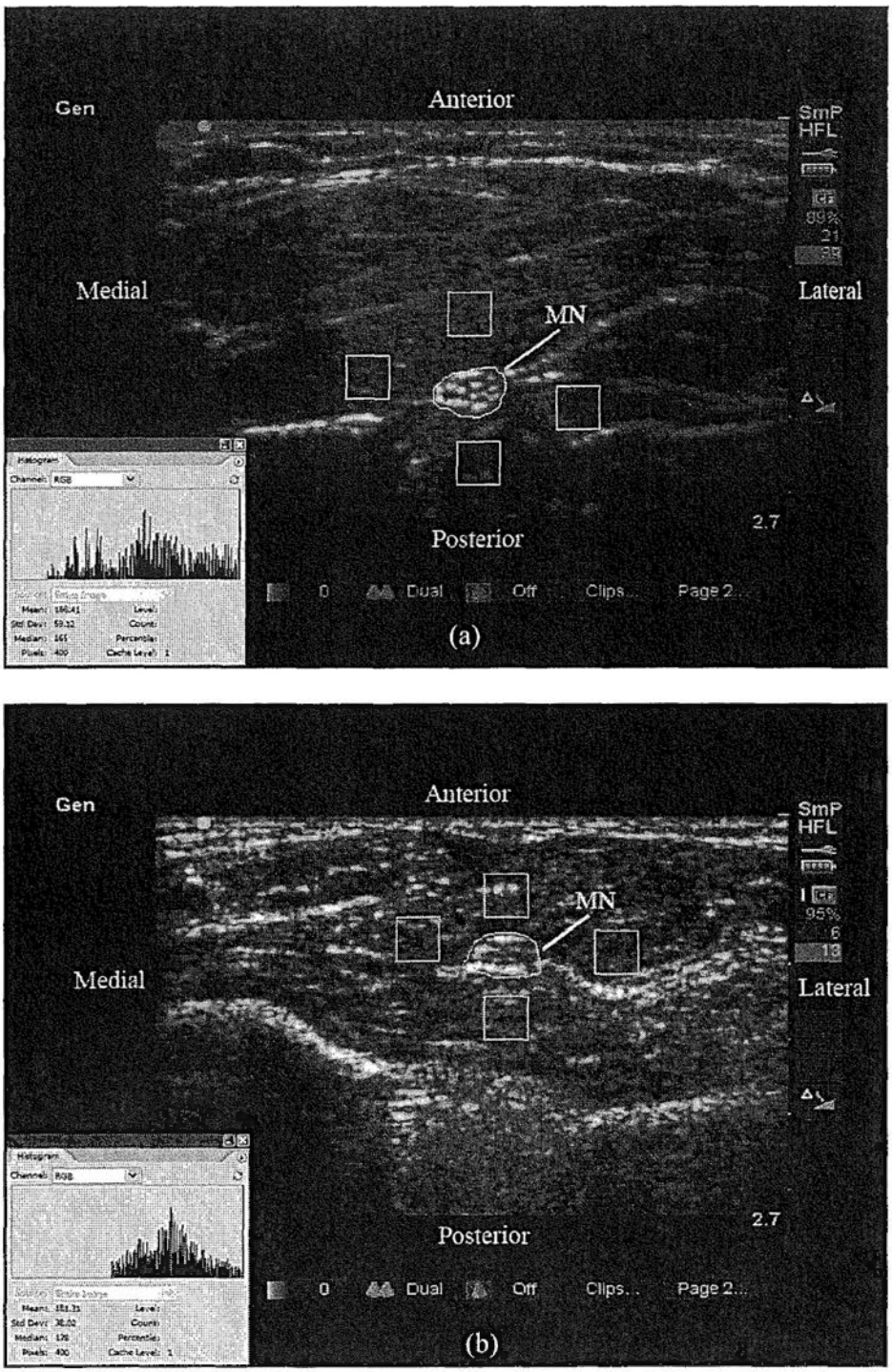

Figure 7-2. A typical transverse sonogram of the forearm in (a) a young subject (a) and (b) an elderly subject. Note the polygonal region of interest (ROI) that has been placed around the outlines of the median nerve (MN) and the four ROI boxes with dimension 40X40 pixels that have been placed anterior, lateral, posterior and medial to the MN on the flexor muscles (FM) of the forearm. Inset showing the histogram of the echo intensity of the ROI over the MN.

7.2.12 Reproducibility Testing

We have demonstrated that computer assisted gray-scale analysis is a reproducible method of measure EI in an US image (Please refer to **Section 4.2.4-Section 4.2.6** in **Chapter 3** for details).

7.2.13 Statistical Analysis

The data were analyzed using SPSS for windows (version 14, SPSS, Inc., Chicago, IL). The Kolomogorov-Smirnov test was used to test the normality of the data recorded. Since the data were normally distributed they are presented as mean (SD; 95% confidence interval). The mean EI of the MN from the three images from each subject were transformed into one group mean EI for statistical analysis (**Table 7-1**). The mean EI at each ROI box in the FM was also determined for the two study groups and one-way repeated measures ANOVA was used to compare the differences in EI at these four sites (**Table 7-2**). The mean EI of the FM from the four ROI boxes were then transformed into one overall mean EI for the study group (**Table 7-1**). The contrast between the MN and the FM was also determined by subtracting the EI of the FM from that of the MN (**Table 7-1**).

Independent sample t-test was used to compare the differences in the EI of the MN, the FM, and the contrast between the MN and the FM, between the two study groups. Univariate analysis of variance was also used to test the effect of the study groups on the EI of the MN and the FM, and the contrast between the nerve and muscles. Chi-square test was used to compare the number of male and female subjects in the two study groups. A p-value less than 0.05 was considered statistical significant.

7.3 Results

7.3.1 Demographic Data

The mean (SD; range) age of the young group was 25.8 (3.44; 19-30) yrs, and that of the elderly group was 81.7 (7.48; 67-89) yrs. The number of male and female subjects in each study group (Group Y 7 male and 6 female; Group E 2 male and 9 female) was comparable (p=0.08). The mean (SD; range) weight (kg), height (cm) and BMI in group Y was 61.5 (8.92; 48-76), 166 (6.19; 156-175) and 21.5 (2.53; 19.4-27.3) respectively. Accurate measures of weight and height could not be obtained in group E because most had fractures in their lower limbs and could not be moved out of bed.

7.3.2 Echo Intensity of the Flexor Muscles

The mean EI of the FM at the four sites (anterior, lateral, posterior and medial to the MN) are presented in **Table 7-2**. There was a significant difference in the mean EI of the FM at the 4 sites in the Group Y (p=0.024) but not in Group E (p=0.09). The overall mean EI of the FM in Group E was also significantly higher than that in Group Y; p<0.0005. (**Table7-1**)

7.3.3 Echo Intensity of the Median Nerve

The mean EI of the MN in Group E was significantly higher than that in Group Y, p<0.0005 (**Table 7-1**).

7.3.4 Contrast between the Median Nerve and the Flexor Muscles

The mean contrast between the MN and the FM was significantly higher in group Y than in group E (p=0.04) (Table 7-1).Univariate analysis showed that the study group

had a significant affect on the EI of the MN ($p=0.001$) and the FM ($p<0.001$), and also on the contrast between the MN and the FM ($p=0.001$).

7.4 Discussion

In this study we used computer assisted grey-scale analysis to measure the EI of the MN and the FM at the forearm in the young and the elderly. We have demonstrated that the EI of the MN and the FM in the forearm are significantly increased, and there is a reduction in the contrast between the MN and the adjoining FM, in the elderly.

7.4.1 Reproducibility of Echo Intensity Measurement

We have demonstrated in **Section 4-3** of **Chapter 4** that computer assisted gray-scale analysis is a valid and reproducible method of measuring EI in the still US images. This is in agreement with previous reports, which have demonstrated that computer assisted gray-scale analysis is a sensitive, quantitative, (Maurits et al., 2003, Nielsen et al., 2000) reproducible (Nielsen et al., 2000) and valid (Nielsen et al., 2000) method of analyzing and characterizing US images of skeletal muscles (Nielsen et al., 2000). Computer assisted gray-scale analysis has been used to determine normal muscle parameters, (Maurits et al., 2003, Maurits et al., 2004) and to diagnose (Maurits et al., 2003, Maurits et al., 2004) and follow-up neuromuscular disease. (Maurits et al., 2003) It is more sensitive, accurate, and also achieves a higher interobserver agreement, than visual evaluation of skeletal muscle sonograms. (Pillen et al., 2006b) We therefore believe that the same should apply when computer assisted grey-scale analysis is used to measure the EI of the MN and FM in the forearm.

7.4.2 Effect of Age on the Echo Intensity of the Flexor Muscles

The EI of the FM in the forearm was significantly increased in the elderly subjects. This is in agreement with results previously published by Maurits,(Maurits et al., 2003) who demonstrated a strong correlation between the echo-intensity of muscles and age (EI of the biceps increases 1.8% per year and EI of the quadriceps increases 1.9% per year), and suggested that the increased EI of muscles with increasing age was due to age-related changes in the muscle.(Maurits et al., 2003) In the elderly there is a reduction in skeletal muscle mass (sacropenia),(Evans, 1992, Gallagher et al., 1997) replacement of the contractile elements in the muscle by fat and connective tissue (Maurits et al., 2003) and an increase in extracellular water content in the muscle (Tsubahara et al., 1992). There is also increase in body fat (Evans, 1992). Normally subcutaneous fat, water and skeletal muscle fibers are hypoechoeic but infiltration of skeletal muscles by fat results in increased muscular EI (Reimers et al., 1993b). This may be due to a change in acoustic impedance at the surface of the fat cells and an increase in scattering of the US energy by the intramuscular fat. Therefore the increased EI of the flexor muscles in our elderly subjects can be explained by the infiltration of the muscle by fat and connective tissue.

The EI of the FM posterior to the MN was significantly lower than that in the anterior, lateral and medial sites, in the young but not in the elderly. This is an expected finding and due to attenuation of the US energy as it travels to depths. In contrast the reason why comparable differences were not present in the elderly is not clear but the generalized increase in musculoskeletal EI,(Maurits et al., 2003) increased inhomogenity (Maurits et al., 2003) in skeletal muscle with age, and loss of contrast between the nerve and muscle that we have demonstrated in this study may be some of the reasons.

7.4.3 Effect of Age on the Echo Intensity of the Median Nerve

The EI of the MN was significantly increased in the elderly group. There are no comparable data in the literature but we believe that the increased EI of the MN in our elderly subjects is also due to age related changes in the MN. The MN when examined in the transverse axis, using high frequency US (13-15MHz), shows multiple rounded hypoechoeic areas in a homogenous hyperechoeic background.(Silvestri et al., 1995) The hypoechoeic areas correspond to the neuronal fascicles and the hyperechoeic background corresponds to the connective tissue layer that binds the neuronal fascicles together.(Silvestri et al., 1995) With advancing age, particularly after the sixth decade, there is marked reduction in the number, diameter and average density of nerve fibers,(Jacobs and Love, 1985, Tohgi et al., 1977) and an increase in connective tissue elements (Cottrell, 1940) (hyperechoeic) within a peripheral nerve, which may explain why the EI of the MN was higher in our elderly subjects.

7.4.4 Effect of Age on the Contrast between the Median Nerve and the Flexor Muscles

There was also a reduction in contrast between the MN and the adjoining FM in the elderly. This is not surprising considering that the EI of the MN and FM was higher in the elderly subjects, and may also explain why it is often difficult to accurately delineate a peripheral nerve using US in this age group. Currently there are no data on the success or failure rate, or the incidence of needle related complications after US guided peripheral nerve blockade in the elderly, and further research in this area is warranted. Until such data is available it may be prudent to use peripheral nerve stimulation in conjunction with US for nerve localization during US guided nerve blockade in the elderly.

7.5 Limitations

Our results must be interpreted after considering the following facts. We were unable to obtain accurate data on body habitus (weight, height and body mass index - BMI) in our elderly subjects, for reasons outlined above. It is known that skeletal muscle size and subcutaneous fat thickness varies with age, gender, weight, BMI (Maurits et al., 2003) and whether the muscles are trained or not (Sipila and Suominen, 1993). Variations in muscle size and subcutaneous fat thickness, by altering the acoustic impedance of the tissues, may affect the EI of a musculoskeletal structure. Currently we are not aware of any published data demonstrating differences in EI of a peripheral nerve, our primary outcome variable, with changes in body habitus. Moreover, BMI (20.24) of elderly Hong Kong Chinese patients calculated from data previously published from our institution (Critchley and Conway, 1996) were comparable to that of the young volunteers in the current study. Therefore we believe that our findings are unlikely to have been influenced by a lack of accurate data on body habitus in the elderly subjects. Future studies should investigate the possible affects of body weight, height and BMI on the EI of peripheral nerves. In addition, anisotropy or angular dependence can also affect the echogenicity of an imaged structure (Soong et al., 2005). In this study we tried to minimize the effects of anisotropy by aligning the transducer at right angles to the forearm bones so that it produced maximum echogenicity of the bones, a method that has previously been described, (Maurits et al., 2003, Maurits et al., 2004, Pillen et al., 2006b, Scholten et al., 2003) and used the average of three EI measurements of the MN and FM.

7.6 Conclusion

In conclusion, we have demonstrated that the echo intensity of the median nerve and the flexor muscles of the forearm are significantly increased, and there is a reduction in contrast between the median nerve and the adjoining flexor muscles, in the elderly. Age related changes in the nerve and muscle may explain why the echo intensity of musculoskeletal structures is increased in the elderly, and which often make it difficult to accurately delineate a peripheral nerve using US in this age group.

Table 7-1. Echo-intensity of the median nerve (MN) and flexor muscles (FM) of the forearm, and the contrast between the nerve and muscle in the young and elderly subjects.

	Young (n=13)	Elderly (n=11)	p-value
MN	126 (11.6; 119-133)	153.3 (13.1;144.5-162.2)	< 0.0005
FM	50.7 (5.3; 47.4-53.9)	90.2 (15.6; 79.7-100.6)	< 0.0005
Contrast	75.3 (13.4; 67.2-83.4)	63.2 (15.2; 52.9-73.4)	0.04

Data are presented and mean (SD; 95%CI). n= frequency, p< 0.05 is considered statistically significant.

Table 7-2. Echo-intensity of the flexor muscles of the forearm at the four region of interest (ROI) boxes around (anterior, lateral, posterior and medial) the median nerve.

	Anterior	Lateral	Posterior	Medial	p-value
Young (n=13)	52.4 (10.1;45.6-59.2)	53.3 (9.5;45.9-58.7)	40.7 (9.8;34.1-47.3)	53.9 (7.5;48.9-58.9)	0.024 *
Elderly (n=11)	86.2 (24.2;69.9-102.4)	95.6 (16.9;84.5-107.2)	85.7 (12;77.7-93.8)	89.6 (15.7;79.1-100.2)	0.09

Data are presented as mean (SD; 95%CI).* Indicates anterior vs. posterior p=0.03, lateral vs. posterior p=0.005 and medial vs. posterior p=0.001, with adjustments for multiple comparisons. n= frequency, p<0.05 is considered statistically significant.

Chapter 8

Echotexture of the Median Nerve in the Young and the Elderly

8.1 Introduction and Objective

Using computer assisted gray-scale analysis we have demonstrated that the echo intensity in the median nerve (MN) of the forearm is significantly increased in the elderly (**Chapter 7**). However, the evaluation of EI is a global measurement of the total brightness of the pixels (gray-scale level) in the US image and does not take into account its spatial distribution. The texture of a digital image is attributed to the distribution of gray-scale levels among the pixels in the image. Texture analysis is used to evaluate the position and intensity of pixels in the digital image (Castellano et al., 2004, Russ, 2007b). Computer assisted texture analysis has been used to characterize the texture of a skeletal muscle (Maurits et al., 2004, Nielsen et al., 2006). However, there are no data describing the echotexture of a peripheral nerve. The aim of this study was to evaluate the echotexture of the MN in the forearm and compare the differences in the young and the elderly.

8.2 Materials and Methods

8.2.1 Study Design

This was a non-randomized, case series. The study was approved by Joint The Chinese University of Hong Kong-New Territories East Cluster Clinical Research Ethics Committee 2007 **(CREC Reference No.: CRE-2007.213)** (See Appendix), and it was conducted in the Department of Anesthesia and Intensive Care of The Chinese University of Hong Kong at the Prince Wales Hospital, Shatin, Hong Kong.

8.2.2 Sample Size Estimation

G Power for Windows 3.0.10 was used to estimate the sample size of this study. Prospective power analysis based on pilot data showed that 5 subjects per group would have an 80% power to detect a mean difference of 0.19 in the white area index (WI) of the MN, the primary outcome variable of this study, assuming that the common standard deviation was 0.1 using a two group t-test with a 0.05 two-sided significance level. Twenty Hong Kong Chinese subjects were recruited for this study.

8.2.3 Inclusion and Exclusion Criteria

Ten young healthy volunteers (<30 years old, Group Y) and 10 elderly (>60 years old, Group E) patients who were presenting for orthopedic lower limb surgery at our hospital were recruited for the study. The MN in the mid-forearm was selected for the US scan because it is a relatively superficial structure and is readily accessible for US imaging. The following were the exclusion criteria:

1). No informed consent;

2). Presence of infection or trauma at the site of scan;

3). Patients with diabetes, advanced tumors, neuropathy or musculoskeletal disorders;

4). ASA physical status >III.

8.2.4 Equipment and Software Used

The US scans were performed by a single investigator, the project supervisor (MK), who is experienced in US imaging, using the same US system (Version V 3.1, ARM 30.80.301.014 with no auto-gain or compound imaging facilities) and a high frequency linear array transducer (HFL38, 13-6 MHz, 38 mm footprint) (**Fig. 3-1a**).

A Compact Flash card of the US machine was used to record all image data from the US system (**Fig. 3-1b**). All US images from the SD card of the US machine were transferred to a personal computer using the Site-Link Manager 3.4.1 software (**Fig. 3-1d**). Adobe® Premier Pro 2.0 software was used to capture a still image from the video loop and was stored as a TIFF image for data analysis (**Fig. 3-1c**). Adobe® Photoshop CS2 software was used to normalize the image and calculate the EI using the standard histogram function (**Fig. 3-1d**). Image-Pro® Plus 6.2 was used to perform measurements of CSA of the MN and determine the texture of the US image (**Fig. 3-1 f**).

8.2.5 Standardization of the Ultrasound System Setting

As outlined in **Section 7.2.5** of **Chapter 7** the setting of the US system was standardized for every subject. This was done by setting the Delta key in the US system to 'reset to factory defaults' (**Fig. 3-5**) at the advice of the manufacturer. As a result, the same setting of the US system was applied for every patient whenever an examination was commenced after booting the US machine. The "small parts" preset, "general" image optimization setting and the "dynamic range" (preset = 0) were chosen before every scan, and the MN was focused so that it was at the centre of the image. The "depth-setting" was also standardized to 2.7 cm, which was considered adequate for imaging the MN in the mid-forearm. These standardized scan settings were used in every subject studied.

8.2.6 Preparation for Subjects

The ultrasound scans were performed on the left mid-forearm with the subject lying comfortably in supine position. The left arm was abducted and externally rotated, with the palm of the hand facing the ceiling and resting on a padded arm rest.

8.2.7 Scan Method

As outlined in **Section 7.2.7** of **Chapter 7**, the US scans were performed on the left mid-forearm. Liberal amounts of US gel was applied to the skin over the area scanned for acoustic coupling and US transducer was positioned midway between the flexor crease of the elbow joint and the distal flexor crease of the wrist joint. A transverse scan of the MN and the FM of the forearm were thereby obtained (**Fig. 7-1**). Care was taken not to exert undue pressure over the area scanned because pressure can affect the grey-scale intensity of the pixels in the image. Moreover to minimize anisotropy (angular dependence) the transducer was also aligned such that it was perpendicular to the forearm bones. This was done by gently tilting the transducer during the scan until maximum echogenicity of the bones, a method that has previously been described during computer assisted gray-scale analysis. (Maurits et al., 2003,Maurits et al., 2004,Pillen et al., 2006b,Scholten et al., 2003)

8.2.8 Image Acquisition and Transfer

As outlined in **Section 7.2.8** of the **Chapter 7**, once an optimal image of the MN was obtained, three video loops (AVI format, 6 seconds each) were recorded on to the Compact Flash card of the ultrasound machine in each subject for analysis at a later date. SiteLink Image Manager 3.4.1 (Sonosite Inc., Bothell, USA) software was used to transfer the video loops from the ultrasound system to a laptop computer. Still images (3 per subject, TIFF format, 720×480 pixels and 8-bit gray levels) were then captured from the video loops using Adobe Premier Pro 2.0 (Adobe Systems Inc, San Jose, CA, USA).

8.2.9 Image Normalization

As outlined in **Section 7.2.9** of the **Chapter 7**, the still images were then "normalized" (Adobe® Photoshop CS2) to ensure that the brightness and contrast of the whole image were at the same level before any grey-scale median (GSM) measurement. Normalization was performed by initially defining the GSM of two reference points (background and text) in the 2D (TIFF) image. Algebraic (linear) scaling was then performed using the" Curves Function" in Adobe Photoshop CS2 such that the GSM of the pure black equaled 0 and that of the pure white equaled 255 in the resultant image. This way, the grey-scale values of all pixels in the image were adjusted according to the input and output values of the two reference points.

8.2.10 Echo Intensity Measurement

A polygonal region of interest (ROI) was drawn around the outlines of the MN using the freehand lasso tool in Adobe Photoshop CS2. The grey-scale intensity or echo intensity [mean (SD) and median (range) value of the pixels inside the MN was determined separately using the standard histogram function in Adobe® Photoshop CS2. An EI value of 0 represents 'pure black' and a value of 255 represents pure white.

8.2.11 Cross Sectional Area Measurement

8.2.11.1 Spatial Calibration

A reference US image was imported into IPP 6.2 window. A reference line, calibration scale, was set to match the depth scale (2.7 cm) marked on the US image vertically. The spatial calibration, 13.6 pixels /mm in the horizontal (X) and vertical (Y) axes of the US image was determined. Since the depth setting was standardized

in this study, the spatial calibration scale was valid for all the US images. Details of spatial calibration are outlined in **Section 3.5.2** of **Chapter 3**.

8.2.11.2 "Off-cart" Measurement

The appropriate reference spatial calibration scale (13.6 pixels /mm) previously saved was selected. A polygon ROI, surrounding the outline of MN in the US image, was created using the freehand polygon feature irregular tool. A closed color figure of MN (**Fig.8-1**) was thereby produced. Thereafter, the result of CSA was determined using IPP and results were expressed in mm. More details are outlined in **Sections 3.5.1 to 3.5.3** of **Chapter 3**.

8.2.12 Echotexture Measurement

Quantitative texture analysis was then performed to evaluate the spatial distribution of the pixels. In the resultant binary image, a white or black area was considered ro be any contiguous group of pixels sharing a specified range of gray-scale values. The white and black areas in the digital image of the MN were identified, measured and counted using IPP.

8.2.12.1 Noise Reduction and ROI Selection

The normalized image was imported into IPP window and magnified to 200%. The median filter was applied to remove the impulse noise from the US image. (Russ, 2007b) Then a ROI surrounding the outline of the MN was carefully drawn using the freehand irregular tool (**Fig.8-1**). Details are outlined in **Section 3.7.3** of **Chapter 3**.

8.2.12.2 Thresholding

Threshold (rang from a minimum to a maximum value) is defined as a range of gray-scale values in an image. Thresholding is a selection process used to extract the

regions within a defined gray-scale range as the foreground, and to reject all of the other regions to the background. After thresholding process, an input gray-scale image is transformed to a binary image using white and black color to distinguish these regions. (Nielsen et al., 2006,Russ, 2007b). During thresholding process, the individual pixels in an US image are marked as a white object if their gray-scale value is greater than the set threshold value or as a black background otherwise.

The thresholding process was performed in this study to segment the white and black areas in the MN image. Today there are no accepted standards for defining a threshold range in the image of a peripheral nerve. Therefore, the gray scale value of 128, which corresponds to the median value of the gray scale ranges (0-255), was used as the common threshold to differentiate the echotexture of the MN in this study. Thereby, a gray-scale image of the MN was segmented into a binary image (**Fig. 3-9; Fig. 3-10; Fig. 8-1a, b**). More details are outlined in **Section 3.7.4** of **Chapter 3**.

8.2.12.3 Black and White Area Index Measurement

In the resultant binary image, an area (white or black) was defined as a region of at least three connected pixels (corresponding to an area of 0.015mm^2) with gray-scale values in the definite threshold (black 0-128, white128-255). As a result, the black area index (BI) was defined as the ratio of the black area to the total CSA of the MN, and the white area index (WI) was defined as the ratio of the white area to the total CSA of the MN.

8.2.13 Reproducibility Testing

We have demonstrated that "off-cart" measurement of CSA, computer assisted gray-scale and texture analyses are reproducible methods of measure CSA and WI in an US image. Please refer to **Section 4.3.2** in **Chapter 4**.

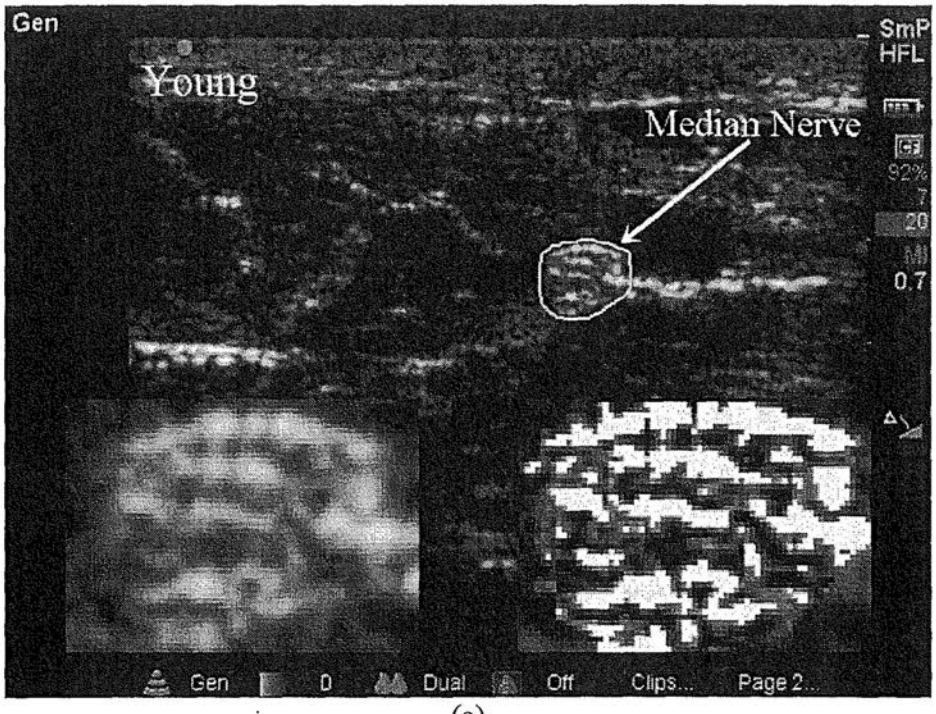

(a)

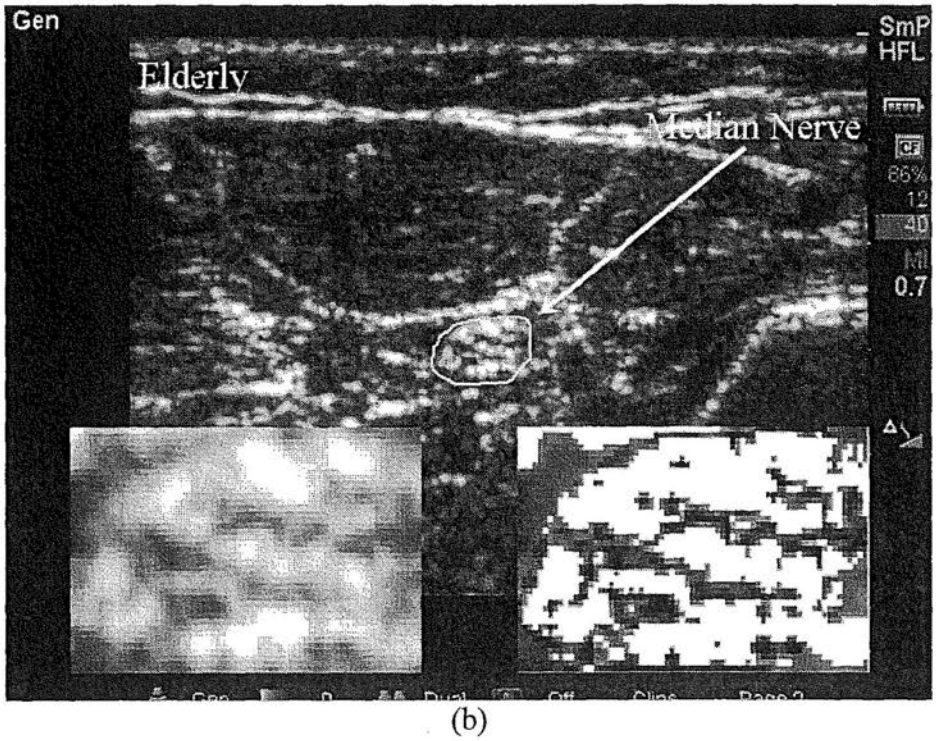

(b)

Figure 8-1. A typical transverse sonogram of the median nerve in the mid-forearm (a) in a young subject (male, 25 yrs old) (b) in an elderly subject (female, 85 yrs old). The region of interest (ROI) is placed around the outlines of the median nerve. Inset shows the normalized median nerve on the left, and the segmented median nerve magnified to 400% on the right in both images.

8.2.14 Statistical Analysis

Statistical Package for the Social Sciences (SPSS) for Windows 14.0 (SPSS Inc, Chicago, IL, USA) was used for the statistical analysis. The Kolmogorov-Smirnov test was used to test the normality of the data recorded. Chi-square test was used to compare the number of male and female subjects in the two study groups. The value of the CSA, EI, WI and BI from the three images from each subject was transformed to one average value for statistical analysis which minimized the variation of data. Since the data were normally distributed they are presented as mean (SD; 95% confidence interval). Pearson product-moment correlation coefficient (r) was used to describe the strength and the direction of the linear relationship between the EI and WI of MN. Independent samples t-test was also used to compare the differences in WI, BI, CSA, and EI of the MN between Group Y and Group E. In addition, one samples t-test was performed to compare WI and BI against 0.5 (50%) within each group separately. A p-value less than 0.05 was considered statistically significant.

8.3 Results

8.3.1 Demographic Data

The mean (SD; range) age of the young group was 25.8 (3.77; 19-30) years, and that of the elderly group was 78.2 (8.94; 62-88) years. The number of male and female subjects in each group (Group Y, 5 male and 5 female; Group E, 3 male and 7 female) was comparable (p=0.33). The mean (SD; range) weight (kg), height (cm) and BMI of the two study groups was also comparable (**Table 8-1**).

8.3.2 Cross Sectional Area, Echo Intensity and Echotexture of the Median Nerve

The mean CSA of the MN in Group E was significantly smaller than that in Group Y, (p=0.002). The mean EI of the MN in Group E was significantly greater than that in Group E, p=0.0017. In Group Y, the mean WI was significantly lower than the BI in the MN (p=0.006) but not in Group E (p=0.213). The mean WI of the MN in Group E was also significantly higher than that in Group Y (P=0.012), and the mean BI in Group E was correspondingly lower than that in Group Y significantly (p=0.012).

8.3.3 Correlation between Echo Intensity and White Area Index of the Median Nerve

As seen in **Fig. 8-2**, there was a strong correlation between the EI and WI of MN, r=0.66, n=20, p=0.02. This means that higher levels of EI are associated with higher levels of WI in the MN.

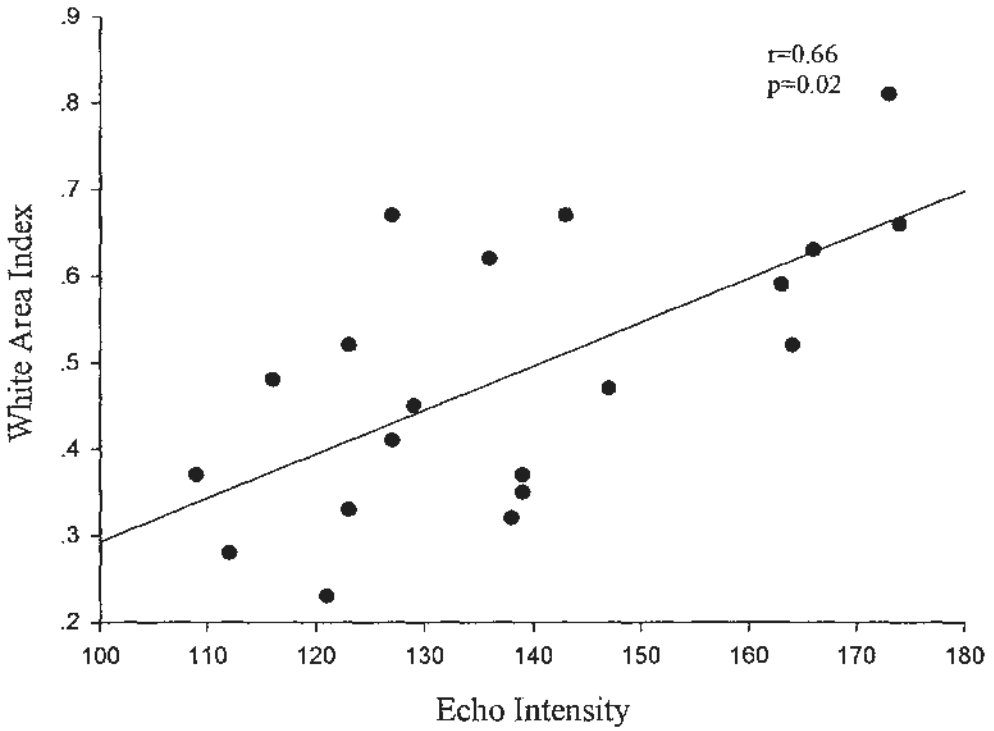

Figure 8-2. Correlation between the echo intensity (EI) and white area index (WI) of the median nerve in the 20 subjects studied.

8.4 Discussion

In this study we used quantitative ultrasonography to evaluate the CSA, EI and the spatial texture of the MN, and compared these parameters between the young and the elderly. We have demonstrated a reduction in CSA and BI, and an increase in the WI and EI, in the MN of the elderly compared with the young. In addition, we have also demonstrated that the BI was larger than the WI in the MN in the young but no in the elderly.

8.4.1 Reproducibility of Measurements

We have demonstrated a good reproducibility of the quantitative ultrasonography methods used to measure the CSA, EI and WI in the musculoskeletal sonogram using

computer assisted image analysis. The method for "off-cart" measurement of CSA using software in the sonographic image also has a good reproducibility. This is in agreement with published data. (Nakamichi and Tachibana, 2000) Please refer to **Section 4.3.2** and **Section 4.4.1** in **Chapter 4.** We have also demonstrated that computer assisted gray-scale analysis is a valid and reproducible method of measuring EI of a nerve in still US images. Although there are no comparable data, the EI measurements in the skeletal muscle also showed a good reproducibility. (Maurits et al., 2003, Nielsen et al., 2000, Pillen et al., 2006a, Pillen et al., 2006b) Moreover, the echotexture measurement of the MN using computer assisted texture analysis also has a good reproducibility. There are no comparable data in the literature. However, there was a good correlation between the measurements of tissue components predicted with computer assisted texture analysis (IPP) and the histologic measurements of that made on the explanted carotid plaques (Lal et al., 2002). These findings indicate that computer assisted texture analysis (IPP) is a valid and reproducible method. We therefore believe that the same applies when computer assisted texture analysis is used to evaluate WI and BI of the MN in the forearm. More details are outlined in **Section 4.4.2** in **Chapter 4.**

8.4.2 Cross Sectional Area of the Median Nerve

The CSA of the MN at the mid-forearm was smaller in the elderly. There are no comparable data published in the literature. Furthermore, there is some controversy about the CSA of a peripheral nerve with age in the literature. Heinemeyer and Reimers (Heinemeyer and Reimers, 1999) suggested that the thicknesses of peripheral nerves in the upper and lower limbs showed a Gaussian distribution, and age and weight had no significant influence on the nerve thickness, whereas height was correlated significantly with the thickness (r^2 between 0.18 and 0.59). In contrast,

Martinoli (Martinoli et al., 2002) demonstrated no linear correlation between gender, height and BMI and the area of the MN, which was measured at the middle third of the forearm with a 12-5 MHz transducer in 50 healthy subjects (17-89 years). However, Cartwright (Cartwright et al., 2009) also illustrated that the area of the MN at the wrist correlated with weight ($r=0.411$, $p=0.003$) and age ($r=0.413$, $p=0.029$) in 50 volunteers (15-80 years) using a 15 MHz transducer. These differences are perhaps due to the different locations used and its research population. With advancing age, particularly after the sixth decade, there is a marked reduction in the number, diameter, and average density of nerve fibers,(Jacobs and Love, 1985, Tohgi et al., 1977) a decrease in the number of the nerve fascicles (Sladjana et al., 2008) and a marked increase in the connective tissue elements within a peripheral nerve (Cottrell, 1940). This may explain the decreased CSA of the MN at the mid-forearm level in the elderly in the present study. Further investigation is warranted in a larger population.

8.4.3 Echo Intensity of the Median Nerve

There was a significant increase in the EI of the MN in the elderly. This confirms our finding in **Chapter 7**.

8.4.4 Echotexture of the Median Nerve

We have demonstrated that WI was significantly lower than the BI of the MN in the young but not in the elderly. Moreover, we also demonstrated that there was an increase in the WI and a reduction in the BI of the MN in the elderly as compared to that in the young.

There are no quantitative data evaluating the echotexture of a peripheral nerve in the literature. The peripheral nerve consists of fascicles bound together loosely by a

connective tissue framework. (Sunderland, 1965,Sunderland and Bradley, 1949,Sunderland and Bradley, 1952) The echotexture of a peripheral nerve is closely related to its histological structure. (Fornage, 1988,Silvestri et al., 1995) The hypoechoic regions in a nerve correspond to the neuronal fascicles, and hyperechoic regions correspond to the connective tissues. (Fornage, 1988,Silvestri et al., 1995) Therefore, we believe that the difference in the echotexture of the MN that we have demonstrated in the young and the elderly may be due to the age-related differences in the peripheral nerve.

The WI of the MN was significantly lower than the BI in the young but not in the elderly. We are not aware of any data comparing the WI and BI of the MN in the literature. However, our finding is in agreement with the histological findings previously published by Bonnel (Bonnel, 1984), who in a cadaver study of comparable age (67-85 years) demonstrated that the perineurial and epineurial connective tissue comprised 73% of the MN. This indicates that the percentage of connective tissue is significantly larger than that of the fascicles in the MN of the elderly. Moreover, Slajana et al. have also (Sladjana et al., 2008) demonstrated that total number of the fascicles in the sciatic nerve of the young (age< 30 years) 61-70 is larger than that in the elderly (age> 60 years) 27-52. There are no data quantifying the percentage of connective tissue in a peripheral nerve of the young. However, the increase in the proportion of the connective tissue (hyperechoic) and the decrease in the number of the fascicles (hypoechoic) in a peripheral nerve of the elderly may explain why the WI was higher and the BI was lower in our elderly subjects.

There was also an increase in the WI and a reduction in the BI of the MN in the elderly compared to that in the young. Currently, there are no comparable data in the

literature but these alterations seen in echotexture are in accordance with age-related histological changes in a peripheral nerve. With aging, morphographic changes occur within a peripheral nerve. There is a marked reduction in the number, diameter and average density of nerve fibers, and thus a reduction in the proportion and number of fascicles in a nerve (Azcoitia et al., 2003, Jacobs and Love, 1985, Sladjana et al., 2008, Tiago et al., 2007, Tohgi et al., 1977). Moreover, the degenerating fascicles are replaced by adipose tissue and connective tissue elements (Cottrell, 1940, Sladjana et al., 2008). Such changes in the nerve architecture may lead to changes in the acoustic impedance of a nerve, which causes scattering of the US beam, and may explain the increased WI in the MN of the elderly.

It was not surprising to see a positive relationship between the EI and WI of the MN, indicating that an increase in EI of a nerve is associated with a larger WI.

8.5 Limitations

Our findings must be interpreted after considering the following facts. An evaluation of echotexture is based on the gray scale level in an image. To data, there are no accepted standards for a threshold range for echotexture measurements in an image of a peripheral nerve. We selected the median value (128) of the gray scale (0-255) as the gray-scale value threshold. Our results on the WI and BI using this median threshold are in accordance with the histological findings of Bonnel (Bonnel, 1984), indicating that the selection of the median value of the gray scale range is reasonable. Previous investigation have used 25%–75% quartiles of the mean EI (Nielsen et al., 2006) or visible method (Maurits et al., 2003) as the threshold for computer assisted texture analysis. We are not aware of any published data demonstrating the effect of different thresholds on the WI of a peripheral nerve. Future research should evaluate

the effect of varying the threshold on the echotexture of a peripheral nerve. Moreover, in the present study age-related differences were only compared between two pre-determined age groups, Group Y <30 years old and Group E >60 years old. Thus, further studies should evaluate the echotexture of a peripheral nerve by stratifying subjects into several age groups.

8.7 Conclusion

Using computer assisted texture analysis we have demonstrated that there is an increase in the echo intensity and white area index, and a reduction in the black area index and the cross sectional area in the median nerve of the elderly. These finding may explain why the median nerve is smaller in size, and appears whiter and brighter on a sonogram in elderly subjects.

Table 8-1. Demographic data of the young and elderly subjects.

	Gender(n)	Age(yr)	Weight(kg)	Height(cm)	BMI
Group Y	**5M/5F**	25.8 (3.77; 19-30)	60.3 (8.77; 48-76)	166 (6; 156-173)	22.0 (2.92; 17.0-26.8)
Group E	**3M/7F**	78.2 (8.94; 62-88)	58.2 (9.51; 40-70)	162 (7; 152-173)	22.1 (3.02; 17.3-27.1)

Data are presented as Mean (SD; range). n=frequency; M=male; F=female and BMI=body mass index.

Table 8-2. The cross sectional area, echo intensity, white area index and black area index of the MN in the young and the elderly

Parameter	Young (n=10)	Elderly (n=10)	p-value
CSA (mm^2)	13.6 (2.18; 12.0-15.2)	9.90 † (3.28; 6.73-11.43)	0.002
EI	128.0 (16.1; 116.5-139.5)	148.7 † (18.9; 135.2-162.3)	0.0017
WI	0.40 * (0.09; 0.34-0.46)	0.57 † (0.17; 0.45-0.69)	0.012
BI	0.60 (0.09; 0.54-0.66)	0.43 † (0.17; 0.31-0.55)	0.012

Data are presented as mean (SD; 95%CI). * Indicates a significant difference between the WI and BI within groups, p=0.006; † indicates a significant difference between groups. $p < 0.05$ is considered statistically significant.

Chapter 9

Echogenicity of a Peripheral Nerve during Ultrasound Guided Nerve Blockade

9.1 Introduction and Objective

US has been used to visualize the spread of an injected local anesthetic in real-time during US guided peripheral nerve blocks. Following the injection the nerve appears brighter and is also better delineated on a sonogram. This phenomenon has been described during US guided infraclavicular brachial plexus block (Bloc et al., 2007), sciatic nerve block (Saranteas et al., 2007) and lumbar plexus block (Karmakar et al., 2008). However, there are no data quantifying this observation during US guided peripheral nerve blockade, which this study was designed to investigate.

9.2 Material and Methods

9.2.1 Study Design

This was a non-randomized, case series. This study was approved by the Joint The Chinese University of Hong Kong-New Territories East Cluster Clinical Research Ethics Committee 2008 (**CREC Reference No.: CRE-2008.213**) (See Appendix), and it was performed in the Department of Anesthesia and Intensive Care of The Chinese University of Hong Kong at the Prince Wales Hospital, Shatin, Hong Kong.

9.2.2 Sample Size Estimation

G Power for Windows 3.0.10 was used to estimate the sample size of this study. Prospective power analysis based on pilot data showed that 7 patients would have an 80% power to detect a mean difference of 30 in the EI of the sciatic nerve before and

during local anesthetic injection, the primary outcome variable of this study, assuming that the common standard deviation was 20 using One-way repeated measurement analysis of variance (ANOVA) with a 0.05 two-sided significance level. 12 Hong Kong Chinese patients were recruited for this study.

9.2.3 Inclusion and Exclusion Criteria

12 adult (ASA I-III, <80year) patients who were scheduled to undergo orthopaedic lower limb surgery under US guided SNB at the subgluteal space were recruited for the study. The following patients were excluded from the study:

1). No informed consent;
2). Patients with diabetes, advanced tumors, neuropathy or musculoskeletal disorder;
3). ASA physical status >III;
4). Known allergy to local anesthetic drugs;
5). Pregnancy.
6). If the anticipated duration of operation was less than 30minutes.

9.2.4 Equipment and Software Used

MicroMaxx US system **(Fig. 3-1a)** and a low frequency curved array transducer (C60e, 5-2 MHz, 60 mm footprint) **(Fig. 9-1)** were used for this study. The latter was used because the sciatic nerve is located at a depth. Once an optimal image was obtained, the data from the US system were recorded on a tape using a Sony video camera **(Fig. 3-1b)** from the video output terminal. Adobe® Premier Pro 2.0 **(Fig. 3-1c)** was used to capture the video loop then store it as a still image in a TIFF image for data analysis. Image-Pro® Plus 6.2 **(Fig. 3-1f)** was used to perform "off-cart"

measurements of CSA. All data downloaded for processing or analysis were stored on a personal laptop computer. **(Fig. 3-1g)**

9.2.5 Preparation for Patient

The patients were positioned laterally with the side to be anaesthetized uppermost and with the hip and knees flexed **(Fig. 9-1)**.

9.2.6 Scan Method

The US scan was performed by a single investigator, the project supervisor (MK), who is experienced in US imaging. The lateral prominence of the greater trochanter and the ischial tuberosity were then identified, and a line was drawn between these two landmarks using a skin marking pen **(Fig. 9-1)**. Liberal amounts of US gel was applied to the skin over the area scanned for acoustic coupling. Then, the transducer was positioned parallel to a marked line between the greater trochanter and ischial tuberosity previously drawn with its orientation marker directed laterally to produce a transverse scan of the sciatic nerve at the subgluteal space.

The "Abdomen" preset, "General" image optimization setting and the dynamic range (preset=0) was chosen before every scan, and the sciatic nerve was focused so that it was at the centre of the image. The depth setting was adjusted to an appropriate depth for the sciatic nerve (depth range: 4.7-9.1 cm) scan, and the amount of gain was also adjusted manually to optimize the image. Once the image was optimized, all settings were kept constant during the whole procedure because changes in US system settings can affect the EI of an US image.

The sciatic nerve arises from the sacral plexus and exits the pelvis through the greater sciatic foramen, between the piriformis and the superior gemellus muscles, to

enter the subgluteal space below the piriformis muscle (Di Benedetto et al., 2002), which is a hypoechoic area between the hyperechoic perimysium of the gluteus maximus and the quadratus femoris muscles. It extended from the greater trochanter laterally to the ischial tuberosity medially. The sciatic nerve is seen as an oval hyperechoic nodule approximately 1.5-2 cm in diameter within the subgluteal space. (**Fig. 9-2**) Care was taken not to exert undue excess pressure over the area scanned as pressure can affect the grey scale intensity of the pixels in the image. Moreover, to minimize anisotropy the transducer was aligned so that it was perpendicular to the nerve which was judged by its maximum echogenicity.

9.2.7 Ultrasound Guided Sciatic Nerve Blockade

The US scan and US-guided SNB were performed by a single investigator using the technique previously described by Karmakar et al. (Karmakar et al., 2007) Under aseptic precautions an insulated nerve block needle was advanced towards the sciatic nerve under real-time US guidance combined with nerve stimulation. Once the tip of needle was confirmed to be close to the sciatic nerve and in the subgluteal space, 25–30 ml of lignocaine 1% and ropivacaine 0.25% with epinephrine 1:400 000 was injected over 2–3 minutes. Distention of the subgluteal space and spread of the local anesthetic around the sciatic nerve was observed and recorded in real-time.

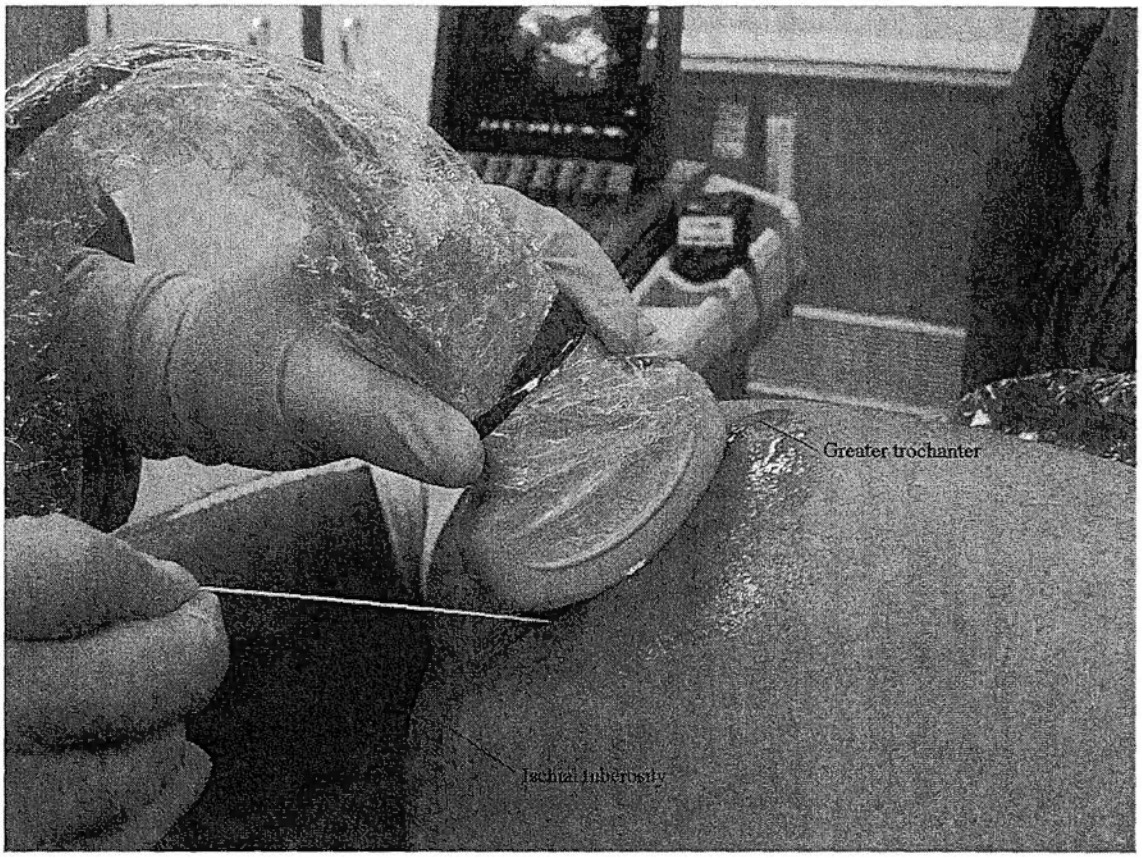

Figure 9-1. Position of the patient and the US transducer during an US-guided SNB at the subgluteal space. Also seen is an insulated nerve block needle being inserted in the long-axis (in-plane) of the US beam (reproduced with permission from (www.aic.cuhk.edu.hk/usgraweb).

9.2.8 Image Acquisition and Transfer

Once an optimal image was obtained, US images were recorded on tape (in AVI format) using a commercial video recorder (Sony Corporation, Ltd., Minato-ku, Tokyo, Japan) via the video output terminal. The stored video from the tape was transferred to a personal computer using Adobe Premier Pro 2.0 and still images were captured (3 per subject, TIFF, 720×576 pixels and 8-bit gray levels) from the movie sequence and stored for data analysis. More details are outlined in **Section 3-4** of **Chapter 3**. The still images were captured at three time points, A (before the LA injection), B (during LA injection) and C (3 minutes after LA injection). The average

velocity of sound through soft tissue is 1540 m/sec and frequency of US in this study was between 5-2 MHz. Thereafter, the resolution of the US system used was 0.31-0.77 mm, and the dimension of a pixel in the study digitized still images was 0.25 X 0.25 mm, so one can conclude that there was no loss of data during the digitization process.

9.2.9 Image Normalization

The still images were then "normalized" (Adobe® Photoshop CS2) to ensure that the brightness and contrast of the whole image was at the same level before any grey-scale median (GSM) measurement. Normalization was performed by initially defining the GSM of 2 reference points (background and text) in the 2D (TIFF) image. Algebraic (linear) scaling was then performed using the" Curves Function" in Adobe Photoshop CS2 such that the GSM of the pure black equaled 0 and that of the pure white equaled 255 in the resultant image. This way, the grey-scale values of all the pixels in the image were adjusted according to the input and output values of the two reference points.

9.2.10 Cross Sectional Area Measurement

IPP 6.2 was used to measure the CSA of the sciatic nerve. Please refer to **Section 3.5** for details.

9.2.10.1 Spatial Calibration

A reference US image was imported into IPP 6.2 (Media Cybernetics, Silver Spring, Maryland, USA) window. A reference line, calibration scale, was set to match the depth scale marked on the US image. Thereafter, the spatial calibration in the horizontal (X) and vertical (Y) axes of the US image was determined, 3.5 pixels/mm

at a depth of 9.1cm, 4.03 pixels/mm at a depth of 7.3cm and 4.52 pixels/mm at a depth of 5.9cm. These different scales were calibrated for this study because different depths were used for scanning the sciatic nerve in the patients studied.

9.2.10.2 "Off-cart" Measurement

The imported image was magnified to 200% to make it easier to identify. The appropriate reference spatial calibration scale that was made and saved to the computer previously was selected. A polygon ROI, surrounding the outline of the sciatic nerve in the US image, was drawn using the freehand polygon feature irregular tool. A closed figure of the sciatic nerve (**Fig.9-2**) was thereby obtained. Thereafter, the CSA of a sciatic nerve was determined and displayed. More details are outlined in **Sections 3.5.1 to 3.5.3** of **Chapter 3**.

9.2.11 Echo Intensity Measurement

A polygonal region of interest (ROI) was drawn around the outlines of the sciatic nerve using the freehand lasso tool in Adobe Photoshop CS2. Computer assisted grey-scale analysis (Adobe® Photoshop CS2) was then performed on these images to measure the EI of the sciatic nerve. The grey-scale intensity or echo intensity [mean (SD) and median (range) value of the pixels inside the MN was determined separately using the standard histogram function in Adobe® Photoshop CS2. An EI value of 0 represents 'pure black' and a value of 255 represents pure white.

9.2.12 Reproducibility Testing

Please refer to the **Section 4.2.8** and **4.2.9** in **Chapter 4**.

9.2.13 Statistical Analysis

The data were analyzed using SPSS for windows (version 14, SPSS, Inc., Chicago, IL). The Kolomogorov-Smirnov test was used to test the normality of the data recorded. Since the data were normally distributed they are presented as mean (SD; 95% CI). The mean EI and CSA of the sciatic nerve from the three images from each subject were transformed into one mean EI and CSA for statistical analysis. The one-way repeated measures ANOVA was used to compare the differences in the EI and CSA of the sciatic nerve at the three time points studied. A p-value less than 0.05 was considered statistical significant.

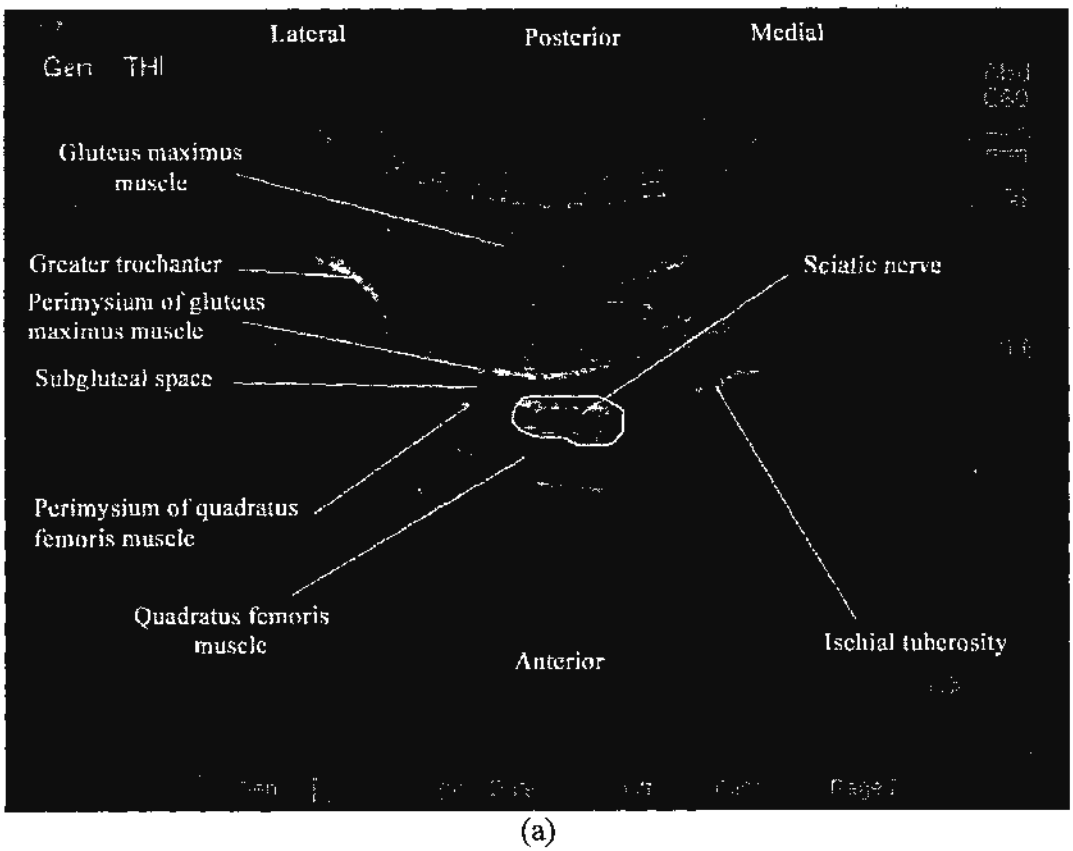

(a)

Figure 9-2a. A typical transverse sonogram of the sciatic nerve is illustrated in the medial aspect of the subgluteal space before local anesthetic injection (reproduced with permission from www.aic.cuhk.edu.hk/usgraweb).

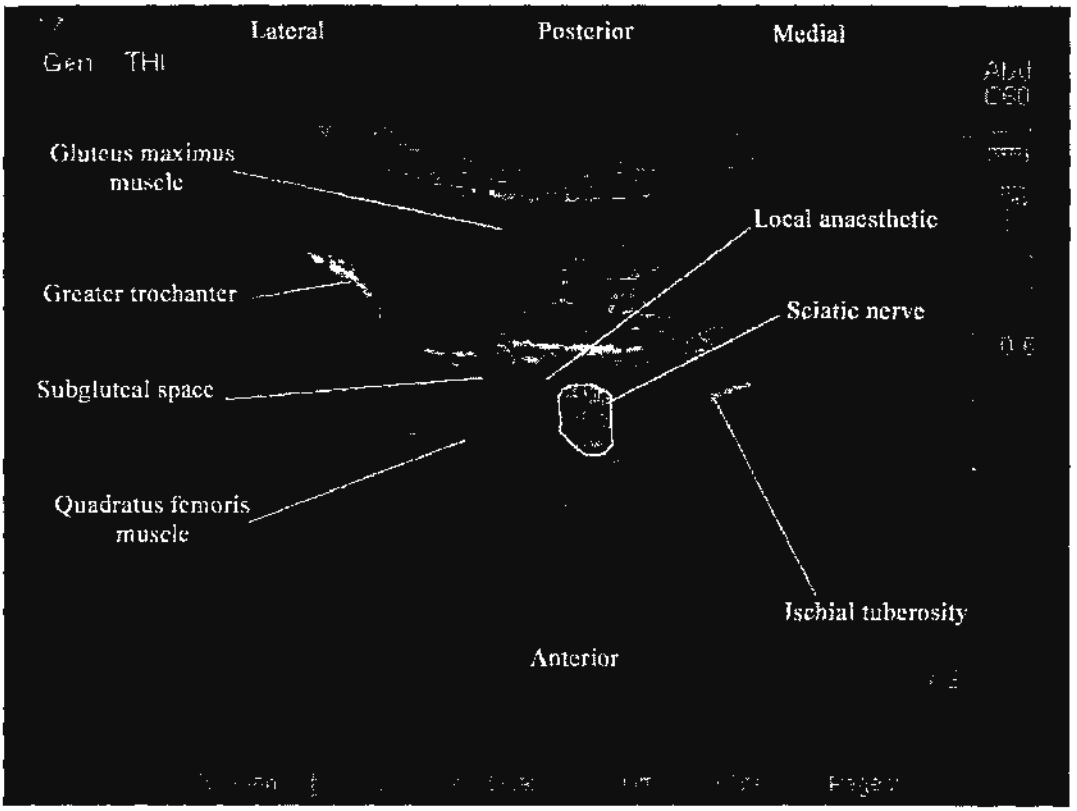

(b)

Figure 9-2b. A typical transverse sonogram of the sciatic nerve at the level of the greater trochanter and ischial tuberosity after 25 ml of local anesthetic injection. Note the distention of the subgluteal space and circumferential spread of local anesthetic around the sciatic nerve (reproduced with permission from www.aic.cuhk.edu.hk/usgraweb).

9.3 Results

9.3.1 Demographic Data

12 patients were recruited for this study. Data from one patient (No.1) was excluded because the depth-setting has to be changed during the procedure. Therefore data from 11 patients (6 male and 5 female) were analyzed. Demographic data are presented in **Table 9-1**.

9.3.2 Changes in Cross Sectional Area of the Sciatic Nerve

The mean CSA of the sciatic nerve at the three time points (Time A, B and C) are presented in **Table 9-2**. The CSA of sciatic nerve at the Time B and C were significantly smaller than that at Time A, p=0.003 and p=0.019, respectively, but there were no difference between that at Time B and C, p=0.578.

9.3.3 Changes in Echo Intensity of the Sciatic Nerve

The mean EI of the sciatic nerve at the three time points (Time A, B and C) are also presented in **Table 9-2**. The EI of the sciatic nerve at Time B and C were significantly higher than that at Time A, p<0.0005 and p=0.019 respectively. However, there was no significant difference in the EI between Time B and C, p=0.062.

9.4 Discussion

We have demonstrated that there is a significant reduction in the CSA and increase in the EI of the sciatic nerve during an US-guided sciatic nerve block at the subgluteal space.

We are not aware of any comparable quantitative data in the literature evaluating changes in the CSA and EI of a peripheral nerve during US guided peripheral nerve blockade. The increase in the EI of the sciatic nerve may be explained by the effects of the LA on the reflection coefficient (α_R) of the US, posterior wall acoustic enhancement of the US signal, and changes in the acoustic impendence (Z).

9.4.1 Reproducibility of Measurements

We have demonstrated that there is a good reproducibility in the measurement of CSA and EI using computer assisted image analysis. For more details please refer to **Section 4.3.2** in **Chapter 4**.

9.4.2 Reflection Coefficient and Echo Intensity

The proportion of the US beam that is reflected from an interface depends on the difference in acoustic impedance (Z) between the tissue medium 1 and 2 of the interface. For an US that is perpendicular to the interface, the amount of incident energy that is reflected between interfaces is expressed as the reflection coefficient (α_R). The α_R value can be calculated from the Z of the two acoustic mediums using the following equation (Karmakar and Kwok, 2009, Marhofer and Frickey, 2006, Rumack et al., 1998):

$$\alpha_R = \left(\frac{Z_2 - Z_1}{Z_2 + Z_1}\right)^2 \quad (9\text{-}1)$$

Currently we are not aware of any published data describing the Z of a human sciatic nerve or LA. It is reasonable to assume that the Z of a LA is comparable to water, the average Z of skeletal muscle is 1.7 kg-m^{-2}-s^{-1} $\times 10^{-4}$, and water is 1.5 kg-m^{-2}-s^{-1} $\times 10^{-4}$ (Hendee and Ritenour, 2002b). Before LA injection the sciatic nerve is surrounded by muscles and soft tissues (Karmakar et al., 2007), and the α_R at the muscle-nerve interface can be determined by subtracting Z value of the muscle and the sciatic nerve. When a LA is injected into the subgluteal space, it rapidly spread around the sciatic nerve and distends the subgluteal space. Thus, the muscle-nerve interface is now replaced by the LA-nerve interface. Since the Z of the LA is lower than that of a skeletal muscle, based on the **equation 9-1** above, the α_R at the LA-nerve interface

now become larger than that at the muscle-nerve interface. With a larger *Z* mismatch at the LA-nerve interface, a greater proportion of the incident US wave is now reflected back to the transducer during LA injection.

9.4.3 Posterior Acoustic Enhancement and Echo Intensity

The gluteus maximus muscle lies above the sciatic nerve along the path of the US beam. When the LA was injected into the subgluteal space it readily spreads around the sciatic nerve and replaces the muscle as the interface. Attenuation of an US beam as it travels through a medium is the sum of both absorption and scattering of the US energy. Attenuation is overcome in most US system by using TGC, which basically amplifies the signals returning from deeper structures and display them as echoes of similar intensity (Hedrick et al., 2005, Hendee and Ritenour, 2002b). The attenuation coefficient α can be calculated by using the following equation:

$$\alpha = \alpha_1 \times v \quad (9\text{-}2)$$

In the equation above, "α" is attenuation coefficient, "α_1" is the attenuation coefficient at 1MHz, and "v" is the frequency of US. The attenuation coefficient of the sciatic nerve of fresh human cadaver specimens is 4.8dB/cm (cross fibers) at 3.4 MHz US (Colombati S and Petralia S, 1950), and that of the human fresh gluteal muscle is 5.17dB/cm at 0.8MHz US (Goss et al., 1978a). In this study the frequency of US used was 5-2 MHz, and based on the **equation 9-2**, the average *α* of the sciatic nerve is 4.94dB/cm and that of gluteal muscle is 22.6dB/cm. To the best of our knowledge, there are no data describing the α of a LA, but as mentioned above, we believe that it is reasonable to assume that it is comparable to that of water. The *α* of water is 0.0022 dB/cm at 1MHz US, so the average α of the LA is 0.077dB/cm at 5-2MHz US. The α of a skeletal muscle is greater than that of the sciatic nerve, but the

α of LA is remarkably smaller that of the sciatic nerve. When LA is injected around the sciatic nerve, less attenuation of an US wave occurs as it travels through the LA to the sciatic nerve compared to that before to the injection. However, the higher intensity of the reflected signals from the deeper structure, sciatic nerve, is still compensated by TGC of the US system. Therefore the greater amplitude of the reflected echoes from the sciatic nerve during LA injection, which is due to overcompensation by the TGC in the US system, also contributes to an increasing brightness of an US image displayed on the monitor.

9.4.4 Change in the Cross Sectional Area of the Sciatic Nerve

The CSA of the sciatic nerve was significant smaller during the LA injection. The acoustic impedance ($Z = \rho \times c$) is determined by the product of the density (ρ) of the medium and the propagation velocity (c) of the sound in the medium. (Hedrick et al., 2005,Hendee and Ritenour, 2002b) Density (ρ) of an object is the mass of a medium per unit volume ($\rho = m/v$). During the injection of LA the CSA of the sciatic nerve decreased probably due to compression of the nerve by the LA in the subgluteal space. Therefore, the ρ increased based on the equation. Since mass of the sciatic nerve was constant during the procedure, the Z of the sciatic nerve may become larger.

9.4.5 Echo Intensity after Local Anesthetic Injection

There was a trend for the EI to reduce after the injection of LA compared to the increase during the injection. However, the difference did not reach statistically significance. We believe that this may be due to a relatively small sample size in our study. It is known that LA spreads rapidly along the course of the sciatic nerve after the LA injection during US guided SNB (Karmakar et al., 2007,Sinha and Chan,

2004). The LA surrounding the sciatic nerve may have decreased due to the spread within the subgluteal space. This may offset the reasons that initially increase the EI of the sciatic nerve at the subgluteal during the LA injection.

9.5 Limitations

Our results must be interpreted after considering the following facts. Anisotropy or angular dependence can affect the echogenicity of an imaged structure (Soong et al., 2005) In this study we tried to minimize the effects of anisotropy by aligning the transducer at right angles so that it produced maximum echogenicity of the sciatic nerve and used the average of three CSA and EI measurements of the sciatic nerve. We observed the changes in the CSA and EI of the sciatic nerve only 3 minutes after the LA injection. One may also question the different baseline setting for each patient unlike the standardized system settings used in the other studies of the project. In the routine clinical practice, the depth and gain settings are commonly changed and rarely kept constant to optimize the image. We believe that the EI measurement of the sciatic nerve in this study is still valid because they were repeated at three different time points, and only differences between the measurements were taken into consideration for the comparison.

9.6 Conclusion

In conclusion, using computer assisted gray-scale analysis we have demonstrated that there is a significant increase in the echo intensity of the sciatic nerve with a reduction of cross sectional area during US guided sciatic nerve blockade. This may explain why the sciatic nerve appears brighter and better delineated during US-guided peripheral nerve blockade.

Table 9-1. Demographic data.

No	Gender (n)	Age (year)	Weight (kg)	Height (cm)	BMI (kg/m^2)
11	6M/5F	53.4 (19.3;26-78)	63.7 (11.8; 43-80)	168 (6.9; 155-178)	22.4 (2.94; 16.4-25.5)

Data are presented as mean (SD; range). n=frequency; M=male; F=female and BMI=body mass index.

Table 9-2. Echo Intensity and cross sectional area of the sciatic nerve during US guided SNB.

	Time A (Before Injection)	Time B (During Injection)	Time C (3min After Injection)	*p*-value
EI	107.3 (19.3; 94.4-120.3)	152.3 (22.7; 137.0-167.5)	131.7 (24.7; 115-148)	<0.0005 *
CSA (mm^2)	156 (57; 117-194)	102 (35; 79-126)	117 (31; 96-138)	<0.0005 †

Data are presented as mean (SD; 95%CI). EI=echo intensity; CSA=cross sectional area. One way repeated measures ANOVA was used to compare the differences in the EI and CSA at these 3 time points. * indicates adjustments for multiple comparisons of EI of nerve between three time points: Time A vs. Time B $p<0.0005$, Time A vs. Time C $p= 0.019$ and Time B vs. Time C $p= 0.062$. † indicates adjustments for multiple comparisons of CSA of nerve between three time points: Time A vs. Time B $p= 0.003$, Time A vs. Time C $p= 0.019$ and Time B vs. Time C $p= 0.578$. $p< 0.05$ is considered statistically significant.

Chapter 10

Summary

Regional anesthetic procedures (peripheral and central neuraxial blocks) are frequently performed for anesthesia or analgesia during the perioperative period. Recently there has been an increase in interest in the use of ultrasound to guide peripheral and central neuraxial blocks in both adults and children. Ultrasound allows the target peripheral nerve and the surrounding structures to be directly visualized in real-time during block placement. It also helps to decide on the best possible site and maximum safe depth for needle insertion, allows real-time guidance of the needle to the target site, and visualize the spread of the injected local anesthetic in real-time. Currently the majority of published data on ultrasound guided regional anesthesia have largely focused on the application and efficacy of ultrasound guidance for peripheral nerve blockade. The peripheral nerves are visualized using ultrasound, and qualitative sonographic characteristics of peripheral nerves have been described in the literature. There are no quantitative data on musculoskeletal structures during ultrasound guided regional anesthesia. Quantitative ultrasonographic methods have been used in radiology to evaluate the echogenicity and echotexture of muscles. Therefore, it seemed plausible to extend these methods to quantify US images during regional anesthesia.

A brief introduction of ultrasound guided regional anesthesia and the objectives of this project are presented in **Chapter 1**. **Chapter 2** describes a brief history of ultrasound guided regional anesthesia, the basic principles of ultrasonography, a review on the validation, reproducibility and reliability of quantitative ultrasonography methods, the anatomy and sonoanatomy of a normal peripheral

nerve, a review of the qualitative echotexture of a peripheral nerve, and limitations of qualitative methods. **Chapter 2** also reviews different methods used to evaluate the echogenicity of musculoskeletal structure in an ultrasound image. My review of the literature shows that quantitative ultrasonographic methods using computer assisted image analysis provide more objective assessment of the echo intensity and echotexture in an ultrasound image, and it is appropriate for research. **Chapter 3** describes in detail the methods and procedures used in this project. This includes the equipment and software used, image acquisition and transfer of data, the procedure for standardizing the ultrasound system settings, image normalization, spatial calibration scale and "off-cart" measurement of dimension (distance and area), EI measurement, noise reduction, thresholding and texture measurements. **Chapter 4** evaluates the reproducibility of the quantitative ultrasonographic method used to measure distance, area, echo intensity and texture. The ultrasound images that were obtained following a standardized scan protocol were analyzed twice to evaluate interobserver agreement and intraobserver consistency. Results of this study demonstrate that the quantitative ultrasonographic methods used in this project are reproducible. **Chapter 5** investigates how changes in ultrasound system setting affect the echo intensity of an ultrasound image. A relationship was established between echo intensity and the parameters of system settings, which include frequency, gain, depth, dynamic range, and power output, using a tissue-mimicking phantom. It further demonstrates a positive linear correlation between the echo intensity of the phantom and the amount of gain and power output used. Moreover, there is also a negative linear correlation of the echo intensity of the phantom and the frequency, dynamic ranges, and depth setting. These results show that it is essential to standardize the settings of an ultrasound system during quantitative ultrasonography.

Chapter 6 evaluates the correlation between measurements made using the "in-cart" (electronic caliper) and "off-cart" method that was developed for this study and describes the sonoanatomy of the left infraclavicular fossa of 98 patients using an "off-cart" measurement method. A saggital scan of the musculoskeletal structures at the left infraclavicular fossa was obtained using a high frequency (6-13 MHz) linear-array transducer. The distance from the skin to the axillary artery and vein, the diameter and cross sectional area of the axillary artery and vein, and the width of the pectoral muscles were measured. This is first report evaluating the correlation between the "in-cart" and "off-cart" measurements in musculoskeletal sonography. We have demonstrated that there was a good correlation between measurements using the "in-cart" (electronic caliper) and "off-cart" method, indicating that "off-cart" (software) measurements can substitute "in-cart" measurements for research purposes. Moreover, in **Chapter 6** using the "off-cart" measurements we were also able to demonstrate age and gender related differences in the measurements of musculoskeletal structure at the infraclavicular fossa. **Chapter 7** determines the echo intensity of the median nerve and flexor muscles at the forearm in 13 young and 11 elderly subjects using computer assisted gray-scale analysis. A high frequency (13-6 MHz) linear-array transducer was used for the scan. The settings of the ultrasound system were standardized, and ultrasound images were normalized. This is the first study to measure the echo intensity of a peripheral nerve. The results have shown that there is an increase in the echo intensity of the median nerve and flexor muscles in the forearm, and a decrease in the contrast between the nerve and muscle. **Chapter 8** compares the echotexture of the median nerve in 10 young and 10 elderly subjects using "off-cart" measurement and computer assisted gray-scale and texture analysis. The settings of the ultrasound system were also standardized, and ultrasound images

were normalized. This is also the first study to demonstrate the echotexture of a peripheral nerve. Results of this study demonstrate that there is an increase in the white area index, and echo intensity, and a reduction in the black area index and cross sectional area of the median nerve in the elderly. Our findings from **Chapter 7** and **Chapter 8** provide an explanation on why the median nerve appears a smaller, whiter and brighter on a brighter background sonogram in the elderly. **Chapter 9** describes the changes in the echogenicity of a sciatic nerve during ultrasound guided sciatic nerve blockade. After the standardization of the system settings and normalization of ultrasound images, using computer assisted gray-scale analysis we have demonstrated that there is an increase in the echo intensity of the sciatic nerve and a reduction in cross sectional area of the nerve after local anesthetic injection during ultrasound guided sciatic nerve blockade. This is the first quantitative report of this phenomenon. Our finding may explain why the sciatic nerve appears brighter and better delineated after local anesthetic injection during ultrasound guided sciatic nerve blockade.

In conclusion, in this project several computer-assisted image analysis methods were developed and used to quantitatively evaluate ultrasound images during ultrasound guided regional anesthesia. Parameters that were evaluated included "off-cart" measurement of distance, area, echo intensity and echotexture. The methods used for computer assisted image analysis were found to be accurate and reproducible. The echo intensity measurement is affected by the settings in the ultrasound system. There is a good correlation between "off-cart" and "in-cart" measurements, and "off-cart" measurements that were made at the infraclavicular fossa demonstrated significant age and gender-related differences in the dimension of the musculoskeletal structure. There are significant differences in the cross sectional area,

echo intensity and echotexture of the median nerve in the young and the elderly. There are also significant differences in the echo intensity of the flexor muscles of the forearm, and contrast between the nerve and the muscles. These changes may be due to age-related histological changes in the nerve and muscle. Moreover, the changes in echo intensity and cross sectional area of the sciatic nerve after local anesthetic injection during ultrasound-guided nerve blockade were quantified. Future research should correlate quantitative echotexture and histology of a peripheral nerve.

Bibliography

Abe T, Brechue W F, Fujita S, Brown J B. Gender differences in FFM accumulation and architectural characteristics of muscle. Med Sci Sports Exerc 1998; (30): 1066-1070.

Abe T, Kearns C F, Fukunaga T. Sex differences in whole body skeletal muscle mass measured by magnetic resonance imaging and its distribution in young Japanese adults. Br J Sports Med 2003; (37): 436-440.

Abramowitz H B, Cohen C. Use of Doppler for difficult axillary block. Anesthesiology 1981; (55): 603.

Arts I M, Pillen S, Overeem S, Schelhaas H J, Zwarts M J. Rise and fall of skeletal muscle size over the entire life span. J Am Geriatr Soc 2007; (55): 1150-1152.

Asbury A K. Peripheral nerves. In: Histology and histopathology of the nervous system. (Eds.Haymaker W, Adams RD). Springfield, Illinois: Charles C Thomas, 1982; 1st: 1566-1610.

Assmann N, McCartney C J, Tumber P S, Chan V W. Ultrasound guidance for brachial plexus localization and catheter insertion after complete forearm amputation. Reg Anesth Pain Med 2007; (32): 93.

Azcoitia I, Leonelli E, Magnaghi V, Veiga S, Garcia-Segura L M, Melcangi R C. Progesterone and its derivatives dihydroprogesterone and tetrahydroprogesterone reduce myelin fiber morphological abnormalities and myelin fiber loss in the sciatic nerve of aged rats. Neurobiol Aging 2003; (24): 853-860.

Bader H. Dependence of wall stress in the human thoracic aorta on age and pressure. Circ Res 1967; (20): 354-361.

Barron D J, Tolan M J, Lea R E. A randomized controlled trial of continuous extra-pleural analgesia post-thoracotomy: efficacy and choice of local anaesthetic. Eur J Anaesthesiol 1999; (16): 236-245.

Becchi C, Al M M, Coppini R, Campolo M, Magherini M, Boncinelli S. Opioid-free analgesia by continuous psoas compartment block after total hip arthroplasty. A randomized study. Eur J Anaesthesiol 2008; (25): 418-423.

Benetos A, Laurent S, Hoeks A P, Boutouyrie P H, Safar M E. Arterial alterations with aging and high blood pressure. A noninvasive study of carotid and femoral arteries. Arterioscler Thromb 1993; (13): 90-97.

Biboulet P, Morau D, Aubas P, Bringuier-Branch, Capdevila X. Postoperative analgesia after total-hip arthroplasty: Comparison of intravenous patient-controlled analgesia with morphine and single injection of femoral nerve or psoas compartment block. a prospective, randomized, double-blind study. Reg Anesth Pain Med 2004; (29): 102-109.

Bigeleisen P E. Nerve puncture and apparent intraneural injection during ultrasound-guided axillary block does not invariably result in neurologic injury. Anesthesiology 2006; (105): 779-783.

Bjarnegard N, Ahlgren A R, Sandgren T, Sonesson B, Lanne T. Age affects proximal brachial artery stiffness; differential behavior within the length of the brachial artery? Ultrasound Med Biol 2003; (29): 1115-1121.

Bjarnegard N, Ryden A A, Sonesson B, Lanne T. The effect of sympathetic stimulation on proximal brachial artery mechanics in humans--differential behaviour within the length of the brachial artery? Acta Physiol Scand 2004; (182): 21-27.

Bloc S, Garnier T, Komly B, Asfazadourian H, Leclerc P, Mercadal L, Morel B, Dhonneur G. Spread of injectate associated with radial or median nerve-type motor response during infraclavicular brachial-plexus block: an ultrasound evaluation. Reg Anesth Pain Med 2007; (32): 130-135.

Bonnel F. Microscopic anatomy of the adult human brachial plexus: an anatomical and histological basis for microsurgery. Microsurgery 1984; (5): 107-118.

Broadbent C R, Maxwell W B, Ferrie R, Wilson D J, Gawne-Cain M, Russell R. Ability of anaesthetists to identify a marked lumbar interspace. Anaesthesia 2000; (55): 1122-1126.

Brockmann K, Becker P, Schreiber G, Neubert K, Brunner E, Bonnemann C. Sensitivity and specificity of qualitative muscle ultrasound in assessment of suspected neuromuscular disease in childhood. Neuromuscul Disord 2007; (17): 517-523.

Cartwright M S, Shin H W, Passmore L V, Walker F O. Ultrasonographic reference values for assessing the normal median nerve in adults. J Neuroimaging 2009; (19): 47-51.

Casati A, Baciarello M, Di C S, Danelli G, De M G, Leone S, Rossi M, Fanelli G. Effects of ultrasound guidance on the minimum effective anaesthetic volume required to block the femoral nerve. Br J Anaesth 2007a; (98): 823-827.

Casati A, Danelli G, Baciarello M, Corradi M, Leone S, Di C S, Fanelli G. A prospective, randomized comparison between ultrasound and nerve stimulation guidance for multiple injection axillary brachial plexus block. Anesthesiology 2007b; (106): 992-996.

Castellano G, Bonilha L, Li L M, Cendes F. Texture analysis of medical images. Clin Radiol 2004; (59): 1061-1069.

Chan V W. Applying ultrasound imaging to interscalene brachial plexus block. Reg Anesth Pain Med 2003; (28): 340-343.

Chan V W, Peng P W, Kaszas Z, Middleton W J, Muni R, Anastakis D G, Graham B A. A comparative study of general anesthesia, intravenous regional anesthesia, and axillary block for outpatient hand surgery: clinical outcome and cost analysis. Anesth Analg 2001; (93): 1181-1184.

Chan V W, Perlas A, McCartney C J, Brull R, Xu D, Abbas S. Ultrasound guidance improves success rate of axillary brachial plexus block. Can J Anaesth 2007; (54): 176-182.

Chan V W, Perlas A, Rawson R, Odukoya O. Ultrasound-guided supraclavicular brachial plexus block. Anesth Analg 2003; (97): 1514-1517.

Chikui T, Kawazu T, Nakamura K, Urashima Y, Yuasa K, Kanda S. Intraoral sonographic features of tongue cancer after radical radiotherapy. Eur J Radiol 2004; (52): 246-256.

Choyce A, Chan V W, Middleton W J, Knight P R, Peng P, McCartney C J. What is the relationship between paresthesia and nerve stimulation for axillary brachial plexus block? Reg Anesth Pain Med 2001; (26): 100-104.

Colombati S, Petralia S. Assorbimento di ultrasuoni in tissuti animali. La Ricerca Scientifica 1950; (Jan-Feb): 71-78.

Cork R C, Kryc J J, Vaughan R W. Ultrasonic localization of the lumbar epidural space. Anesthesiology 1980; (52): 513-516.

Cottrell L. Histologic variations with age in apparently normal peripheral nerve trunks. Arch Neurol Psychiat (Chic) 1940; (43): 1138-1150.

Cousins M J, Bridenbaugh P O, Carr D B, Horlocker T T. Cousins & Bridenbaugh's neural blockade in clinical anesthesia and pain medicine. Lippincott Williams & Wilkins, Philadelphia 2009.

Crews J C, Gerancher J C, Weller R S. Pneumothorax after coracoid infraclavicular brachial plexus block. Anesth Analg 2007; (105): 275-277.

Critchley L A, Conway F. Hypotension during subarachnoid anaesthesia: haemodynamic effects of colloid and metaraminol. Br J Anaesth 1996; (76): 734-736.

Currie J M. Measurement of the depth to the extradural space using ultrasound. Br J Anaesth 1984; (56): 345-347.

Demondion X, Herbinet P, Boutry N, Fontaine C, Francke J P, Cotten A. Sonographic mapping of the normal brachial plexus. Am J Neuroradiol 2003; (24): 1303-1309.

Di Benedetto P, Casati A, Bertini L, Fanelli G. Posterior subgluteal approach to block the sciatic nerve: description of the technique and initial clinical experiences. Eur J Anaesthesiol 2002; (19): 682-686.

Dobrin P B, Mrkvicka R. Failure of elastin or collagen as possible critical connective tissue alterations underlying aneurysmal dilatation. Cardiovasc Surg 1994; (2): 484-488.

Domingo-Triado V, Selfa S, Martinez F, Sanchez-Contreras D, Reche M, Tecles J, Crespo M T, Palanca J M, Moro B. Ultrasound guidance for lateral midfemoral sciatic nerve block: a prospective, comparative, randomized study. Anesth Analg 2007; (104): 1270-4, tables.

Donald I. "Sonar": a new diagnostic echo-sounding technique in obstetrics and gynaecology. Proc R Soc Med 1962; (55): 637-638.

Donald I. Use of ultrasonics in diagnosis of abdominal swellings. Br Med J 1963; (2): 1154-1155.

Donald I, Macvicar J, Brown T G. Investigation of abdominal masses by pulsed ultrasound. Lancet 1958; (1): 1188-1195.

Dussik K T, Frith D J, Kyriazidou M, Sear R S. Measurements of articular tissues with ultrasound. Am J Phys Med 1958; (37): 160-165.

Eichenberger U, Greher M, Kirchmair L, Curatolo M, Moriggl B. Ultrasound-guided blocks of the ilioinguinal and iliohypogastric nerve: accuracy of a selective new technique confirmed by anatomical dissection. Br J Anaesth 2006; (97): 238-243.

Eisele R, Schmid R, Kinzl L, Kramer M, Katzmaier P, Hartwig E. Soft tissue texture analysis by B-mode-ultrasound in the evaluation of impairment in chronic low back pain. Eur J Ultrasound 1998; (8): 167-175.

Evans W J. Exercise, nutrition and aging. J Nutr 1992; (122): 796-801.

Fanelli G, Casati A, Garancini P, Torri G. Nerve stimulator and multiple injection technique for upper and lower limb blockade: failure rate, patient acceptance, and neurologic complications. Study Group on Regional Anesthesia. Anesth Analg 1999; (88): 847-852.

Floch H, Naux E, Pham D C, Dupas B, Pinaud M. Computed tomography scanning of the sciatic nerve posterior to the femur: Practical implications for the lateral midfemoral block. Reg Anesth Pain Med 2003; (28): 445-449.

Forbes G B. Longitudinal changes in adult fat-free mass: influence of body weight. Am J Clin Nutr 1999; (70): 1025-1031.

Fornage B D. Peripheral nerves of the extremities: imaging with US. Radiology 1988; (167): 179-182.

Forsberg F, Shi W T, Merritt C R, Dai Q, Solcova M, Goldberg B B. On the usefulness of the mechanical index displayed on clinical ultrasound scanners for predicting contrast microbubble destruction. J Ultrasound Med 2005; (24): 443-450.

Franco C D, Domashevich V, Voronov G, Rafizad A B, Jelev T J. The supraclavicular block with a nerve stimulator: to decrease or not to decrease, that is the question. Anesth Analg 2004; (98): 1167-1171.

Frontera W R, Hughes V A, Fielding R A, Fiatarone M A, Evans W J, Roubenoff R. Aging of skeletal muscle: a 12-yr longitudinal study. J Appl Physiol 2000a; (88): 1321-1326.

Frontera W R, Suh D, Krivickas L S, Hughes V A, Goldstein R, Roubenoff R. Skeletal muscle fiber quality in older men and women. Am J Physiol Cell Physiol 2000b; (279): C611-C618.

Gallagher D, Visser M, De Meersman R E, Sepulveda D, Baumgartner R N, Pierson R N, Harris T, Heymsfield S B. Appendicular skeletal muscle mass: effects of age, gender, and ethnicity. J Appl Physiol 1997; (83): 229-239.

Galloway S, Bodenham A. Ultrasound imaging of the axillary vein--anatomical basis for central venous access. Br J Anaesth 2003; (90): 589-595.

Gilda C. Breast imaging. Lippincott Williams & Wilkins, Philadelphia 2004.

Gomez R S, Mendes T C. Epidural anaesthesia as a complication of attempted brachial plexus blockade using the posterior approach. Anaesthesia 2006; (61): 591-592.

Goss S A, Frizzell L A, Dunn F. Frequency dependence of ultrasonic absorption in mammalian testis. J Acoust Soc Am 1978a; (63): 1226-1229.

Goss S A, Johnston R L, Dunn F. Comprehensive compilation of empirical ultrasonic properties of mammalian tissues. J Acoust Soc Am 1978b; (64): 423-457.

Graif M, Seton A, Nerubai J, Horoszowski H, Itzchak Y. Sciatic nerve: sonographic evaluation and anatomic-pathologic considerations. Radiology 1991; (181): 405-408.

Grau T, Leipold R W, Conradi R, Martin E, Motsch J. Efficacy of ultrasound imaging in obstetric epidural anesthesia. J Clin Anesth 2002a; (14): 169-175.

Grau T, Leipold R W, Delorme S, Martin E, Motsch J. Ultrasound imaging of the thoracic epidural space. Reg Anesth Pain Med 2002b; (27): 200-206.

Grau T, Leipold R W, Fatehi S, Martin E, Motsch J. Real-time ultrasonic observation of combined spinal-epidural anaesthesia. Eur J Anaesthesiol 2004; (21): 25-31.

Grau T, Leipold R W, Horter J, Conradi R, Martin E, Motsch J. The lumbar epidural space in pregnancy: visualization by ultrasonography. Br J Anaesth 2001a; (86): 798-804.

Grau T, Leipold R W, Horter J, Conradi R, Martin E O, Motsch J. Paramedian access to the epidural space: the optimum window for ultrasound imaging. J Clin Anesth 2001b; (13): 213-217.

Gray A T. Ultrasound-guided regional anesthesia: current state of the art. Anesthesiology 2006; (104): 368-373.

Greher M, Retzl G, Niel P, Kamolz L, Marhofer P, Kapral S. Ultrasonographic assessment of topographic anatomy in volunteers suggests a modification of the infraclavicular vertical brachial plexus block. Br J Anaesth 2002; (88): 632-636.

Griffin D R. Echolocation by blind men, bat and radar. Science 1944; (100): 589-590.

Gruber H, Peer S, Kovacs P, Marth R, Bodner G. The ultrasonographic appearance of the femoral nerve and cases of iatrogenic impairment. J Ultrasound Med 2003; (22): 163-172.

Gurkan Y, Acar S, Solak M, Toker K. Comparison of nerve stimulation vs. ultrasound-guided lateral sagittal infraclavicular block. Acta Anaesthesiol Scand 2008; (52): 851-855.

Hadzic A. Textbook of regional anesthesia and acute pain management. McGraw-Hill, Medical Pub. Division, New York 2007.

Hadzic A, Arliss J, Kerimoglu B, Karaca P E, Yufa M, Claudio R E, Vloka J D, Rosenquist R, Santos A C, Thys D M. A comparison of infraclavicular nerve block versus general anesthesia for hand and wrist day-case surgeries. Anesthesiology 2004; (101): 127-132.

Hadzic A, Karaca P E, Hobeika P, Unis G, Dermksian J, Yufa M, Claudio R, Vloka J D, Santos A C, Thys D M. Peripheral nerve blocks result in superior recovery profile

compared with general anesthesia in outpatient knee arthroscopy. Anesth Analg 2005a; (100): 976-981.

Hadzic A, Williams B A, Karaca P E, Hobeika P, Unis G, Dermksian J, Yufa M, Thys D M, Santos A C. For outpatient rotator cuff surgery, nerve block anesthesia provides superior same-day recovery over general anesthesia. Anesthesiology 2005b; (102): 1001-1007.

Heckmatt J Z, Dubowitz V. Diagnostic advantage of needle muscle biopsy and ultrasound imaging in the detection of focal pathology in a girl with limb girdle dystrophy. Muscle Nerve 1985; (8): 705-709.

Heckmatt J Z, Dubowitz V. Ultrasound imaging and directed needle biopsy in the diagnosis of selective involvement in muscle disease. J Child Neurol 1987; (2): 205-213.

Heckmatt J Z, Leeman S, Dubowitz V. Ultrasound imaging in the diagnosis of muscle disease. J Pediatr 1982; (101): 656-660.

Heckmatt J Z, Pier N, Dubowitz V. Real-time ultrasound imaging of muscles. Muscle Nerve 1988; (11): 56-65.

Hedrick W R, Hykes D L, Starchman D E. Ultrasound physics and instrumentation. Elsevier Mosby, St. Louis, Mo. 2005.

Heinemeyer O, Reimers C D. Ultrasound of radial, ulnar, median, and sciatic nerves in healthy subjects and patients with hereditary motor and sensory neuropathies. Ultrasound Med Biol 1999; (25): 481-485.

Hendee W R, Ritenour E R. Ultrasound instrumentation. In: Medical imaging physics. (Ed.Hendee WR RE). New York: Wiley-Liss, 2002a; 4th: 331-341.

Hendee W R, Ritenour E R. Ultrasound wave. In: Medical imaging physics. (Ed.Hendee WR RE). New York: Wiley-Liss, 2002b; 4th: 303-316.

Jacobs J M, Love S. Qualitative and quantitative morphology of human sural nerve at different ages. Brain 1985; (108 (Pt 4)): 897-924.

Jaffe C C, Harris D J. Physical factors influencing numerical echo-amplitude data extracted from B-scan ultrasound images. J Clin Ultrasound 1980; (8): 327-333.

Jan van G G, Tielens L, Gielen M. Ultrasound-guided interscalene brachial plexus block in a child with femur fibula ulna syndrome. Paediatr Anaesth 2006; (16): 330-332.

Jeanneret C, Labs K H, Aschwanden M, Bollinger A, Hoffmann U, Jager K. Physiological reflux and venous diameter change in the proximal lower limb veins during a standardised Valsalva manoeuvre. Eur J Vasc Endovasc Surg 1999; (17): 398-403.

Kamolz L P, Schrogendorfer K F, Rab M, Girsch W, Gruber H, Frey M. The precision of ultrasound imaging and its relevance for carpal tunnel syndrome. Surg Radiol Anat 2001; (23): 117-121.

Kaplan D, Qinglin Ma. On the statistical characteristics of log-compressed Rayleighsignals: theoretical formulation and experimental results. J Acoust Soc Am 1994; (95): 1396.

Kapral S, Krafft P, Eibenberger K, Fitzgerald R, Gosch M, Weinstabl C. Ultrasound-guided supraclavicular approach for regional anesthesia of the brachial plexus. Anesth Analg 1994; (78): 507-513.

Kapral S, Krafft P, Gosch M, Fleischmann D, Weinstabl C. Ultrasound imaging for stellate ganglion block: direct visualization of puncture site and local anesthetic spread. A pilot study. Reg Anesth 1995; (20): 323-328.

Karmakar M K, Critchley L A, Ho A M, Gin T, Lee T W, Yim A P. Continuous thoracic paravertebral infusion of bupivacaine for pain management in patients with multiple fractured ribs. Chest 2003; (123): 424-431.

Karmakar M K, Ho A M, Li X, Kwok W H, Tsang K, Ngan Kee W D. Ultrasound-guided lumbar plexus block through the acoustic window of the lumbar ultrasound trident. Br J Anaesth 2008; (100): 533-537.

Karmakar M K, Kwok W H. Ultrasound-guided regional anesthesia. In: A practice of anesthesia for infants and children. (Eds.Charles JC, Jerrold LI, Todres ID). Philadelphia, PA: Saunders/Elsevier, 2009; 4th: 911-938.

Karmakar M K, Kwok W H, Ho A M, Tsang K, Chui P T, Gin T. Ultrasound-guided sciatic nerve block: description of a new approach at the subgluteal space. Br J Anaesth 2007; (98): 390-395.

Karmakar M K, Li X, Ho A M, Kwok W H, Chui P T. Real-time ultrasound-guided paramedian epidural access: evaluation of a novel in-plane technique. Br J Anaesth 2009.

Kawasaki T, Sasayama S, Yagi S, Asakawa T, Hirai T. Non-invasive assessment of the age related changes in stiffness of major branches of the human arteries. Cardiovasc Res 1987; (21): 678-687.

Klaastad O, Lilleas F G, Rotnes J S, Breivik H, Fosse E. Magnetic resonance imaging demonstrates lack of precision in needle placement by the infraclavicular brachial plexus block described by Raj et al. Anesth Analg 1999; (88): 593-598.

Klaastad O, Lilleas F G, Rotnes J S, Breivik H, Fosse E. A magnetic resonance imaging study of modifications to the infraclavicular brachial plexus block. Anesth Analg 2000; (91): 929-933.

Knipp B S, Zagzebski J A, Wilson T A, Dong F, Madsen E L. Attenuation and backscatter estimation using video signal analysis applied to B-mode images. Ultrason Imaging 1997; (19): 221-233.

Ko G T, Chan J C, Tsang L W, Critchley J A, Cockram C S. Smoking and diabetes in Chinese men. Postgrad Med J 2001; (77): 240-243.

Koscielniak-Nielsen Z J, Rasmussen H, Nielsen P T. Patients' perception of pain during axillary and humeral blocks using multiple nerve stimulations. Reg Anesth Pain Med 2004; (29): 328-332.

Koscielniak-Nielsen Z J, Rotboll-Nielsen P, Rassmussen H. Patients' experiences with multiple stimulation axillary block for fast-track ambulatory hand surgery. Acta Anaesthesiol Scand 2002; (46): 789-793.

Kremkau F W. Diagnostic ultrasound. W.B.Saunders, Philodelphia 2002.

Kuo Y W, Lu I C, Yen M K, Soo L Y, Lu D V, Chu K S. The feasibility of surface landmark for coracoid infraclavicular brachial plexus block by ultrasonographic assessment. Acta Anaesthesiol Taiwan 2007; (45): 27-32.

la Grange P, Foster P A, Pretorius L K. Application of the Doppler ultrasound blood flow detector in supraclavicular brachial plexus block. Br J Anaesth 1978; (50): 965-967.

Lal B K, Hobson R W, Pappas P J, Kubicka R, Hameed M, Chakhtoura E Y, Jamil Z, Padberg F T, Jr., Haser P B, Duran W N. Pixel distribution analysis of B-mode ultrasound scan images predicts histologic features of atherosclerotic carotid plaques. J Vasc Surg 2002; (35): 1210-1217.

Lamont A C, Graebe A C, Pelmore J M, Thompson J R. Ultrasound assessment of renal cortical brightness in infants: is naked eye evaluation reliable? Invest Radiol 1990; (25): 250-253.

Lefebvre F, Meunier M, Thibault F, Laugier P, Berger G. Computerized ultrasound B-scan characterization of breast nodules. Ultrasound Med Biol 2000; (26): 1421-1428.

Lin D C, Nazarian L N, O'Kane P L, McShane J M, Parker L, Merritt C R. Advantages of real-time spatial compound sonography of the musculoskeletal system versus conventional sonography. AJR Am J Roentgenol 2002; (179): 1629-1631.

Liu F C, Liou J T, Tsai Y F, Li A H, Day Y Y, Hui Y L, Lui P W. Efficacy of ultrasound-guided axillary brachial plexus block: a comparative study with nerve stimulator-guided method. Chang Gung Med J 2005; (28): 396-402.

Loewy J. Sonoanatomy of the median, ulnar and radial nerves. Can Assoc Radiol J 2002; (53): 33-38.

Long W B, Rosenblum S, Grady I P. Successful resuscitation of bupivacaine-induced cardiac arrest using cardiopulmonary bypass. Anesth Analg 1989; (69): 403-406.

Marhofer P, Frickey N. Ultrasonographic guidance in pediatric regional anesthesia Part 1: Theoretical background. Paediatr Anaesth 2006; (16): 1008-1018.

Marhofer P, Greher M, Kapral S. Ultrasound guidance in regional anaesthesia. Br J Anaesth 2005; (94): 7-17.

Marhofer P, Nasel C, Sitzwohl C, Kapral S. Magnetic resonance imaging of the distribution of local anesthetic during the three-in-one block. Anesth Analg 2000; (90): 119-124.

Marhofer P, Schrogendorfer K, Koinig H, Kapral S, Weinstabl C, Mayer N. Ultrasonographic guidance improves sensory block and onset time of three-in-one blocks. Anesth Analg 1997; (85): 854-857.

Marhofer P, Schrogendorfer K, Wallner T, Koinig H, Mayer N, Kapral S. Ultrasonographic guidance reduces the amount of local anesthetic for 3-in-1 blocks. Reg Anesth Pain Med 1998; (23): 584-588.

Marhofer P, Sitzwohl C, Greher M, Kapral S. Ultrasound guidance for infraclavicular brachial plexus anaesthesia in children. Anaesthesia 2004; (59): 642-646.

Martinoli C, Bianchi S, Derchi L E. Tendon and nerve sonography. Radiol Clin North Am 1999; (37): 691-711.

Martinoli C, Schenone A, Bianchi S, Mandich P, Caponetto C, Abbruzzese M, Derchi L E. Sonography of the median nerve in Charcot-Marie-Tooth disease. Am J Roentgenol 2002; (178): 1553-1556.

Maurits N M, Beenakker E A, van Schaik D E, Fock J M, van der Hoeven J H. Muscle ultrasound in children: normal values and application to neuromuscular disorders. Ultrasound Med Biol 2004; (30): 1017-1027.

Maurits N M, Bollen A E, Windhausen A, De Jager A E, Van Der Hoeven J H. Muscle ultrasound analysis: normal values and differentiation between myopathies and neuropathies. Ultrasound Med Biol 2003; (29): 215-225.

Mazziotti G, Sorvillo F, Iorio S, Carbone A, Romeo A, Piscopo M, Capuano S, Capuano E, Amato G, Carella C. Grey-scale analysis allows a quantitative evaluation of thyroid echogenicity in the patients with Hashimoto's thyroiditis. Clin Endocrinol (Oxf) 2003; (59): 223-229.

McCartney C J, Xu D, Constantinescu C, Abbas S, Chan V W. Ultrasound examination of peripheral nerves in the forearm. Reg Anesth Pain Med 2007; (32): 434-439.

McDonald J S, Spigos D G. Computed tomography-guided pudendal block for treatment of pelvic pain due to pudendal neuropathy. Obstet Gynecol 2000; (95): 306-309.

Merritt C R. Physics of ultrasound. In: Diagnostic ultrasound. (Eds.Rumack CM, Wilson SR, Charboneau JW). St. Louis,Mo.: Mosby, 1998; 2nd: 10-33.

Moayeri N, Bigeleisen P E, Groen G J. Quantitative architecture of the brachial plexus and surrounding compartments, and their possible significance for plexus blocks. Anesthesiology 2008; (108): 299-304.

Morita M, Sasano H, Azami T, Sasano N, Katsuya H. The skin-traction method increases the cross-sectional area of the internal jugular vein by increasing its anteroposterior diameter. J Anesth 2007; (21): 467-471.

Nakamichi K I, Tachibana S. Enlarged median nerve in idiopathic carpal tunnel syndrome. Muscle Nerve 2000; (23): 1713-1718.

Neal J M. How close is close enough? Defining the "paresthesia chad". Reg Anesth Pain Med 2001; (26): 97-99.

Newman P G, Rozycki G S. The history of ultrasound. Surg Clin North Am 1998; (78): 179-195.

Nielsen K C, Guller U, Steele S M, Klein S M, Greengrass R A, Pietrobon R. Influence of obesity on surgical regional anesthesia in the ambulatory setting: an analysis of 9,038 blocks. Anesthesiology 2005; (102): 181-187.

Nielsen K C, Steele S M. Outcome after regional anaesthesia in the ambulatory setting--is it really worth it? Best Pract Res Clin Anaesthesiol 2002; (16): 145-157.

Nielsen P K, Jensen B R, Darvann T, Jorgensen K, Bakke M. Quantitative ultrasound image analysis of the supraspinatus muscle. Clin Biomech (Bristol , Avon) 2000; (15 Suppl 1): S13-S16.

Nielsen P K, Jensen B R, Darvann T, Jorgensen K, Bakke M. Quantitative ultrasound tissue characterization in shoulder and thigh muscles--a new approach. BMC Musculoskelet Disord 2006; (7): 2.

Nishiyama M, Naganuma K, Amaki Y. A new approach for brachial plexus block under fluoroscopic guidance. Anesth Analg 1999; (88): 91-97.

Oberndorfer U, Marhofer P, Bosenberg A, Willschke H, Felfernig M, Weintraud M, Kapral S, Kettner S C. Ultrasonographic guidance for sciatic and femoral nerve blocks in children. Br J Anaesth 2007; (98): 797-801.

Ootaki C, Hayashi H, Amano M. Ultrasound-guided infraclavicular brachial plexus block: an alternative technique to anatomical landmark-guided approaches. Reg Anesth Pain Med 2000; (25): 600-604.

Orebaugh S L, Pennington S. Variant location of the musculocutaneous nerve during axillary nerve block. J Clin Anesth 2006; (18): 541-544.

Orebaugh S L, Williams B A. Brachial plexus anatomy: normal and variant. ScientificWorldJournal 2009; (9): 300-312.

Orebaugh S L, Williams B A, Kentor M L. Ultrasound guidance with nerve stimulation reduces the time necessary for resident peripheral nerve blockade. Reg Anesth Pain Med 2007; (32): 448-454.

Pavlin D J, Rapp S E, Polissar N L, Malmgren J A, Koerschgen M, Keyes H. Factors affecting discharge time in adult outpatients. Anesth Analg 1998; (87): 816-826.

Peer S. High resolution sonography of the peripheral nervous system: general consideration and technical concept. In: High resolution sonography of the peripheral nervous system. (Eds.Peer S, Bodner G). Berlin, Heidelberg: Springer, 2008; 2nd: 1-15.

Peer S, Kovacs P, Harpf C, Bodner G. High-resolution sonography of lower extremity peripheral nerves: anatomic correlation and spectrum of disease. J Ultrasound Med 2002; (21): 315-322.

Perlas A, Chan V W, Simons M. Brachial plexus examination and localization using ultrasound and electrical stimulation: a volunteer study. Anesthesiology 2003; (99): 429-435.

Perlas A, Niazi A, McCartney C, Chan V, Xu D, Abbas S. The sensitivity of motor response to nerve stimulation and paresthesia for nerve localization as evaluated by ultrasound. Reg Anesth Pain Med 2006; (31): 445-450.

Pillen S, Morava E, Van K M, Ter Laak H J, De Vries M C, Rodenburg R J, Zwarts M J. Skeletal muscle ultrasonography in children with a dysfunction in the oxidative phosphorylation system. Neuropediatrics 2006a; (37): 142-147.

Pillen S, van K M, Nievelstein R A, Verrips A, van Kruijsbergen-Raijmann W, Zwarts M J. Skeletal muscle ultrasonography: Visual versus quantitative evaluation. Ultrasound Med Biol 2006b; (32): 1315-1321.

Pinkney M N. Instrumentation. In: Ultrasonography : an introduction to normal structure and functional anatomy. (Eds.Curry RA, Tempkin BB). Philadelphia: W.B. Saunders Co., 1995a; 1st: 8-21.

Pinkney M N. Physics. In: Ultrasonography: an introduction to normal structure and functional anatomy. (Eds.Curry RA, Tempkin BB). Philadelphia: W.B. Saunders Co., 1995b; 1st: 2-7.

Plunkett A R, Brown D S, Rogers J M, Buckenmaier C C, III. Supraclavicular continuous peripheral nerve block in a wounded soldier: when ultrasound is the only option. Br J Anaesth 2006; (97): 715-717.

Pohle R, von Rohden L, Fisher D. Skeletal muscle sonography with texture analysis. Hanson, Kenneth M. Medical Imaging 1997: Image Processing 3034[1], 772-778. 1997. Newport Beach, CA, USA, SPIE.
Ref Type: Conference Proceeding

Portney L G, Watkins M P. Foundations of clinical research: applications to practice. Prentice Hall Health, Upper Saddle River, N.J. 2000.

Proctor D N, O'Brien P C, Atkinson E J, Nair K S. Comparison of techniques to estimate total body skeletal muscle mass in people of different age groups. Am J Physiol 1999; (277): E489-E495.

Rasmussen L S, Johnson T, Kuipers H M, Kristensen D, Siersma V D, Vila P, Jolles J, Papaioannou A, Abildstrom H, Silverstein J H, Bonal J A, Raeder J, Nielsen I K, Korttila K, Munoz L, Dodds C, Hanning C D, Moller J T. Does anaesthesia cause postoperative cognitive dysfunction? A randomized study of regional versus general anaesthesia in 438 elderly patients. Acta Anaesthesiol Scand 2003; (47): 260-266.

Redborg K E, Sites B D, Chinn C D, Gallagher J D, Ball P A, Antonakakis J G, Beach M L. Ultrasound improves the success rate of a sural nerve block at the ankle. Reg Anesth Pain Med 2009; (34): 24-28.

Reeves N D, Maganaris C N, Narici M V. Ultrasonographic assessment of human skeletal muscle size. Eur J Appl Physiol 2004; (91): 116-118.

Reimers C D, Fleckenstein J L, Witt T N, Muller-Felber W, Pongratz D E. Muscular ultrasound in idiopathic inflammatory myopathies of adults. J Neurol Sci 1993a; (116): 82-92.

Reimers K, Reimers C D, Wagner S, Paetzke I, Pongratz D E. Skeletal muscle sonography: a correlative study of echogenicity and morphology. J Ultrasound Med 1993b; (12): 73-77.

Retzl G, Kapral S, Greher M, Mauritz W. Ultrasonographic findings of the axillary part of the brachial plexus. Anesth Analg 2001; (92): 1271-1275.

Rominger C J. The normal axillary venogram. Am J Roentgenol Radium Ther Nucl Med 1958; (80): 217-224.

Rosenberg I H. Summary comments: epidemiological and methodological problems in determining nutritional status of older persons. Am J Clin Nutr 1989; (50 (suppl)): 1231-1233.

Rosenblatt M A, Abel M, Fischer G W, Itzkovich C J, Eisenkraft J B. Successful use of a 20% lipid emulsion to resuscitate a patient after a presumed bupivacaine-related cardiac arrest. Anesthesiology 2006; (105): 217-218.

Royse C E, Sha S, Soeding P F, Royse A G. Anatomical study of the brachial plexus using surface ultrasound. Anaesth Intensive Care 2006; (34): 203-210.

Rumack C M, Wilson S R, Charboneau J W. Diagnostic ultrasound. Mosby, St. Louis, Mo. 1998.

Russ J C. Acquiring images. In: The image processing handbook. (Ed.Russ JC). Boca Raton, FL: CRC Press, 2007a; 5th: 1-76.

Russ J C. Segmentation and thresholding. In: The image processing handbook. (Ed.Russ JC). Boca Raton, FL: CRC Press, 2007b; 5th: 397-439.

Sample W F, Mitchell S P, Bledsoe R C. Parathyroid ultrasonography. Radiology 1978; (127): 485-490.

Sanada K, Kearns C F, Midorikawa T, Abe T. Prediction and validation of total and regional skeletal muscle mass by ultrasound in Japanese adults. Eur J Appl Physiol 2006; (96): 24-31.

Sandhu N S, Capan L M. Ultrasound-guided infraclavicular brachial plexus block. Br J Anaesth 2002; (89): 254-259.

Sandhu N S, Maharlouei B, Patel B, Erkulwater E, Medabalmi P. Simultaneous bilateral infraclavicular brachial plexus blocks with low-dose lidocaine using ultrasound guidance. Anesthesiology 2006; (104): 199-201.

Saranteas T, Chantzi C, Zogogiannis J, Alevizou A, Anagnostopoulou S, Iatrou C, Dimitriou V. Lateral sciatic nerve examination and localization at the mid-femoral level: an imaging study with ultrasound. Acta Anaesthesiol Scand 2007; (51): 387-388.

Schafhalter-Zoppoth I, Zeitz I D, Gray A T. Inadvertent femoral nerve impalement and intraneural injection visualized by ultrasound. Anesth Analg 2004; (99): 627-628.

Scholten R R, Pillen S, Verrips A, Zwarts M J. Quantitative ultrasonography of skeletal muscles in children: normal values. Muscle Nerve 2003; (27): 693-698.

Schroeder S, Enderle M D, Baumbach A, Ossen R, Herdeg C, Kuettner A, Karsch K R. Influence of vessel size, age and body mass index on the flow-mediated dilatation (FMD%) of the brachial artery. Int J Cardiol 2000; (76): 219-225.

Schwemmer U, Schleppers A, Markus C, Kredel M, Kirschner S, Roewer N. Operative management in axillary brachial plexus blocks: comparison of ultrasound and nerve stimulation. Anaesthesist 2006; (55): 451-456.

Scorza A. A novel method for automatic evaluation of the effective dynamic range of medical ultrasound scanners. Sloten, J. V., Verdonck, P., Nyssen, M., and Haueisen, J. 4th European Conference of the International Federation for Medical and Biological Engineering. ECIFMBE 2008 22[1], 1607-1611. 2009. Antwerp, Belgium, Springer Berlin Heidelberg. IFMBE Proceedings. Magjarevic, R. and Nagel, J. H. 11-23-0080. Ref Type: Conference Proceeding

Shah S, Hadzic A, Vloka J D, Cafferty M S, Moucha C S, Santos A C. Neurologic complication after anterior sciatic nerve block. Anesth Analg 2005; (100): 1515-7, table.

Sharrock N E, Fischer G, Goss S, Flynn E, Go G, Sculco T P, Salvati E A. The early recovery of cognitive function after total-hip replacement under hypotensive epidural anesthesia. Reg Anesth Pain Med 2005; (30): 123-127.

Sheppard D G, Iyer R B, Fenstermacher M J. Brachial plexus: demonstration at US. Radiology 1998; (208): 402-406.

Silvestri E, Martinoli C, Derchi L E, Bertolotto M, Chiaramondia M, Rosenberg I. Echotexture of peripheral nerves: correlation between US and histologic findings and criteria to differentiate tendons. Radiology 1995; (197): 291-296.

Singelyn F J, Deyaert M, Joris D, Pendeville E, Gouverneur J M. Effects of intravenous patient-controlled analgesia with morphine, continuous epidural analgesia, and continuous three-in-one block on postoperative pain and knee rehabilitation after unilateral total knee arthroplasty. Anesth Analg 1998; (87): 88-92.

Sinha A, Chan V W. Ultrasound imaging for popliteal sciatic nerve block. Reg Anesth Pain Med 2004; (29): 130-134.

Sipila S, Suominen H. Ultrasound imaging of the quadriceps muscle in elderly athletes and untrained men. Muscle Nerve 1991; (14): 527-533.

Sipila S, Suominen H. Muscle ultrasonography and computed tomography in elderly trained and untrained women. Muscle Nerve 1993; (16): 294-300.

Sipila S, Suominen H. Quantitative ultrasonography of muscle: detection of adaptations to training in elderly women. Arch Phys Med Rehabil 1996; (77): 1173-1178.

Sites B D, Beach M L, Spence B C, Wiley C W, Shiffrin J, Hartman G S, Gallagher J D. Ultrasound guidance improves the success rate of a perivascular axillary plexus block. Acta Anaesthesiol Scand 2006; (50): 678-684.

Sites B D, Gallagher J, Sparks M. Ultrasound-guided popliteal block demonstrates an atypical motor response to nerve stimulation in 2 patients with diabetes mellitus. Reg Anesth Pain Med 2003; (28): 479-482.

Sladjana U Z, Ivan J D, Bratislav S D. Microanatomical structure of the human sciatic nerve. Surg Radiol Anat 2008; (30): 619-626.

Smith-Levitin M, Blickstein I, brecht-Shach A A, Goldman R D, Gurewitsch E, Streltzoff J, Chervenak F A. Quantitative assessment of gray-level perception: observers' accuracy is dependent on density differences. Ultrasound Obstet Gynecol 1997; (10): 346-349.

Soeding P E, Sha S, Royse C E, Marks P, Hoy G, Royse A G. A randomized trial of ultrasound-guided brachial plexus anaesthesia in upper limb surgery. Anaesth Intensive Care 2005; (33): 719-725.

Solbiati L, De P L, Ierace T, Bellotti E, Derchi L E. High-resolution sonography of the recurrent laryngeal nerve: anatomic and pathologic considerations. Am J Roentgenol 1985; (145): 989-993.

Sonesson B, Hansen F, Stale H, Lanne T. Compliance and diameter in the human abdominal aorta--the influence of age and sex. Eur J Vasc Surg 1993; (7): 690-697.

Soong J, Schafhalter-Zoppoth I, Gray A T. The importance of transducer angle to ultrasound visibility of the femoral nerve. Reg Anesth Pain Med 2005; (30): 505.

Stuart R M, Koh E S, Breidahl W H. Sonography of peripheral nerve pathology. Am J Roentgenol 2004; (182): 123-129.

Sunderland S. The adipose tissue of peripheral nerves. Brain 1945; (68): 118-122.

Sunderland S. The connective tissues of peripheral nerves. Brain 1965; (88): 841-854.

Sunderland S, Bradley K C. The cross-sectional area of peripheral nerve trunks devoted to nerve fibers. Brain 1949; (72): 428-449.

Sunderland S, Bradley K C. The perineurium of peripheral nerves. Anat Rec 1952; (113): 125-141.

Tagliafico A, Resmini E, Nizzo R, Bianchi F, Minuto F, Ferone D, Martinoli C. Ultrasound measurement of median and ulnar nerve cross-sectional area in acromegaly. J Clin Endocrinol Metab 2008; (93): 905-909.

Thierry Maisonobe J-J H. Changes in the Peripheral Nervous System. In: Principles of neural aging. (Ed.Sergio U.Dani AHGFW). Amsterdam ; Oxford : Elsevier, 1997; 304-316.

Tiago R, Pontes P, do Brasil O C. Age-related changes in human laryngeal nerves. Otolaryngol Head Neck Surg 2007; (136): 747-751.

Ting P L, Sivagnanaratnam V. Ultrasonographic study of the spread of local anaesthetic during axillary brachial plexus block. Br J Anaesth 1989; (63): 326-329.

Tohgi H, Tsukagoshi H, Toyokura Y. Quantitative changes with age in normal sural nerves. Acta Neuropathol 1977; (38): 213-220.

Tsubahara A, Chino N, Ishii H, Akaboshi K, Takahashi H, Saitoh M. Objective parameters in magnetic resonance imaging (MRI) for neuromuscular diagnosis: preliminary findings. Disabil Rehabil 1992; (14): 163-167.

Urmey W F, Stanton J. Inability to consistently elicit a motor response following sensory paresthesia during interscalene block administration. Anesthesiology 2002; (96): 552-554.

van der Heijden-Spek JJ, Staessen J A, Fagard R H, Hoeks A P, Boudier H A, Van Bortel L M. Effect of age on brachial artery wall properties differs from the aorta and is gender dependent: a population study. Hypertension 2000; (35): 637-642.

Wallace D H, Currie J M, Gilstrap L C, Santos R. Indirect sonographic guidance for epidural anesthesia in obese pregnant patients. Reg Anesth 1992; (17): 233-236.

Wang F Y, Wu S H, Lu I C, Hsu H T, Soo L Y, Tang C S, Chu K S. Ultrasonographic examination to search out the optimal upper arm position for coracoid approach to infraclavicular brachial plexus block--a volunteer study. Acta Anaesthesiol Taiwan 2007; (45): 15-20.

Watanabe M, Sawai T, Nagura H, Suyama K. Age-related alteration of cross-linking amino acids of elastin in human aorta. Tohoku J Exp Med 1996; (180): 115-130.

Williams S R, Chouinard P, Arcand G, Harris P, Ruel M, Boudreault D, Girard F. Ultrasound guidance speeds execution and improves the quality of supraclavicular block. Anesth Analg 2003; (97): 1518-1523.

Willschke H, Marhofer P, Bosenberg A, Johnston S, Wanzel O, Sitzwohl C, Kettner S, Kapral S. Epidural catheter placement in children: comparing a novel approach using ultrasound guidance and a standard loss-of-resistance technique. Br J Anaesth 2006; (97): 200-207.

Wilson J L, Brown D L, Wong G Y, Ehman R L, Cahill D R. Infraclavicular brachial plexus block: parasagittal anatomy important to the coracoid technique. Anesth Analg 1998; (87): 870-873.

Yang W T, Chui P T, Metreweli C. Anatomy of the normal brachial plexus revealed by sonography and the role of sonographic guidance in anesthesia of the brachial plexus. Am J Roentgenol 1998; (171): 1631-1636.

Young A, Stokes M, Crowe M. Size and strength of the quadriceps muscles of old and young women. Eur J Clin Invest 1984; (14): 282-287.

Young A, Stokes M, Crowe M. The size and strength of the quadriceps muscles of old and young men. Clin Physiol 1985; (5): 145-154.

Zaidman C M, Holland M R, Anderson C C, Pestronk A. Calibrated quantitative ultrasound imaging of skeletal muscle using backscatter analysis. Muscle Nerve 2008; (38): 893-898.

Zuberi S M, Matta N, Nawaz S, Stephenson J B, McWilliam R C, Hollman A. Muscle ultrasound in the assessment of suspected neuromuscular disease in childhood. Neuromuscul Disord 1999; (9): 203-207.

Appendices

Ethical Approval of Research Protocol

香港中文大學醫學院
Faculty Of Medicine
The Chinese University Of Hong Kong

醫院管理局
Hospital Authority
New Territories East Cluster

Joint The Chinese University of Hong Kong – New Territories East Cluster
Clinical Research Ethics Committee
香港中文大學–新界東醫院聯網 臨床研究倫理 聯席委員會

Flat 3C, Block B, Staff Quarters, Prince of Wales Hospital, Shatin, HK
Tel : (852) 2632 3935 Fax : (852) 2646 6653 Website : http://www.crec.cuhk.edu.hk

To: Xiang LI (PhD Student) 8 June 2007
Dept. of Anaesthesia and Intensive Care
The Chinese University of Hong Kong

Ethics Approval of Research Protocol

CREC Ref. No.:	**CRE-2007.213**
Date of Approval:	**08 June 2007***
Protocol Title:	**Quantitative Evaluation of the Echogenicity of Peripheral Nerves in Young and Elderly Subjects**
Investigator(s):	**Xiang LI, W.H. KWOK, Kristie H.S. TSANG and Anna LEE**
Supervisor(s):	**Prof. Manoj Kumar KARMAKAR**

I write to inform you that ethics approval has been given to you to conduct the captioned study in accordance with the following document(s) submitted:

- Clinical Trial Protocol
- Patient Informed Consent Form in English and Chinese Version

This ethics approval* will be valid for 12 months. Application for further renewal can be made by submitting the Ethics Renewal and Research Progress Report Form to the CREC (*Download the electronic form template from the* http://www.crec.cuhk.edu.hk or http://intec/home/Research%20Ethics/main.asp). It will be much appreciated if the completion of the project will be reported to the Committee in due course.

The Joint CUHK-NTEC Clinical Research Ethics Committee serves to confirm that research complies with the Declaration of Helsinki, ICH GCP Guidelines, local regulations, HA and University policies.

(Ms. Eva Kong)
Hospital Administrator
Joint CUHK-NTEC
Clinical Research Ethics Committee

EK/si

PATIENT CONSENT FORM
病人參與研究同意書

Department of Anaesthesia and Intensive Care

The Chinese University of Hong Kong

香港中文大學

麻醉及深切治療學系

Title of Study

Quantitative Evaluation of the Echogenicity of Peripheral Nerves in Young and Elderly Subjects

研究主題

對青年人群和老年人群的外周神經超聲定量評估研究

Background

Regional anaesthesia (peripheral nerve block or a central neuraxial block) is frequently performed for anaesthesia or analgesia during the preoperative period because it improves postoperative outcomes. Success of these techniques depends on the ability to accurately place the needle and thereby the local anaesthetic drugs close to the target nerve. Recently ultrasound has been used to guide regional anaesthetic procedure in both adults and children. Ultrasound guidance speeds the execution of peripheral nerve blocks, reduces the discomfort experienced during block placement, reduces the amount of local anaesthetic required, speeds the onset of sensory blockade, improves the quality of sensory-motor blockade, and prolongs the duration of sensory blockade. Therefore ultrasound guidance for regional anaesthesia is becoming increasingly popular amongst anesthesiologists including our group. However we have observed marked differences in the echogenicity of musculoskeletal structures between the young and the elderly patients, which makes ultrasound delineation of peripheral nerves and thus USGRA procedures in the elderly more difficult. Review of the literature shows that there is a strong linear correlation between age and muscle echo intensity making muscles appear whiter in the elderly patient. We are not aware of any published data quantifying age related differences in echogenicity of peripheral nerves which we plan to study in this research project.

研究背景

區域麻醉显著改善手術病人術後的預後情況，已經成為臨床外科手術中和術後麻醉鎮痛的常用技術。在进行操作时準確的穿刺針定位和局麻藥物在目標神經周圍的擴散是這項操作技術成功的關鍵。最近，超聲波技術被引入到成人和兒童的區域麻醉的操作之中，這項技術明顯縮短操作時間，減少病人術中不適

感， 而且在減少麻醉藥品的使用劑量的同時，加快了藥物感覺－運動阻滯起效時間並延長了作用時間和增強了神經阻滯的作用效果。因此，這項技術已經進一步獲得包括我們在內的很多麻醉醫生的歡迎。但是我們發現在年輕人和老年人的骨骼肌在超聲回聲結構上存在明顯差異，這種差異使的應用超聲識別老年人的周圍神經結構時出現更多的困難。通過文獻的檢索老年人的肌肉組織的超聲回聲密度更高，而且這種回聲密度的變化和年齡之間存在明顯線性相關，但是目前我們沒有在公開發表的文獻資料上發現關於這種差異的量化研究資料和資料，因此我們計畫開展這項科學研究專案。

The objectives of this study

To compare the echogenicity of peripheral nerves between the young and the elderly.

研究目標

比较年輕人与老年人的外週神經影像超声回声結構中的差异

Procedures

If you agree to participate, the following things will happen:

You will undergo ultrasound imaging of the median nerve in your dominant upper limb. During the ultrasound imaging you will lie supine in bed with the arm relaxed. Ultrasound imaging will take no more than 15 minutes.

程序

若你同意參與，將有以下的程式：

檢查上肢時候，請仰臥并且放鬆上肢。我們會用超聲波獲得你的前臂正中神經圖像。 全部超聲掃描檢查需要15分鐘時間。

Benefits

There may be no direct benefits to you from participating in the study. The results of this study will help anesthesiologists who perform ultrasound guided regional anaesthesia in the future.

利益

你不會因為參與這項研究，而得到任何直接益處；但是這研究結果可有助於日後麻醉科醫生以後應用超聲引導區域麻醉的技術。

Risks

Ultrasound is non-invasive and clinical ultrasonography carries NO risks.

危險

超聲掃描是無創技術， 這項研究風險極微。

Ethical Approval

This study has been approved by the Research Ethics Committee of the Joint CUHK-NTEC Clinical Research Ethics Committee.

道德評審

此研究經已通過香港中文大學一新界東區醫院聯盟的臨床研究倫理委員會之道德審核。

Confidentiality

All information obtained in this study will be considered confidential and used only for research purposes. Your identity will be kept confidential in so far as the law allows.

保密

一切因這研究而得的資料，都視作機密，亦只作研究用途；你的個人資料會在法律保障下，得到保密處理。

Questions

The researcher has discussed with you and offered to answer your questions. If you have further questions, you can contact the research nurse or Michael.

問題

研究員已和你討論過及已回答你的問題；若有其他疑問，你可撥電2632 2735聯絡Michael或研究護士。

Right to refuse or withdraw

You understand that to participate or not in this study is voluntary, and will not affect the medical management you will receive. You also understand you have the right to withdraw from the study anytime, if you wish to do so.

拒絕參加及退出的權利

你明白參加與否是自願的，任何決定也不會影響你將接受的醫療服務，你有權隨己意隨時退出這項研究。

Department of Anaesthesia and Intensive Care

The Chinese University of Hong Kong

香港中文大學

麻醉及深切治療學系

Title of Study

Quantitative Evaluation of the Echogenicity of Peripheral Nerves

In Young and Elderly Subjects

研究主題

對青年人群和老年人群的外周神經超聲定量評估研究

Consent

I agree to participate in this study. I have read the information provided and understand the information that has been provided.

同意書

我已閱讀所提供資料，並瞭解一切向我所說明的解釋，我同意參加這項研究。

....

Name & signature of participant Name & signature of investigator

參加者姓名及簽署 研究員姓名及簽署

.....

Date 日期

Patient Details (Gum

香港中文大學醫學院
Faculty Of Medicine
The Chinese University Of Hong Kong

醫院管理局
Hospital Authority
New Territories East Cluster

Joint The Chinese University of Hong Kong – New Territories East Cluster Clinical Research Ethics Committee
香港中文大學—新界東醫院聯網 臨床研究倫理 聯席委員會

Flat 3C, Block B, Staff Quarters, Prince of Wales Hospital, Shatin, HK
Tel : (852) 2632 3935 / 2144 5936 Fax : (852) 2646 6653 Website : http://www.crec.cuhk.edu.hk

11 FEB '09

To: Dr. Xiang Li
PhD Student
Dept. of Anaesthesia & Intensive Care
Prince of Wales Hospital

Ethics Approval of Research Protocol

CREC Ref. No.:	**CRE-2008.591**
Date of Approval:	**04 February 2009***
Study Title:	**Quantitative Evaluation of the Echogenicity of A Peripheral Nerve During Ultrasound Guided Nerve Blockade**
Investigator(s):	**Xiang Li**
Academic Supervisor(s):	**Manoj Kumar KARMAKAR**
Site Supervisor(s):	**Manoj Kumar KARMAKAR**

I write to inform you that ethics approval has been given for you to conduct the captioned study in accordance with the following document(s) submitted:

- Clinical Trial Protocol
- Patient Information Sheet, English and Chinese Version
- Patient Consent Form, English and Chinese Version

This ethics approval* will be valid for 12 months. Application for further renewal can be made by submitting the Ethics Renewal and Research Progress Report Form to the CREC (Download the electronic form template from the http://www.crec.cuhk.edu.hk or http://intec.home/Research%20Ethics/main.asp). You are kindly requested to report to the Committee upon completion of the project.

The Joint CUHK-NTEC Clinical Research Ethics Committee is organized and operates according to ICH-GCP and the applicable laws and regulations.

Miss Winkie Lo
CREC Officer
Joint CUHK-NTEC
Clinical Research Ethics Committee

WLol

PATIENT CONSENT FORM

病人參與研究同意書

Department of Anaesthesia and Intensive Care

The Chinese University of Hong Kong

香港中文大學

麻醉及深切治療學系

Title of Study

Quantitative Evaluation of the Echogenicity of a Peripheral Nerve during Ultrasound Guided Nerve Blockade

研究主題

外周神經阻滯術中的神經超聲回聲密度變化研究

Background

Ultrasound guided peripheral nerve blocks improves the quality of blockade comparing the traditional technique for surgery. Therefore it is becoming popular amongst anesthesiologists including our group. In our clinical jobs we have observed the echogenicity of nerve is increased significantly during block on a sonogram. But until now not any published data can quantify it.

研究背景

超聲波引導區域麻醉這項技術明顯提高了外科手術的神經阻滯效果。因此，這項技術已經進一步獲得包括我們在內的很多麻醉醫生的歡迎。在臨床工作過程中我們觀察到一些現象，在局部麻醉藥物被成功注射到神經組織周圍后，神經組織的回聲密度出現了顯著性改變，對于這一現象目前仍然沒有文獻數據能够進行過量化的客觀解釋。

The objectives of this study

To perform quantitative evaluation of the echogenicity of peripheral nerve during block using computer assisted grey-scale analysis in the subjects.

研究目標

使用計算機輔助灰度分析定量評價周圍神經的超聲圖像在區域麻醉過程中的變化規律。

Procedures

If you agree to participate, the following things will happen:

Record Demographic data: age, gender, height (cm), weight (kg) and the body mass index (BMI).

Only ultrasound imaging of yours will be recorded during ultrasound guided block.

The ultrasound imaging recorded at three time points, including before blockade, during injection and after local anesthetic injection, will be analyzed.

程序

若你同意參與，將有以下的程式：

您的年齡性別、身高、體重和體總指數將會被記錄。您進行超聲引導下區域麻醉時的超聲圖像將會在以後被記錄。超聲掃描檢查錄像(術前、注射麻醉藥物和注射完畢后)將會被分析。

Benefits

There may be no direct benefits to you from participating in the study. The results of this study will improve the medical service of ultrasound guided peripheral nerve block in the future.

利益

你不會因為參與這項研究，而得到任何直接益處；但是這研究結果可有助促進日後麻醉科醫生以後應用超聲引導區域麻醉的技術。

Risks

We ONLY analyze your ultrasound image, there is NO risk.

危險

我們僅僅對于你的超聲圖像進行研究, 無風險。

Ethical Approval

This study has been approved by the Research Ethics Committee of the Joint CUHK-NTEC Clinical Research Ethics Committee.

道德評審

此研究經已通過香港中文大學－新界東區醫院聯盟的臨床研究倫理委員會之道德審核。

Confidentiality

All information obtained in this study will be considered confidential and used only for research purposes. Your identity will be kept confidential in so far as the law allows.

保密

一切因這研究而得的資料，都視作機密，亦只作研究用途；你的個人資料會在法律保障下，得到保密處理。

Questions

The researcher has discussed with you and offered to answer your questions. If you have further questions, you can contact the research nurse or Michael.

問題

研究員已和你討論過及已回答你的問題；若有其他疑問，你可撥電2632 2735聯絡*Dr. Michael Li*或研究護士。

Right to refuse or withdraw

You understand that to participate or not in this study is voluntary, and will not affect the medical management you will receive. You also understand you have the right to withdraw from the study anytime, if you wish to do so.

拒絕參加及退出的權利

你明白參加與否是自願的，任何決定也不會影響你將接受的醫療服務，你有權隨已意隨時退出這項研究.

Department of Anaesthesia and Intensive Care

The Chinese University of Hong Kong

香港中文大學

麻醉及深切治療學系

Quantitative Evaluation of the Echogenicity of a Peripheral Nerve during Ultrasound Guided Nerve Block

外周神經在外周神經阻滯術中的回聲密度變化研究

Consent

I agree to participate in this study. I have read the information provided and understand the information that has been provided.

同意書

我已閱讀所提供資料，並瞭解一切向我所說明的解釋，我同意參加這項研究。

....

Name & signature of participant Name & signature of investigator

參加者姓名及簽署 研究員姓名及簽署

.....

Date

日期

Patient Details (Gum

香港中文大學醫學院
Faculty Of Medicine
The Chinese University Of Hong Kong

醫院管理局
Hospital Authority
New Territories East Cluster

Joint The Chinese University of Hong Kong – New Territories East Cluster
Clinical Research Ethics Committee
香港中文大學–新界東醫院聯網 臨床研究倫理 聯席委員會

Flat 3C, Block B, Staff Quarters, Prince of Wales Hospital, Shatin, HK
Tel : (852) 2632 3935 / 2144 5926 Fax : (852) 2646 6653 Website : http://www.crec.cuhk.edu.hk

11 MAR '09

To: Dr. Xiang LI
PhD Student
Dept. of Anaesthesia & Intensive Care
Prince of Wales Hospital

Ethics Approval of Research Protocol

CREC Ref. No.:	**CRE-2009.096**
Date of Approval:	**03 March 2009***
Study Title:	**Correlation between "In-cart" and "Off-cart" Measurements in Musculoskeletal Ultrasound Imaging**
Investigator(s):	**Xiang LI**
Academic Supervisor(s):	**M.K. KARMAKAR**
Site Supervisor(s):	**M.K. KARMAKAR**

I write to inform you that ethics approval has been given for you to conduct the captioned study in accordance with the following document(s) submitted:

- Clinical Trial Protocol, revised on 28 February 2009
- Participant Informed Consent Form, English and Chinese Version, revised on 02 March 2009

This ethics approval* will be valid for 12 months. Application for further renewal can be made by submitting the Ethics Renewal and Research Progress Report Form to the CREC (Download the electronic form template from the http://www.crec.cuhk.edu.hk or http://intra.hospital.research%20/Ethics/main.asp). You are kindly requested to report to the Committee upon completion of the project.

The Joint CUHK-NTEC Clinical Research Ethics Committee is organized and operates according to ICH-GCP and the applicable laws and regulations.

Miss Winkie Lui
CREC Officer
Joint CUHK-NTEC
Clinical Research Ethics Committee

WLui

PATIENT CONSENT TO PARTICIPATE IN A RESEARCH STUDY

病人參與研究同意書

Department of Anaesthesia and Intensive Care

The Chinese University of Hong Kong

香港中文大學

麻醉及深切治療學系

Title of Study

Correlation between "In-cart" and "Off-cart" Measurements in Musculoskeletal Ultrasound Imaging

研究主題

對于骨骼肌超聲圖像在綫和離綫觀察方法的相關性比較研究

Background

Ultrasound has been used to identify and measure musculoskeletal structures before performing common interventions in the daily clinical practice. The more popular measuring method ("in-cart" method) is commonly used to measure objective size directly on the screen using the electronic callipers incorporated into the ultrasound machine. But this process is time-consuming. As a possible alternative to it, another measuring method ("off-cart" method) was introduced, which means measurement can be performed on the still ultrasound image. However, to date there has been no data on the evaluation of correlation between the two methods. Gender-related variation of the skeletal muscle thickness has been previously reported using ultrasound, but it is not clear whether gender-related differences also exist in the pectoralis major and pectoralis minor muscles.

研究背景

超聲波是在臨床工作中進行骨骼肌機構測量的常用手段。日常進行測量是采取在綫方法，即是用超聲波機器上的測量器對目標進行直接測量，但是這種檢測方法需要消耗較多的時間。目前可以采用離綫方法進行測量，即使采取只針對病人已經記錄下的超聲波圖像使用圖像軟件進行測量，但是這兩種方法之間的相關性未曾進行評價。此外，既往的研究證實某些骨骼肌結構存在性別差异，但是對于性別相關的鎖骨下的骨骼肌結構的差异沒有使用超聲波進行評價。

The objectives of this study

Our objective is to access the correlation between the "off-cart" and "in-cart" measurement methods in still and if there is a gender-related difference in the musculoskeletal sonoanatomy of the infraclavicular region.

研究目標

評價兩種方法的相關性和鎖骨下區域骨骼肌結構性別差別。

Procedures

If you agree to participate, the following things will happen:

For measurements, you will lie supine with the arm slightly relaxed on the bed. You will answer questions about your weight, height and age. The research nurse/investigators will collect data from your medical record. We will spend about 5 minutes on all scanning.

程式

若你同意參與，將有以下的程式：

請仰臥并且放鬆上肢。我們需要詢問你的身高，體重和年齡。進行研究時候需要收集你的病歷資料。全部超聲掃描檢查需要5分鐘時間。

Benefits

There may be no direct benefits to you from participating in the study. The results of this study may improve the way anesthesiologists manage, diagnosis and treatments in future patients.

利益

你不會因為參與這項研究，而得到任何直接益處；這研究結果可有助改善日後麻醉科醫生處理手術病人和一些其他專科診斷治療方法。

Risks

There is NO risk if you participate in the study.

危險

這項研究無風險。

Ethical Approval

This study has been approved by the Joint CUHK-NTEC Clinical Research Ethics Committee.

道德評審

此研究經已通過中大—新界東聯網醫院聯合臨床研究倫理委員會之道德審核。

Confidentiality

All information obtained in this study will be considered confidential and used only for research purposes. Your identity will be kept confidential in so far as the law allows.

保密

一切因這研究而得的資料，都視作機密，亦只作研究用途；你的個人資料會在法律保障下，得到保密處理。

Questions

The researcher has discussed with you and offered to answer your questions. If you have further questions, you can contact the research nurse or Dr. Kamakar on 2632 2735.

問題

研究員已和你討論過及已回答你的問題；若有其他疑問，你可撥電2632 2735聯絡Dr. Kamakar M.K.或研究護士。

Right to refuse or withdraw

You understand that to participate or not in the study are voluntary, and will not affect the medical management you will receive. You also understand you have the right to withdraw from the study anytime, if you wish to do so.

拒絕參加及退出的權利

你明白參加與否是自願的，任何決定也不會影響你將接受的醫療服務，你有權隨已意隨時退出這項研究。

Department of Anaesthesia and Intensive Care

The Chinese University of Hong Kong

香港中文大學

麻醉及深切治療學系

Title of Study

Correlation between "In-cart" and "Off-cart" Measurements in Musculoskeletal Ultrasound Imaging

研究主題

對于骨骼肌超聲圖像在綫和離綫觀察方法的相關性比較研究

Consent

I agree to participate in this study. I have read the information provided and understand the explanation that has been given to me.

同意書

我已閱讀所提供資料，並瞭解一切向我所說明的解釋，我同意參加這項研究。

....

Name & signature of participant Name & signature of investigator

參加者姓名及簽署 研究員姓名及簽署

.....

Date

日期

Patient Details (Gum